Master thesis:

Dynamic behaviour of long jetty structures under seismic conditions

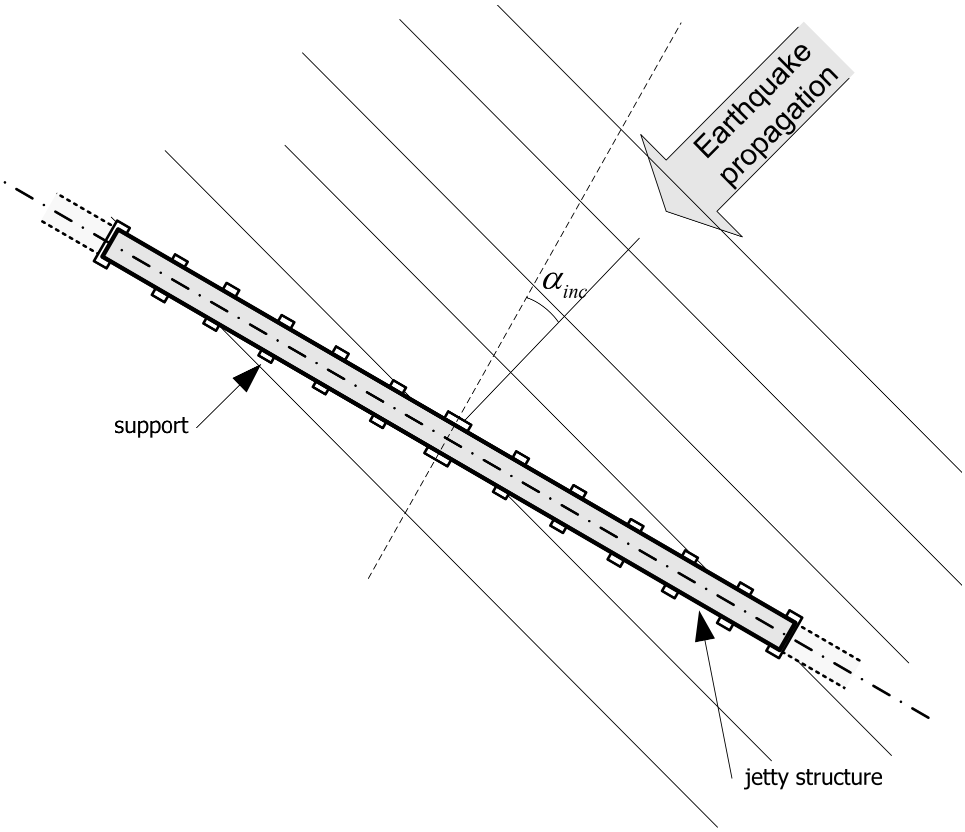

Editor:	W.H. de Brabander jr
Supervision Committee:	Prof. Drs. Ir. J.K. Vrijling Ir. L.A.M. Groenewegen Dr. sc. A. Metrikine Ir. W.F. Molenaar

Date:	20 October 2006
Status:	Final
Number of Pages:	109

Master thesis:

Dynamic behaviour of jetty structures under seismic conditions

Editor:	W.H. de Brabander jr
Supervision Committee:	Prof. Drs. Ir. J.K. Vrijling Ir. L.A.M. Groenewegen Dr. sc. A. Metrikine Ir. W.F. Molenaar

Date:	20 October 2006
Status:	Final
Number of Pages:	109

Summary

Jetty structures are relatively long structures. Codes applied to seismic engineering, e.g. eurocode 8, do not make a differentiation to relatively long structures. So, what is the effect of uneven excitation on relatively long structures?

The earthquake load, according to the eurocode 8, is modelled by a modal response spectrum. Consequently, this modal response spectrum is applied on a modal analysis. The only information a modal response spectrum contains, is the information about the maximum response of a single degree of freedom model during a design earthquake event. The modal response spectrum does not contain information about the time delay in excitation. Therefore it is not possible to implement the effect of uneven excitation when applying the modal analysis.

This research investigates the effect of uneven excitation on a jetty structure by the time history method. A model has been set up according the Euler- Bernoulli beam model. The calculation is done for the Alkion earthquake for variable incidence angles. For particular incidence angles does the maximum bending moment peak. The cause of this response amplification is discovered in the transfer functions.

The transfer function describes the steady state response of a harmonic load. The peak bending moments calculated with the time history analysis corresponds the peaks calculated with the transfer functions. The additional peaks are caused by the frequency of the harmonic loading and the shape of the load. For particular values of the incidence angle does the shape the load match the mode shape.

Information of the time delay in loading turns out to be important for the occurring maximum forces, bending moments. E.g. the time history calculations give an 5x amplification of the structural bending moments. Building codes should inherit design rules for relatively long structures because bending moment do increases for particular incidence angles.

Contents

Figures

Tables

Preface

This master thesis finalizes my master study civil engineering at Delft Technical University (DTU). The project is worth 42 ECTS which equals a workload of 8 months. This research is being executed in cooperation with DTU and Delta Marine Consultants (DMC). Prof. A. van der Horst, managing director of DMC brought me in contact with L.A.M Groenewegen, senior consultant of DMC and also member of the supervision committee. Mr Groenewegen had some questions about the amplification of structural stresses when an earthquake is moving towards a relatively long structure under an angle. The building codes, API, Eurocode and BS do not make a differentiation for relatively long structures. A problem description is given in chapter one.

An area, which is struck by a major earthquake, often needs emergency relief supplies to take care of the casualties or to repair the structural damage. For a coastal area a jetty is often the primary chain in this supply. The understanding of earthquake loads on jetty structures is therefore very important.

The first chapter starts with the problem description and the case where the research is applied on. Chapter two is about the modelling of earthquakes. How it is triggered and how to calculate the earthquake load, which can be applied onto the model. The earthquake modelling techniques available are the time history analysis or a modal response spectrum analysis. The time history analysis is discussed in this chapter. Chapter three is about structural modelling. Deferent structural modelling techniques are available. The applied model is based on the Euler – Bernoulli beam.
Chapter four is about the analysis of the model applied to the case. The maximum structural response is calculated and an explanation is comparison is made to a SDOF calculation. The last chapter finalizes the report with conclusions and recommendations.

Many thanks to my supervision committee. L.A.M. Groenewegen for the generation of the thesis subject and the study facilities at DMC, A. Metrikine for his supervision in the set up of the model and the availability of a study room/ facilities at the section of Structural Mechanics. W.F. Molenaar for his feedback on the reports, Prof. Vrijling, chairman of the supervision committee, for his overall monitoring. Further I would like to thank T. van Eck from the KNMI- seismology division, for providing the earthquake datasets.
Special thanks to Marieke, my parents, family, friends and fellow students for their great support.

W.H. de Brabander jr.

List of symbols

A	area	[m^2]
a_x	acceleration in x direction	[m/s^2]
a_y	base acceleration	[m/s^2]
$\mathbf{C}$	damping matrix	[kg/s]
c_w	wave celerity	[m/s]
c	damping parameter	[kg/s]
c_{cr}	critical damping	[kg/s]
D	shear force	[N]
d	span length	[m]
E	young's modulus	[N/m^2]
E_{disp}	dissipated energy	[j]
E_n	energy	[j]
F_x	Force in x direction	[N]
f_0	natural frequency	[Hz]
H_{Da}	base acceleration – structural shear force transfer function	[kg]
H_{Ma}	base displacement – structural acceleration transfer function	[Ns^2]
H_{My}	base displacement – structural bending moment transfer function	[N]
H_{vy}	base displacement – structural displacement transfer function	[-]
I	moment of inertia	[m^4]
I_m	mass moment of inertia	[kgm^2]
i	complex number	[-]
$\mathbf{K}$	stiffness matrix	[N/m]
k	stiffness parameter	[N/m]
k_n	time domain sample number	[-]
k_r	rotational stiffness parameter	[N/m]
k_t	transverse stiffness parameter	[Nm]
k_{total}	total stiffness parameter	[N/m]
$\mathbf{M}$	mass matrix	[kg]
M	bending moment	[Nm]
M_{cap}	mass of concrete cap	[kg]
M_w	mass of added water	[kg]
M_{pile}	mass of pile	[kg]
$M_{\sup}$	mass of support	[kg]
M_l	Richter magnitude	[-]
M_s	surface wave magnitude	[-]
M_b	body wave magnitude	[-]
M_0	seismic moment	[-]
M_w	Moment magnitude	[-]
m	mass	[kg]
m_{total}	total mass	[kg]
N	normal force	[N]

N_s	number of samples	[-]
$N_{\sup}$	number of supports	[-]
n	frequency domain sample number	[-]
S_Y	frequency domain base motion	
s	support number	[-]
T_0	natural period	[s]
T_y	bending moment	[Nm]
t	time	[s]
V	transverse displacement in the frequency domain	[ms]
v	transverse displacement in the time domain	[m]
$\dot{v}$	transverse velocity in the time domain	[m/s]
$\ddot{v}$	transverse acceleration in the time domain	[m/s^2]
v'	rotation	[-]
v''	curvature	[-/m]
x	x - coordinate	[m]
y	y - coordinate	
Y_b	transverse base motion amplitude	[m]
y_b	transverse base motion	[m]
y_{NS}	North – South earthquake motion	[m]
y_{EW}	East – West earthquake motion	[m]
y_{long}	longitudinal earthquake motion	[m]
y_{trans}	transverse earthquake motion	[m]
r	radius	[m]
z	z - coordinate	[m]
α	damping factor	[s]
α_{inc}	angle of incidence	[^{0}]
β	wave propagation angle	[^{0}]
ε	strain	[-]
Φ	rotation amplitude	[-]
ϕ	rotation	[-]
γ	wave number	[rad/m]
κ	curvature	[-/m]
ρ	specific weight	[kg/m^3]
σ	stress	[N/m^2]
θ	jetty angle	[^{0}]
ω	frequency	[rad/s]
ω_0	natural frequency	[rad/s]
ξ	critical damping percentage	[-]
τ	time delay	[s]

Chapter 1 Project description

The problem description for this thesis is given in the first part of this chapter. The second part of this chapter discusses the case where the problem is applied on. The case is a jetty structure near Melaka, Malaysia. The definition of a jetty (Tsinker, 1997):

> *A structure projected into the water, enabling mooring of ships at an angle to the shoreline.*

1.1 Problem description

Building codes prescribes modal response spectra, or more simplified, a linear static analysis to model earthquakes. In these simplified modelling techniques, the effect of uneven excitation of the jetty is not taken into account. The problem description is given in the next paragraphs.

1.1.1 Analysis of a jetty

Jetty structures can be very long. Consequently, an earthquake will not excite the structure at every support at the same time but more likely at every support with some time delay (see Figure 1-1). In the building codes this time delay isn't taken into account. This effect can cause an additional dynamic amplification or reduction on the jetty behaviour. This research will be focused on this effect on a jetty. A study will be done on the influence of structural parameters on structural behaviour.

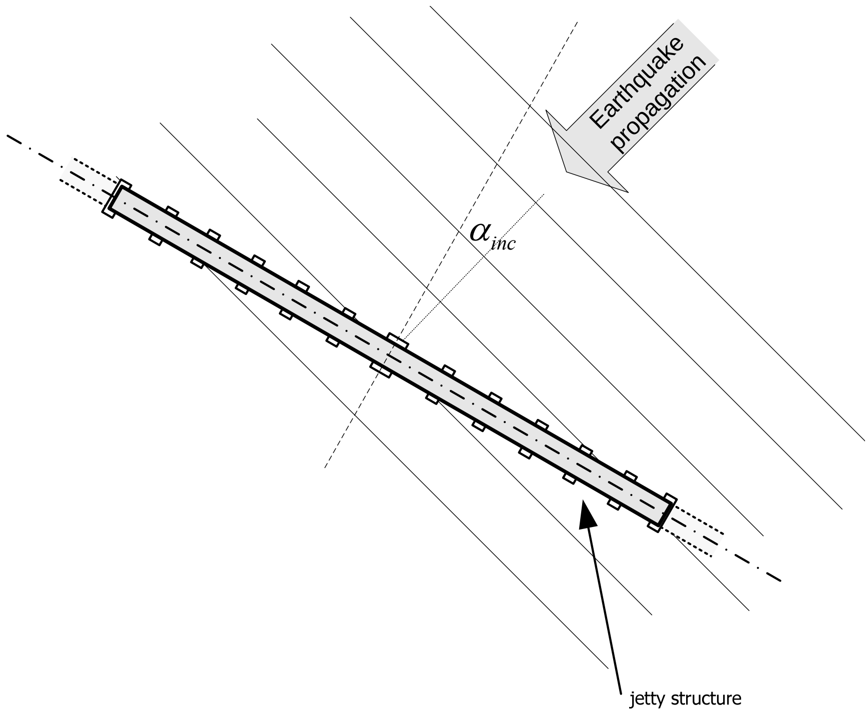

Figure 1-1 earthquake approaching jetty structure

1.1.2 Relation between structural dynamics and pipe limits

Pipes which lay on a jetty usually have a fixed connection. It is required that the pipe on a jetty won't collapse. If the pipe is constructed with free connection it allows the pipe to move in transversal direction with respect to the support. This research will be focused on the allowance of some dynamic movement of the pipeline relative to the jetty. To allow some movement, the energy induced by the earthquake does not have to be dissipated by the structure directly and the pipe will experience less bending.

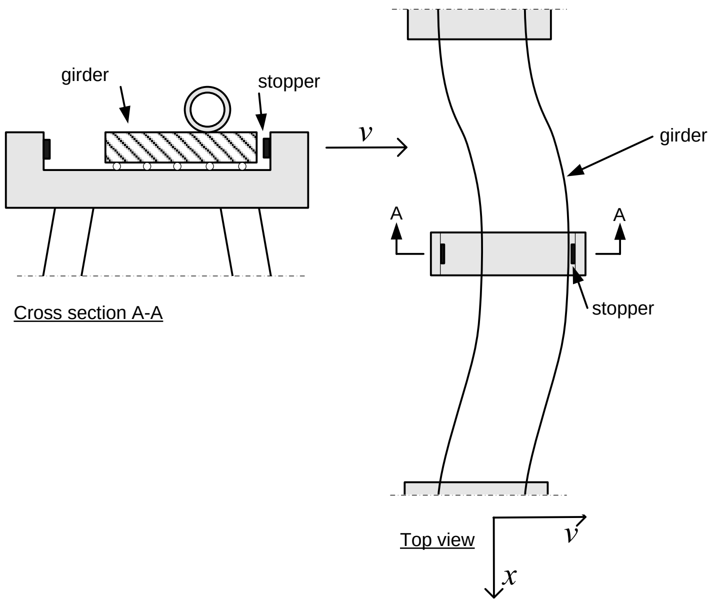

Figure 1-2 Behaviour tubular pipe support

1.2 Case

A bulk cargo carrier jetty near Melaka is chosen to investigate. The first 13 supports are analysed for this case. At the 1st and 13th support exists an expansion joint. A jetty can be modelled as a stand alone structure between its extension joints (Maritime Navigation Commission Working Group 34, 2001). The influence of the interaction between the extension joints is then neglected. Therefore, during this research, the jetty between its expansion joints will be modelled as a stand alone structure. The middle support exists of a strong point with two rows of piles. A survey is given in Figure 1-3. Due to thermal expansions, the structure expands and shortens. Near the strong points, the deck is fixed. The deck expands/ shortens away from the expansion joints. The longitudinal deflection is zero in the expansion joints.

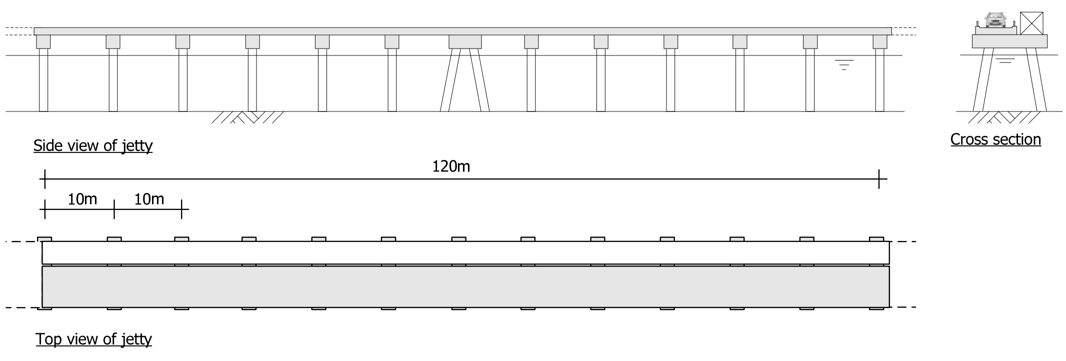

Figure 1-3 Survey of jetty near Melaka

1.2.1 Pile-Cap Properties

The piles have the following properties:

Length	7.0m
D (Diameter)	0.610m

t (Width)	0.016m
A (area)	0.030m2
I (inertia)	0.00132m4
E (Young's modulus)	2.1e11[N/m2]
ρ (specific weight)	7700 kg/m3
Pile weight	1617 kg (one pile)

The cap has the following properties

Length	7.6~9.2m
Width	1.2m
Height	1.71m
V (volume)	11.5~18.9m^3
E (Young's modulus)	3.5e10[N/m2]
ρ (specific weight)	2500 kg/m3
Cap weight	39,500 kg (average)

Added mass to the pile, due to water, is given by:

$$M_w = \rho \cdot C_m \cdot \pi \cdot r^2 \text{ [kg/m]} \tag{1-1}$$

For this application holds C_m = 1 ,hollow pile (Sarpkaya and Isaacson, 1981). The added water mass per pile is given by:

$$M_w = 1023 \cdot 1 \cdot \pi \cdot 0.61^2 = 1196 \text{ [kg/m]} \tag{1-2}$$

The contribution of the pile mass to the jetty deck is estimated at approximate 24% (Spijkers et al., 2005). Therefore, the total mass concentrated onto the jetty deck is given by:

$$M_{\sup} = 0.24\left(M_{water} + M_{pile}\right) + M_{cap} \quad \text{[kg]} \tag{1-3}$$

The water height is 4m, thus the concentrated mass at the jetty deck is given by:

$$M_{\sup} = 0.24\left(4 \times 1196 + 2 \times 1617\right) + 39500 = 40964.24 \quad \text{[kg]} \tag{1-4}$$

Near the strong point are located 4 piles instead of 2. So the support mass is:

$$M_{\sup} = 2 \times \left(1273\right) + 39,500 = 42,046 \quad \text{[kg]} \tag{1-5}$$

1.2.2 Deck

A cross section of the deck – girder is given Figure 1-4.

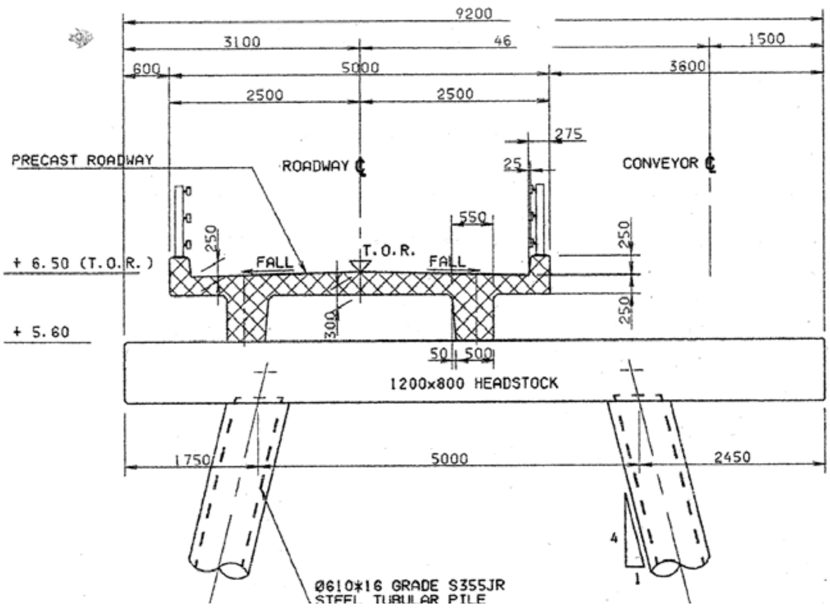

Figure 1-4 Typical cross section jetty

The girder properties are given by:

d (span)	10.0m
A (area)	2.759m2
I (intertia)	1.37m4
E (Young's modulus of B35, uncracked)	3.1e12[N/m2]
ρ (specific weight)	2500 kg/m3
Conveyor/ deck appurtenances	3000 kg/m

Chapter 2 Earthquakes

An earthquake is a sudden and sometimes catastrophic movement of a part of the Earth's surface. This may cause several types of effects, which can be direct or indirect. Direct effects are e.g. ground shaking and ground sliding. Indirect effects are e.g. tsunamis. This chapter discusses the earthquake phenomenon, the mechanism, measuring and the modelling of an earthquake. Figure 2-1 gives the acceleration in the north- south and east- west direction of El Centro earthquake in may 2, 1940. In table 2-1 are the magnitudes given for heavy earthquakes in the past century.

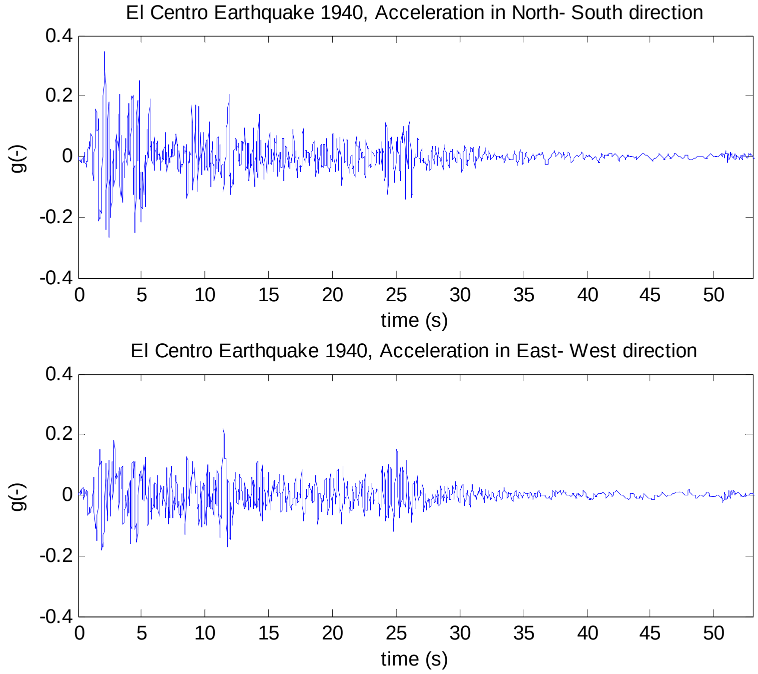

Figure 2-1 El Centro earthquake 1940 acceleration in g (9.81 m/s^2)

year	Place	Magnitude Richter scale
1905	China	8.7
1906	Colombia	8.9
1906	Chili	8.6
1911	Russia	8.7
1914	Japan	8.7
1922	Chili	8.4
1928	Chili	8.4
1933	Japan	8.9
1938	Alaska	8.7
1939	Chili	8.3
1943	Chili	8.3
1950	India	8.7

table 2-1 Heavy earthquakes (Spijkers et al., 2005)

Conversion of Richter scale to peak ground acceleration is done by equation (2.1).

$$\hat{a}_L = Ae^{0.8M}\left(R+R_0\right)^{-2} \quad (2.1)$$

Where:

A 56e6 m/s^2

M_L Local magnitude (Richter)

R	Distance to epicentre
R_0	40m

2.1 Triggering

The earth consists of multiple plates which move freely from each other according to the plate theory. Where two plates meet each other faulting occurs. The different types of faulting are given in Figure 2-2:

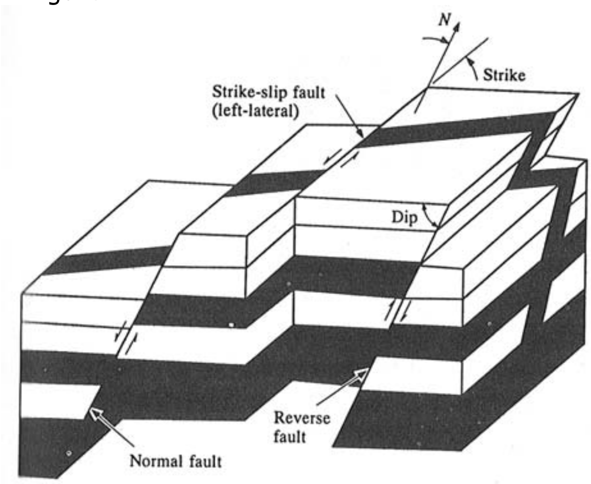

Figure 2-2 different types of faulting (Clough and Penzien, 1993)

The types of faults are (Figure 2-2):

- thrust or reverse fault
- extensional or normal fault
- strike- slip fault

The relative movement of the plate determines the type of faulting. Stresses are being built up, during movement,. When the stresses exceed the resistance between two plates, the accumulated stress or energy will be released in the form of ground shaking. Consequently seismic intensity will be higher at plate boundaries. The seismic data of most locations on earth is available. E.g. at GSHAP.

Figure 2-3 Zones where heavy earthquakes occur. (Spijkers et al., 2005)

2.2 Propagation

An earthquake initially produces waves that propagate through the earth’s interior in the form of body waves. Where the waves meet the surface, the earthquake continues in the form of surface waves.

2.2.1 Body waves

Body waves follow curved paths because of anisotropy (Figure 2-4). Anisotropy is caused by the variation in density and composition of the Earth's interior. Within an earth layer the velocity of the wave is higher in the direction to the inner core.

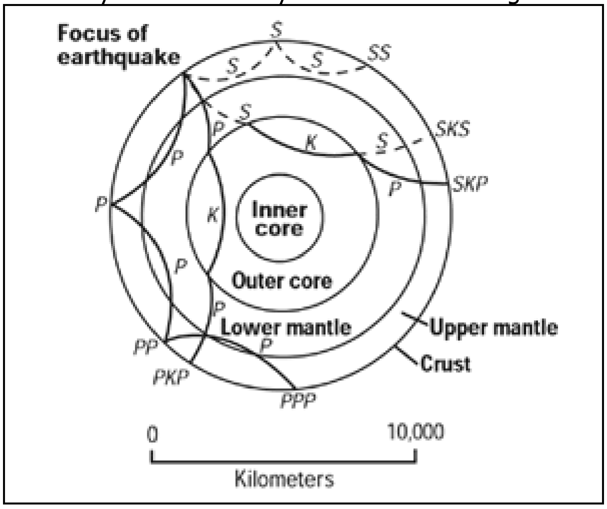

Figure 2-4 Propagation of Body waves

Bodywaves are P- waves and S-waves. P-waves are, like sound waves, longitudinal or compression waves. The wave celerity depends on the density of the material. (Through air does it propagate with the speed of sound.) The propagation of a P-wave is caused by a pressure difference. P-waves are also known as pressure waves.
S-waves are transverse or shear waves, this means that the movement of the ground is perpendicular to the direction of the wave propagation direction. The propagation of the wave is caused by shear stresses. This is why S- waves propagate only through solids, because fluids and gasses do not support shear forces. In Figure 2-5 are the P- and S-waves schematised. The velocities of P/S – waves are given in table 2-2.

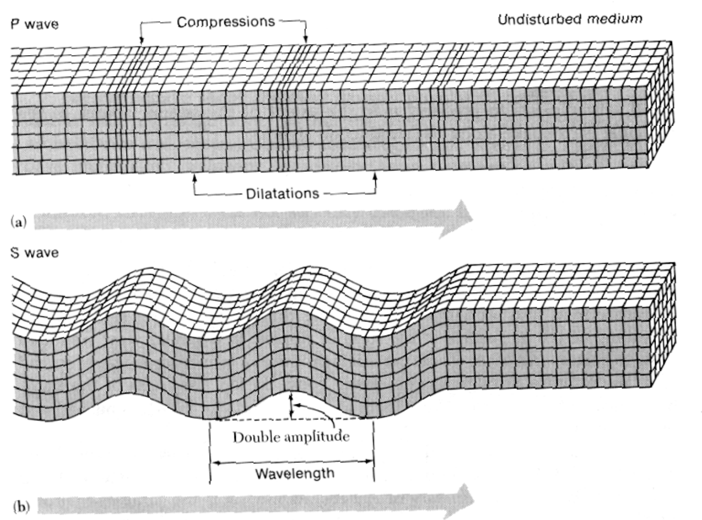

Figure 2-5 bodywaves a) p- wave b) s- wave

Body waves	Velocity	Direction
P- wave	330 m/s in air 1450 m/s in water 5000 m/s granite	Longitudinal

S- wave	+/-58% of the speed of an P-wave	Transversal

table 2-2 velocity of p/s waves

2.2.2 Surface waves

Surface waves are analogous to water waves and travel over the earth's surface. They are more likely than body waves to stimulate resonance in structures and therefore the most destructive type of seismic wave. There are two types of surface waves: Rayleigh waves and Love waves.
Rayleigh waves, also called ground roll, are surface waves that travel as ripples similar to those on the surface of water. L. Rayleigh and J.W. Strutt predicted the existence of the waves in 1885. Surface waves are slower than body waves and can readily be seen in an open space.
Love waves are surface waves that cause horizontal shearing of the ground. They are named after A.E.H. Love, a British mathematician who created a mathematical model of these waves in 1911. They are usually slightly faster than Rayleigh waves.

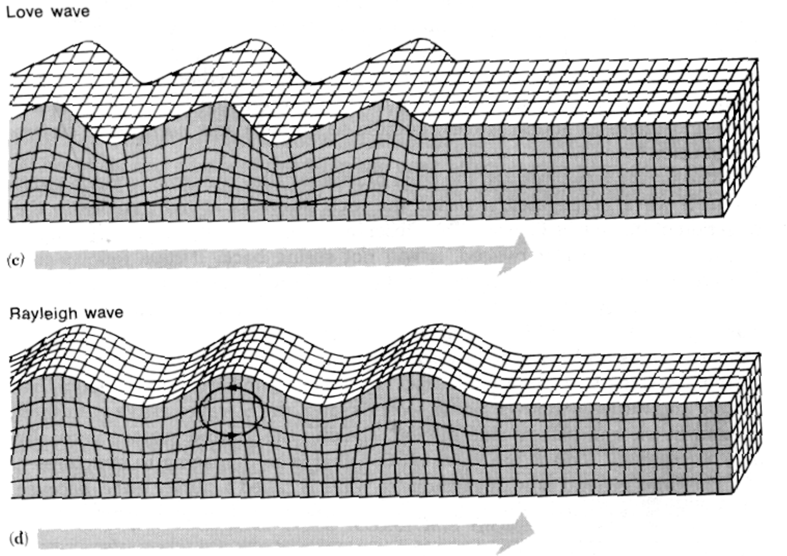

Figure 2-6 Mechanism of body and surface waves

ground type	description of the ground type	v (m/s)
A	Rock or tougher rock- like geological formation, including at most 5 m of weaker material at the surface	>800
B	Deposits of very dense sand, gravel or very stiff clay, at least several tens of m in thickness, characterised by a gradual increase of mechanical properties with depth	360-800
C	Deep deposits of dense or medium-dense sand, gravel or stiff clay with thickness from several tens to many hundreds of meter	180-360
D	Deposits of loose-to-medium cohesion less soil (with or without some soft cohesive layers), or of predominantly soft-to-firm cohesive soil	<180

table 2-3 ground types (Nederlands Normalisatie-Instituut, 1995)

The different ground types (table 2-3) are determined according the value of the average shear wave velocity given in the table. Ground motion is a complex phenomenon near the surface. The surface can vibrate locally when soft soil is located on top of rock or stiff soil. The composition of the soil is very important for local dominant vibrations.

2.3 Measuring

2.3.1 The modified Mercalli Intensity Scale

The Mercalli intensity scale consists of a series of certain key responses such as people awakening, movement of furniture, damage to chimneys, and finally - total destruction. Although numerous intensity scales have been developed over the last several hundred years to evaluate the effects of earthquakes, the one currently used in the United States is the Modified Mercalli (MM) Intensity Scale. It was originally developed by Mercalli and modified in 1931 by the American seismologists Harry Wood and Frank Neumann. This scale, composed of 12 increasing levels of intensity that range from imperceptible shaking to catastrophic destruction, is designated by Roman numerals. It does not have a mathematical basis; instead it is an arbitrary ranking based on observed effects.

2.3.2 Earthquake magnitudes

Since 1900 all over the world earthquakes have been measured by various seismographs. To translate the measurements into an analytic value, several magnitudes are in use:

Symbol	Name	Formula
• M_L	Local ("Richter") Magnitude	ML = log A - log A_o defined by Richter (1935) where A is the maximum trace amplitude in millimetres recorded on a standard short-period seismometer and log Ao is a standard value as a function of distance where distance ≤ 600 kilometres.
• M_s	Surface Wave Magnitude (Gutenberg and Richter,1936)	Ms = log A + 1.66 log Δ + 2.0 Where: A = the maximum ground amplitude in micrometers (microns) Δ = the epicentral distance of the seismometer measured in degrees
• M_b	Body Wave (P-wave) Magnitude	M_b = log A – log T + 0.01 Δ+ 5.9
• M_o	Seismic Moment	$M_0 = \mu A\overline{D}$ Where: μ = rupture strength A = rupture area $\overline{D}$ = average amount of slip
• M_w	Moment Magnitude	The measured ground $M_w = \frac{\log M_0}{1.5} - 10.7$ where: M_0 = seismic moment
• E_n	Energy	The total energy released from a seismic activity is often estimated from the relationship: log E_n = 11.8 + 1.5 M_s Where: E_n = the amount of energy expressed in ergs

	M_s = The surface wave magnitude 1 erg = 1 dyne · 1 cm. Where one dyne is a force to bring over an acceleration of 1 cm/s^2 to a mass of 1 gram. So 1 dyne = 10-5 N and 1 erg = 10-7 J = 10-7 N·m

table 2-4 used magnitudes

The surface magnitude is most commonly used to describe the size of shallow (less than about 70 km focal depth) earthquake with a moderate to large distant (farther than about 1000km). The body wave magnitude (Gutenberg, 1945) is a worldwide magnitude scale based on the amplitude of the first few cycles of p-waves which are not strongly influenced by the focal depth. For strong earthquakes, the measured ground-shaking characteristics become less sensitive to the size of the earthquake than for smaller earthquakes. This phenomenon is called "saturation". The moment Magnitude is the only magnitude that is not subjected to saturation. Therefore it is a good magnitude to apply to very strong earthquake
In practice all magnitudes are used. Depending on the earthquake or the phenomenon which is of importance a magnitude has to be chosen. E.g. the released energy during an earthquake doesn't have to be proportional to the maximum acceleration of an earthquake. For relatively small earthquakes, the Richter magnitude is being used. For strong magnitudes the moment magnitude.

2.4 Greece earthquake

The transverse structural motion is investigated in this research. The earthquake motion, on the other hand, is given in multiple directions. An earthquake motion is a 3 dimensional motion in x, y and z direction. This paragraph determines the transverse base motion. Also the time delay between the arrival time of the earthquake is determined.
During this research is used the dataset of the Alkion earthquake in Greece (Ambraseys N., 2000) which occurred on 1981-02-24 at 20:53:59. One of the seismograms, which measured this earthquake was located at Xilokastro – OTE building. The recordings are given in Figure 2-7. The measurement data is in three directions:

- longitudinal
- transversal
- vertical

The response spectra for the longitudinal earthquake motion are given in Figure 2-8. For the calculation of the response spectra is referred to Appendix E. This calculation has been done in the time domain.

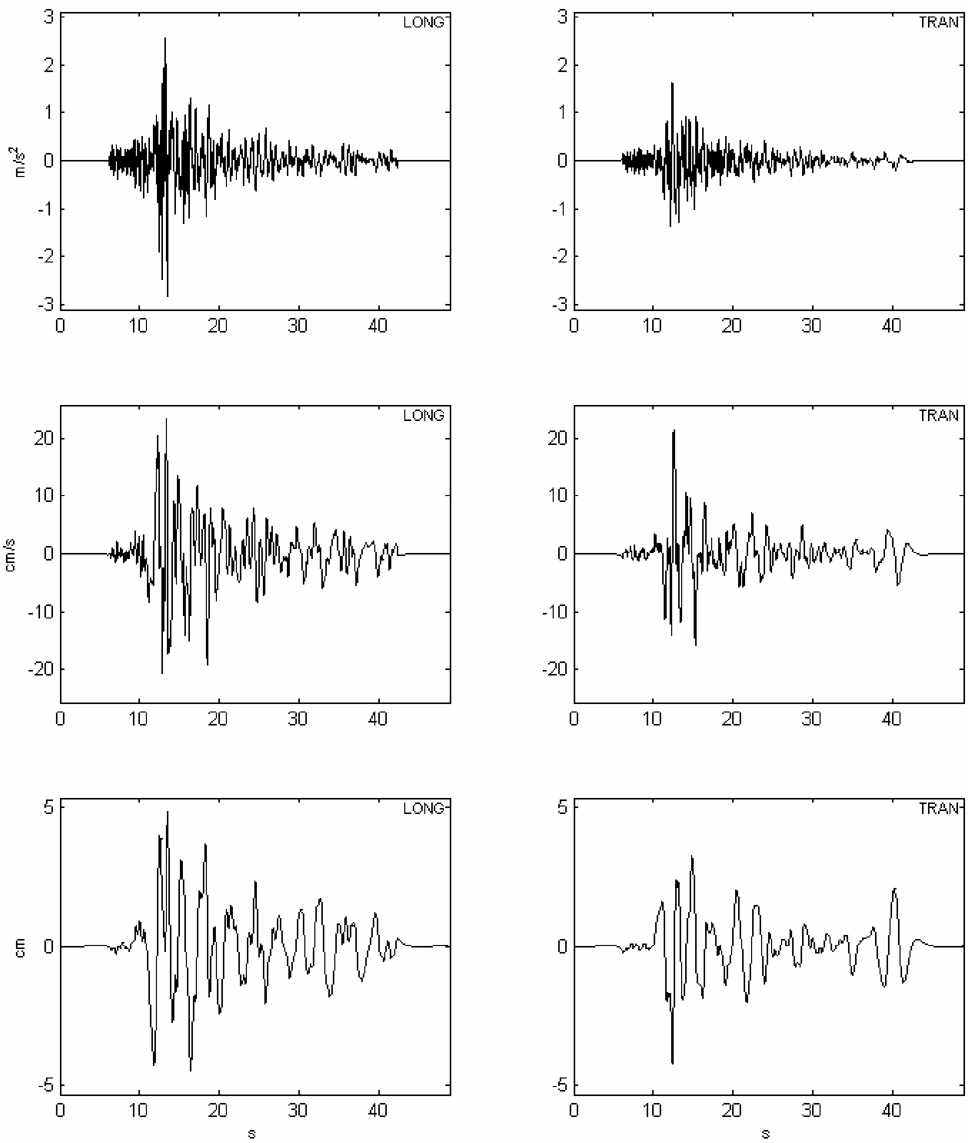

Figure 2-7 Alkion Earthquake Greece, first row: acceleration, second row: velocity, third row: displacement, first column: longitudinal direction, second column: transverse direction.

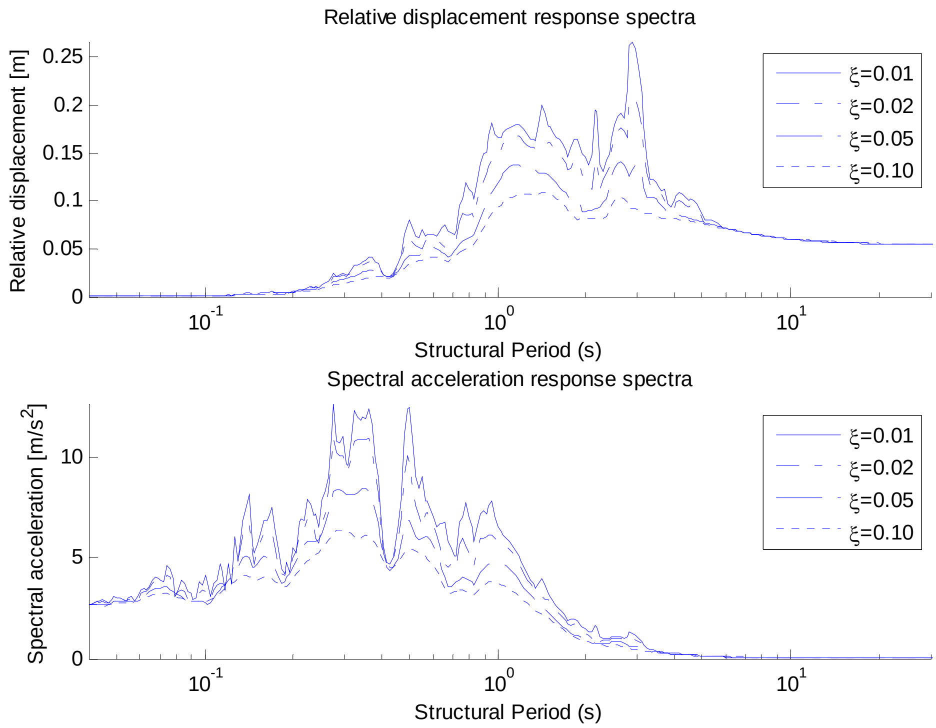

Figure 2-8 Response spectra for Alkion earthquake longitudinal motion. Pseudo acceleration and relative displacement for different damping values.

Figure 2-9 Location of epicentre and seismogram

Some values of the earthquake are:

- Ms: 6.68 surface wave magnitude
- Mb: 6.1 body wave
- ML: 6.8 richter scale
- Mw:6.4 moment magnitude

The epicentre of the earthquake is given in the dashed box (Figure 2-9). The earthquake displacement signal taken onto the jetty is the measurement data from the Xilokastro – OTE building (number 334 on the map).

2.5 Time delay

What is the influence of the time delay (τ) in excitation of the supports onto the structure? This is the main question during this research. The time delay is dependent on the angle of incidence (α_{inc}) of the incoming earthquake waves.
In Figure 2-10 is seen the time delay τ of an earthquake peak. The time delay (τ) is depending on the angle of incidence (α_{inc}) and is given by:

$$\tau = \frac{d}{c}\sin\alpha_{inc} \tag{2.2}$$

where:

α_{inc} = angle of incidence
d = length between supports
c = earthquake wave celerity

(α_{inc}) is dependent on the position of the jetty (θ) and the propagation direction (β) of the earthquake. The angle of incidence (α_{inc}) is given by:

$$\alpha_{inc} = 90 + \beta - \theta \tag{2.3}$$

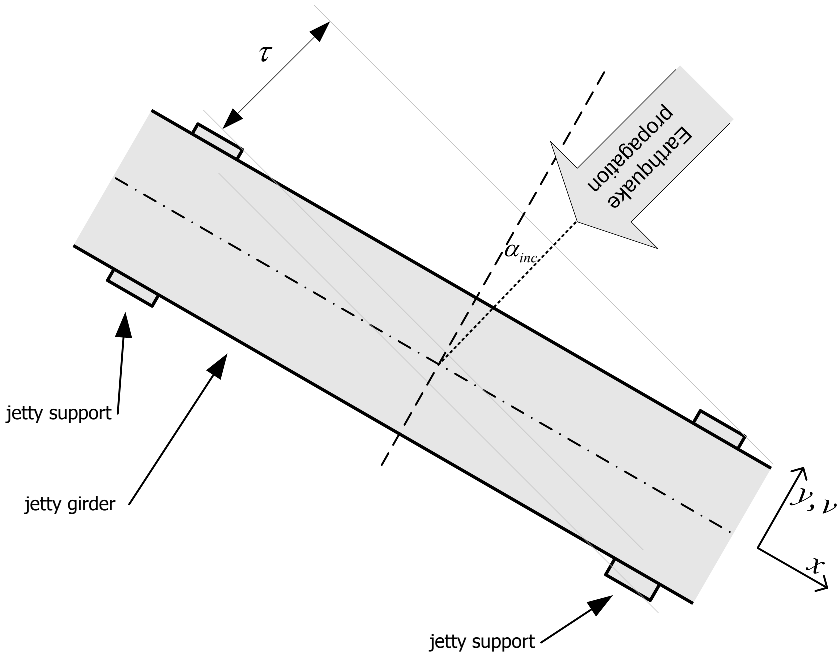

Figure 2-10 Time delay tau

β and θ are given in the figure below:

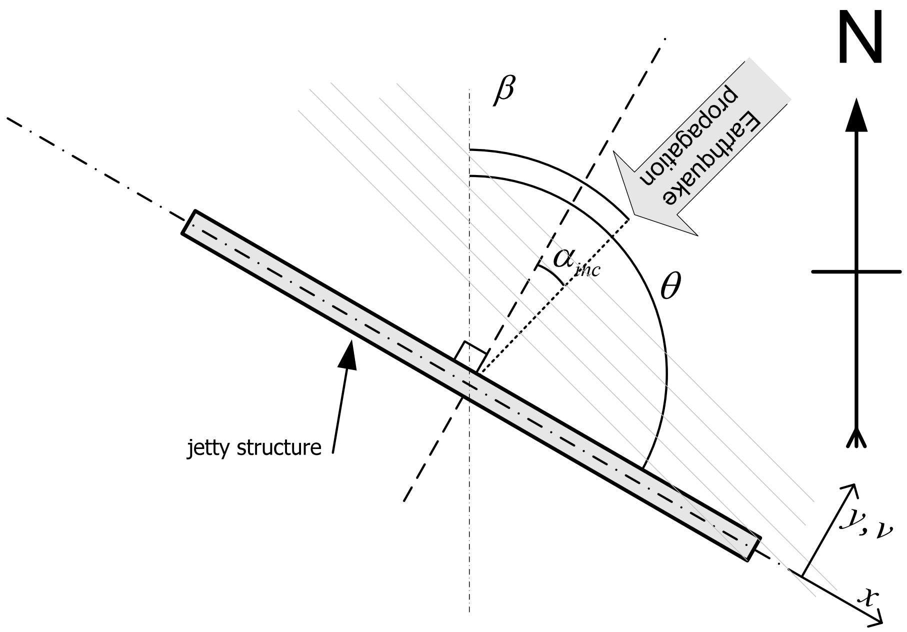

Figure 2-11 angle of propagation/ jetty/ incidence

In this research is assumed that the propagation direction (β) of the earthquake is coming from the epicentre (β is 85^0) so equation (2.2) becomes:

$$\tau = \frac{d}{c_w}\sin\alpha_{inc} = \frac{d}{c_w}\sin\left(90+85-\theta\right) = \frac{d}{c_w}\sin\left(175-\theta\right) \tag{2.4}$$

The motion investigated, is the transverse motion with respect to the jetty. With a constant propagation direction of the earthquake, the transverse base motion is changing with a changing position of the structure. The transverse base motion (y-direction, perpendicular to the jetty) is therefore given by (see Figure 2-12) :

$$y_{base\_trans} = -y_{long}\cos\alpha_{inc} - y_{trans}\sin\alpha_{inc} \tag{2.5}$$

The longitudinal base motion is given by:

$$x_{base\_long} = -y_{long}\sin\alpha_{inc} + y_{trans}\cos\alpha_{inc} \tag{2.6}$$

With these assumptions, the time delay and the base vibration are both depending on α_{inc} which is depending on the position of the jetty (θ).

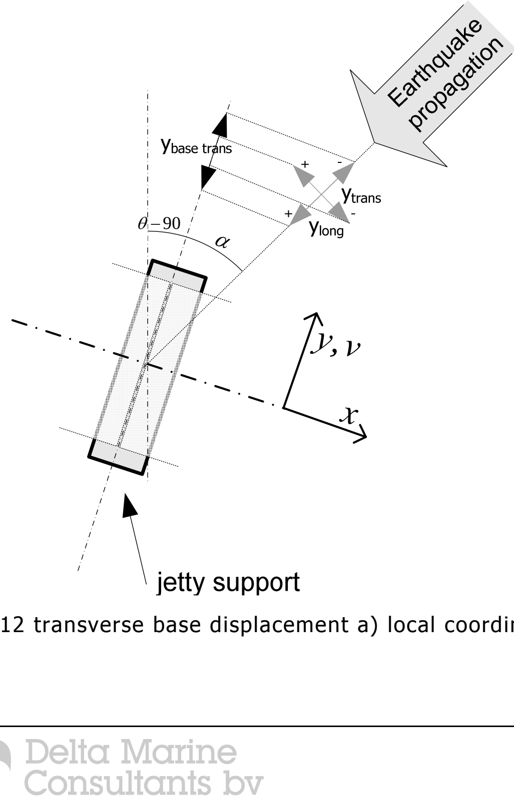

Figure 2-12 transverse base displacement a) local coordinates b) global coordinates

The base motion in transverse direction changes with a chancing α_{inc}. In the following figures is given the base motion for different α_{inc}.

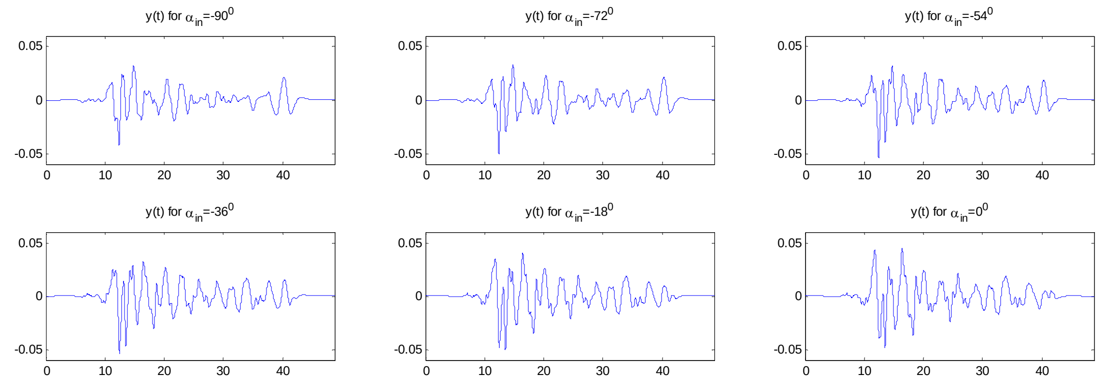

Figure 2-13 base motion [m] in transverse direction v for different α_{inc}

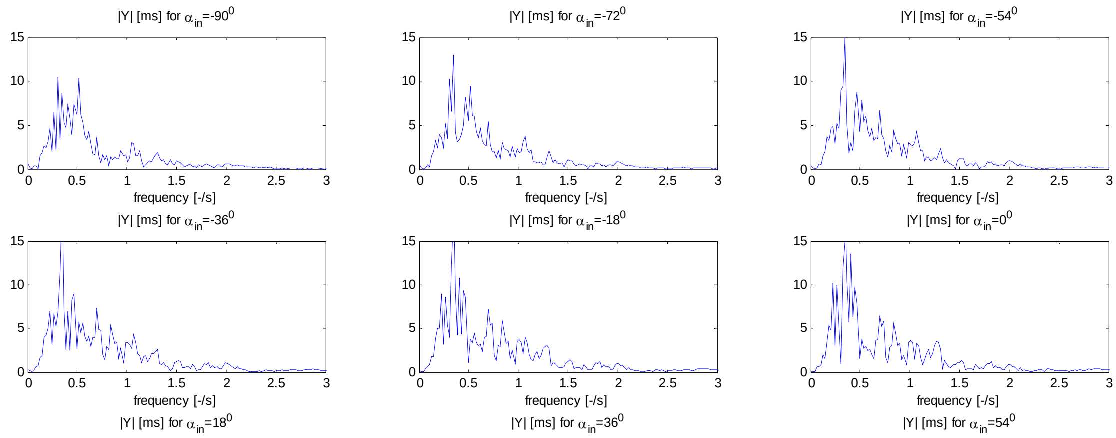

Figure 2-14 amplitude base motion (time domain) in transverse direction v for different α_{inc}

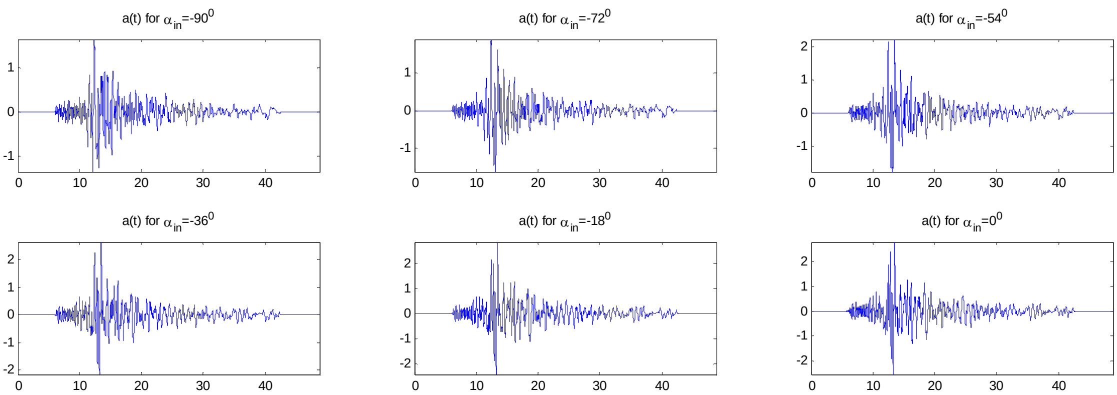

Figure 2-15 base acceleration [m/s^2] in transverse direction v for different α_{inc}

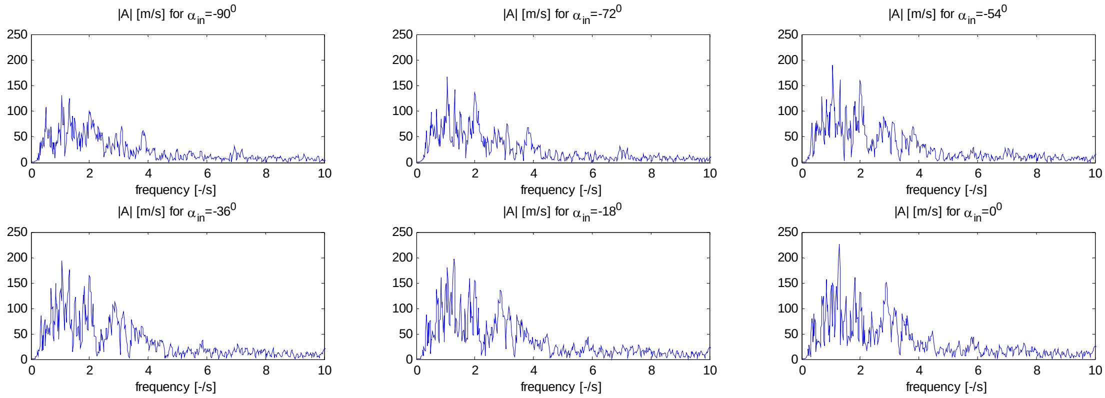

Figure 2-16 amplitude base acceleration (time domain) in transverse direction v for different α_{inc}

It can be concluded that the dominant frequencies of the displacement are between 0 and 1 hz and that the dominant acceleration frequencies are between 0 and 5 hz.

Chapter 3 Modelling

The jetty under investigation consists of continuous girders supported by piles. For the time being is chosen to model the jetty as a stand alone structure between its expansion joints (Maritime Navigation Commission Working Group 34, 2001). A survey of the jetty is given in Figure 3-1.

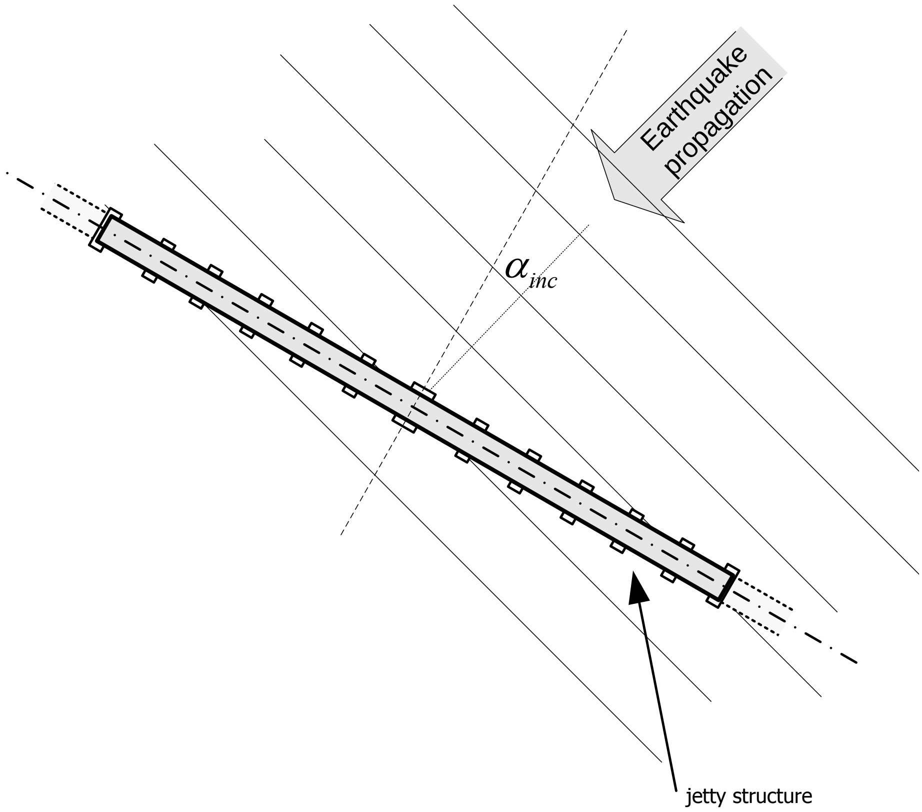

Figure 3-1 Jetty survey

This chapter discusses the possible modelling techniques. There are different modelling approaches available. These employ:

- Discrete systems (paragraph 3.1)
- Continuous systems (paragraph 3.2)

3.1 Discrete mass model

Discrete mass systems are systems where the mass is concentrated in certain nodes. Figure 3-2 shows an example of a SDOF model. In here, the mass is centred in the top of the structure. The pile resistance is modelled as a spring in horizontal direction. In this model only one degree of freedom is investigated.

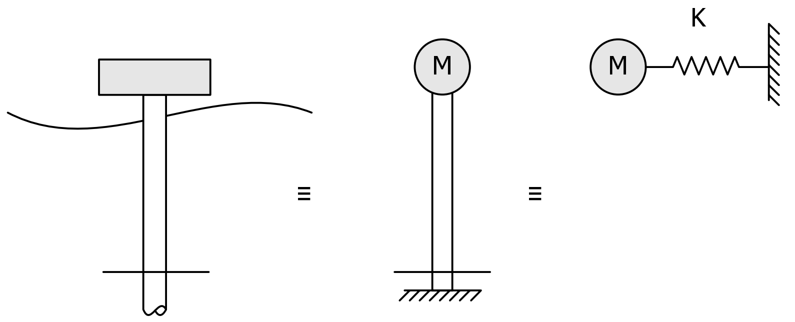

Figure 3-2 SDOF model setup

The equation of motion for a SDOF model is given by:

$$m\ddot{x} + c\dot{x} + kx = f(t) \tag{3.1}$$

where:

$m =$	lumped mass
$c =$	dashpot
$k =$	spring
$f(t) =$	force
$x =$	location
$\dot{x} =$	velocity
$\ddot{x} =$	acceleration

Discrete mass systems are also applicable with multiple concentrated masses. In Figure 3-3 is given a beam with 6 degree of freedom. The two ends of the beam represent the nodes of the beam where the mass is lumped. The stiffness matrix for a 6DOF beam is given in Appendix D. More than one degree of freedom structures are called multi degree of freedom (MDOF) structures.

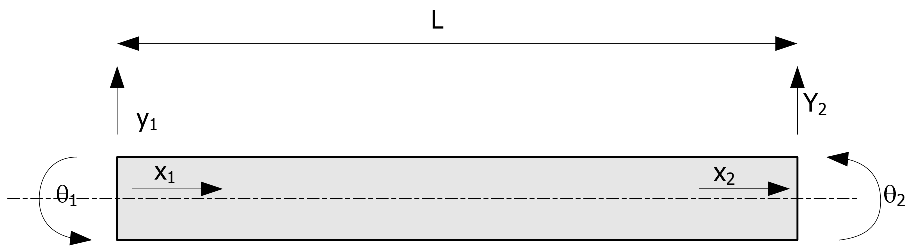

Figure 3-3 MDOF beam

The equation of motion for a MDOF model is given by:

$$\mathbf{M}\ddot{\mathbf{x}} + \mathbf{C}\dot{\mathbf{x}} + \mathbf{K}\mathbf{x} = \mathbf{f(t)} \tag{3.2}$$

where:

$\mathbf{M} =$	lumped mass matrix
$\mathbf{x} =$	location vector
$\dot{\mathbf{x}} =$	velocity vector
$\ddot{\mathbf{x}} =$	acceleration vector
$\mathbf{C} =$	dashpot matrix
$\mathbf{K} =$	spring matrix
$\mathbf{f(t)} =$	force vector

The determination of the stiffness, damping and mass matrix for beam is given in Appendix D. A combination of beams is given in Figure 3-4. Frame structures can be represented by multiple beams. A principle sketch and the accompanying stiffness matrix is given in Figure 3-4. Finite element software is based on this principle. More degrees of freedom, then the beam discussed, can be used.

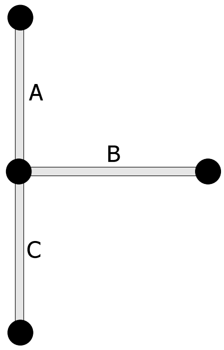

$$\mathbf{K_g} = \begin{bmatrix} \mathbf{A_{11}} & \mathbf{A_{12}} & \mathbf{0} & \mathbf{0} \\ \mathbf{A_{21}} & \mathbf{A_{22}} + \mathbf{B_{11}} + \mathbf{C_{11}} & \mathbf{B_{12}} & \mathbf{C_{12}} \\ \mathbf{0} & \mathbf{B_{21}} & \mathbf{B_{22}} & \mathbf{0} \\ \mathbf{0} & \mathbf{C_{21}} & \mathbf{0} & \mathbf{C_{22}} \end{bmatrix}$$

Figure 3-4 example structure off multiple beams (left), transformation partial beam stiffness to integral stiffness matrix

For more detail on lumped mass modelling is referred to Appendix D and Dynamics of structures (Clough and Penzien, 1993).

3.2 Continuous model (Euler – Bernoulli beam)

Another modelling approach is continuous modelling. This paragraph discusses the Euler – Bernoulli beam model, which is a continuous model. The opposite to discrete or lumped mass systems is that the mass isn't lumped into nodes. The mass is distributed over the length of the beam.

Considering an elastic beam, the displacement in the positive y-direction is indicated by the symbol $v(x,t)$, this represents the degree of freedom, which is a continuous function of the position x, and time t (Figure 3-5). The beam has a flexural stiffness EI [Nm^2], a cross- sectional area A[m^2] and a mass density ρ [kg/m^3].

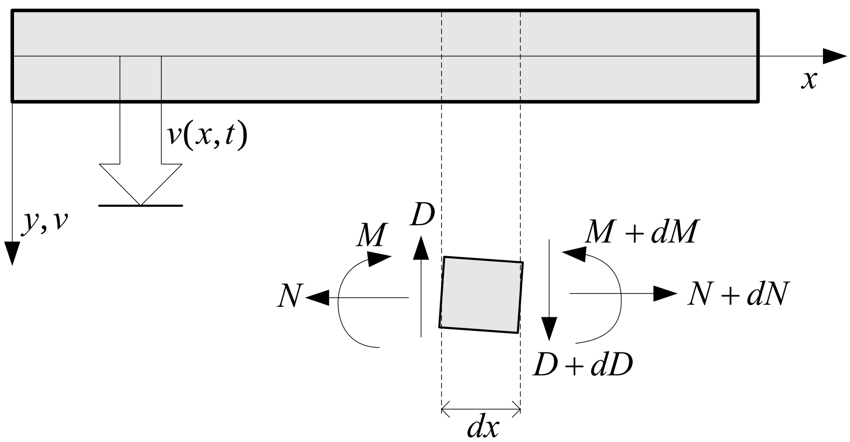

Figure 3-5 sign convention of the beam

In the following paragraphs, is derived for the Euler – Bernoulli beam, the:

- kinematic relation
- constitutive relation
- equation of motion

3.2.1 Kinematic relations

The kinematic relation represent the deformations to the degree of freedom $v(x,t)$.

$$\phi = -\frac{dv}{dx} \tag{3-3}$$

$$\kappa = \frac{d\phi}{dx} \tag{3-4}$$

$$\varepsilon(y) = y\kappa \tag{3-5}$$

The relationship (3-3) assumes that no shear force deformation occurs. The cross-section of the beam remains always perpendicular to the neutral line. The relationship (3-5) is a result of the assumption that plane cross- sections remain plane.

3.2.2 Constitutive relation

The behaviour of the material is formulated by Hooke's law. With this law, a statement is made about the relationship between the deformation quantity κ (the curvature) and the internal quantity M (bending moment). This relationship is called the constitutive relation.

$$\sigma(y) = \varepsilon(y)E \tag{3-6}$$

Equation (3-6) combined with (3-5) gives a linear stress function across the width of the beam:

$$\sigma(y) = y\kappa E \tag{3-7}$$

Consequently, the bending moment becomes:

$$M(x) = \int y\sigma(y)dA = \kappa E \int y^2 dA \rightarrow M = EI\kappa \tag{3-8}$$

3.2.3 Equation of motion

Newton's second law, which relates the acceleration to the internal forces and the external load, is given for the three directions by:

- x – direction

$$\sum F_x = ma_x \tag{3-9}$$

- phi – direction

$$\sum T_z = \rho I dx \frac{d^2\phi}{dt^2} \rightarrow dM - Ddx = \rho I dx \frac{d^2\phi}{dt^2} \tag{3-10}$$

The rotational inertia is posed as ρI=0, equation (3-10) is therefore reduced to a relation know in statics:

$$\frac{dM}{dx} = D \tag{3-11}$$

- z – direction

$$\sum F_y = ma_y \rightarrow dD = \rho A dx \frac{d^2 v}{dt^2} \tag{3-12}$$

Hence:

$$\frac{d^2 M}{dx^2} = \rho A \frac{d^2 v}{dt^2} \tag{3-13}$$

Combining (3-13) with (3-3), (3-4) and (3-8) gives the equation of motion for an Euler-Bernoulli beam:

$$\overbrace{EI\frac{\partial^4 v(x,t)}{\partial x^4}}^{\text{stiffness term}} + \overbrace{\rho A \frac{\partial^2 v(x,t)}{\partial t^2}}^{\text{inertia term}} = 0 \tag{3-14}$$

From (3-14) follows two more relations that are of great importance when bringing the boundary conditions into account:

$$M(x,t) = -EI\frac{d^2 v(x,t)}{dx^2} \quad \text{(bending moment)} \tag{3-15}$$

$$D(x,t) = -EI\frac{d^3 v(x,t)}{dx^3} \quad \text{(shear force)} \tag{3-16}$$

The deformation due to shear force and the influence of the rotational inertia has not been taken into account, which is justified for slender beams and low natural frequencies. The general solution of equation (3-14) is:

$$v(x,t) = Ve^{i(\omega t - \gamma x)} \tag{3-17}$$

where:

$$\gamma^4 = \frac{\rho A \omega^2}{EI}$$ wave number [rad/m]

The determination of the wave number is given in Appendix B.

3.3 Adopted structural model

The model chosen in this research is the continuous model (Euler – Bernoulli Beam paragraph 3.2). This model compared to a MDOF model has the following advantages:

- relative easy to generate transfer function
- returns exact solution

The transfer function is a frequency dependent function. E.g. the transfer function between the base displacement and the structural displacement is given by:

$$H_{v_n y}(x,\omega) = \frac{v_n(x,t)}{y(t)} = \frac{V_n(x,\omega)}{Y} \tag{3-18}$$

The transfer function shows the structural response as function of the frequency of the base motion. The resonance frequencies are shown as peaks. A change in parameters will give a change in transfer function. The influence of the parameters is readily seen by comparing different transfer functions,.
The resistance forces of the supports are modelled as discrete springs located at the supports. The jetty is modelled as multiple beams connected to each other (see Figure 3-6).

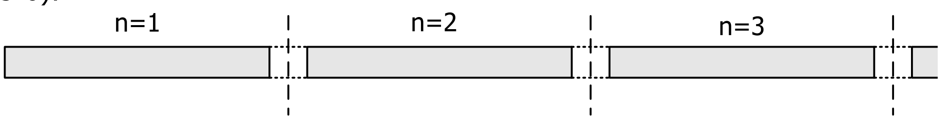

Figure 3-6 Multiple Euler – Bernoulli beams connected

At each support holds:

$$\sum F_{v,s} = m \cdot \frac{d^2 v}{dt^2} \quad \text{(forces equilibrium)} \tag{3.19}$$

$$\sum M_s = I_m \cdot \frac{d^2 \phi}{dt^2} \quad \text{(bending moment equilibrium)} \tag{3.20}$$

Because the beams have fixed connections holds additional the following connection conditions for each intermediate support.

$$v_{left} = v_{right} \tag{3.21}$$

$$v'_{left} = v'_{right} \tag{3.22}$$

The jetty model (top view) is given in Figure 3-7. The degree of freedom in this model is given by $v(x,t)$ which represents the displacement in transverse direction as function of x (location) and t (time). The different spans are connected to each other and the supports are modelled as discrete springs.

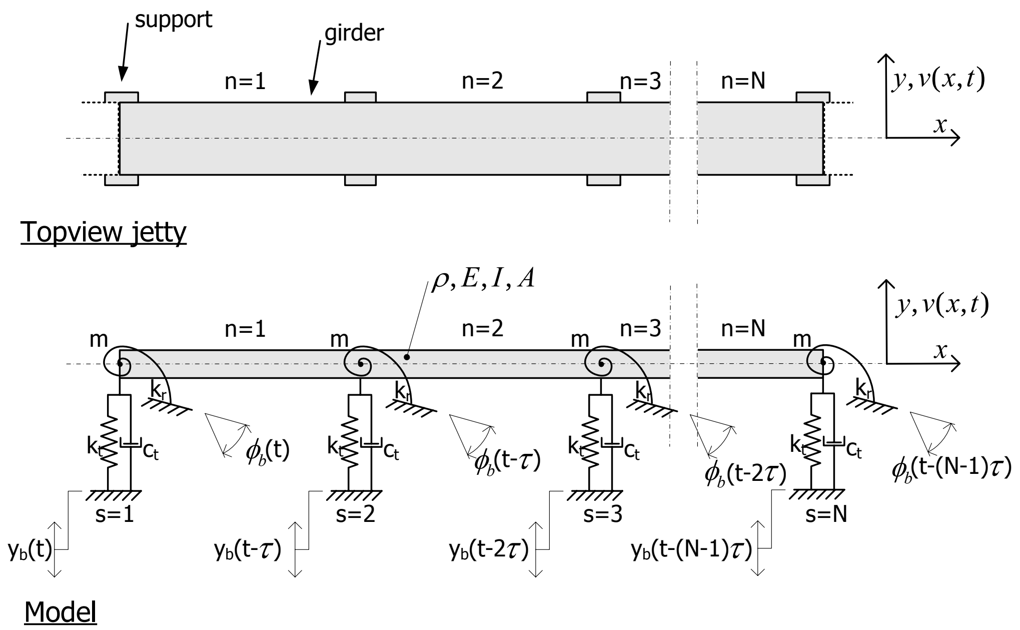

Figure 3-7 jetty model

The base excitation parameters are given by:

$y_b(t)$	displacement motion of the support base [m]
$\phi(t)$	rotation motion of the support base [-]
s	support number
τ	time delay in excitation between supports [s]

The structural parameters are given by:

k_t	support stiffness in transverse direction [N/m]
k_r	support stiffness in rotational direction [m^{-1}]
EI	bending stiffness of the jetty deck in transverse direction [Nm^2]
d	span length [m]
$N_{\sup}$	number of supports [-]
α	damping factor $\frac{c}{k}$ [-]
m	centred mass at supports

The supports are represented by springs in v- and rotational- direction (Figure 3-7). The value of the springs in transverse depends on the pile length. The spring stiffness is defined by:

$$k = \frac{dF}{dv} \tag{3-23}$$

For the case at Melaka, is given the values for transverse stiffness κ in Figure 3-8-a. The supports consist of two 610x16mm^2 piles and a concrete cap of 800 x 1200 mm^2. The strong point exists of four 610x16mm^2 piles and a concrete cap of 800 x 3000 mm^2. See Figure 3-8-b/c/d for a cross-section/ top view of the supports.

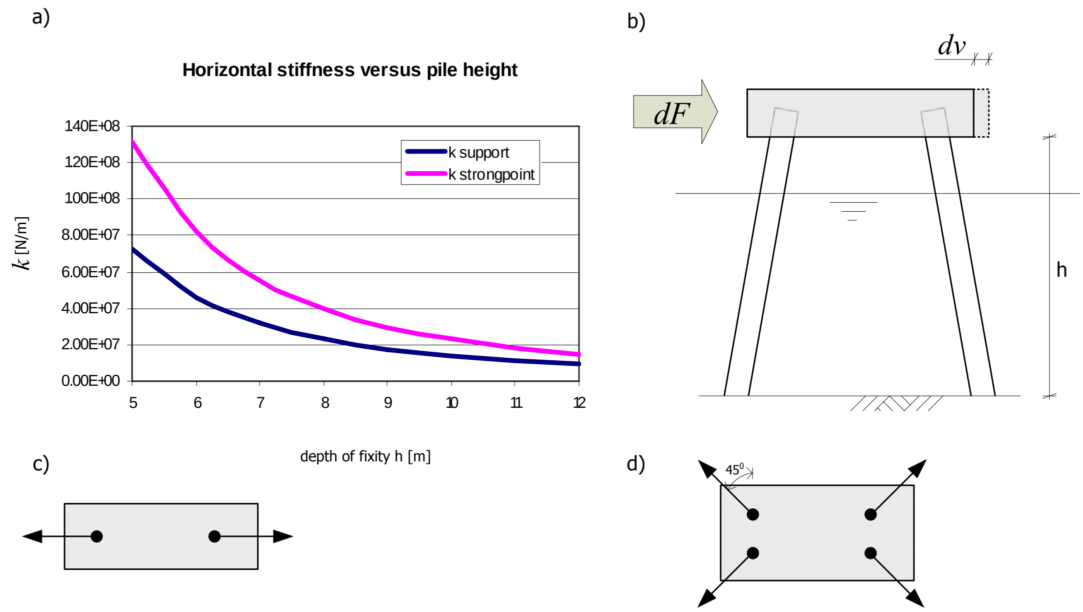

Figure 3-8 a) horizontal resistance as function of the fixity depth b) cross-section support c) normal support, top view d) strong point support top view

The stiffness is increased averagely by 75% at the strongpoint (see Figure 3-8-a). The stiffness of the statically undetermined support structure can be calculated by solving a system of equations or with finite element software (see Appendix I). A top view of the supports is given in Figure 3-8-c/d. The arrows represent the direction of the pile inclination. The piles are constructed with an inclination of 1:4.

3.4 Damping

Damping is a measure of energy dissipation in a vibrating system. This paragraph discusses the modelling of damping. The following table shows the sources of energy dissipation in earthquakes.

- structural damping
    - material damping
    - mechanical damping
    - inelastic behaviour
- hydrodynamic damping
    - radiation damping
    - fluid damping
- soil damping
    - radiation damping
    - material damping

Linear damping is a damping force that is proportional to velocity. Damping causes energy loss in the form of yielding and/ or heating. In reality damping isn't linear but damping is often linearized to make the calculations easier.

3.4.1 Linear Damping

Viscous damping is a convenient way to represent damping (Clough and Penzien, 1993). In the equation of motion is this represented by the symbol C.

$$M\ddot{x} + C\dot{x} + Kx = f(t) \tag{3.24}$$

Viscous damping isn't necessarily the best model for damping in real structures and soils. For a harmonic motion $x = \hat{x} \cdot \sin \omega t$, the spring and the damping forces are respectively:

$$F_k = k\hat{x} \sin \omega t \tag{3.25}$$

$$F_d = c\hat{x}\omega \cos \omega t \tag{3.26}$$

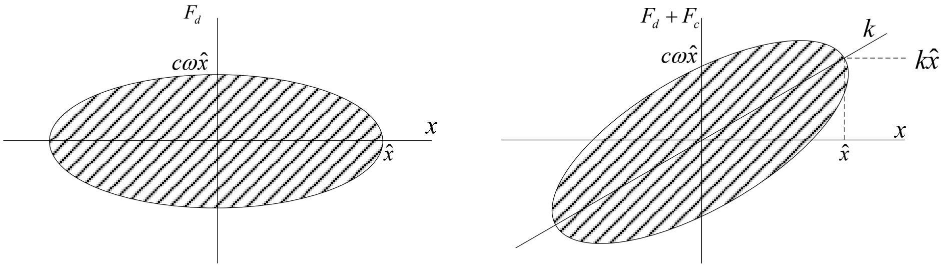

Figure 3-9 development of forces in spring and damper

Where the amplitude of motion $\hat{x}$ is a function of the excitation frequency which is given by(Spijkers et al., 2005):

$$\hat{x} = \frac{\hat{F}}{k} \frac{1}{\sqrt{\left(1 - \frac{\omega^2}{\omega_0^2}\right) + \left(2\zeta \frac{\omega^2}{\omega_0^2}\right)^2}} \tag{3.27}$$

The dissipated energy (hatched area Figure 3-9) can be calculated by:

$$E_{diss} = \int_0^T F dx = \int_0^T F\dot{x} dt = c\pi\omega\hat{x}^2 \tag{3.28}$$

3.4.2 Damping percentage

In practice it is difficult to determine the damping coefficient. Therefore it is common to take a percentage ξ of the critical damping.

$$c = \xi c_{cr} \tag{3.29}$$

where:

$c_{cr} = 2\sqrt{km}$ (critical damping)

The damping percentages are known from field studies. Typical damping ratios for seismic analysis are given in table 3-1. The values for earthquakes are higher than other types of dynamic excitation. This is because damping is in general strain dependent and strain levels will be greater than for other load types. The damping values given here are mainly taken from full scale testes of existing structures and represent average structures, foundations and soil conditions. The critical damping factor ξ is often used to insert damping into the equation of motion. This method, to include damping, can be extended readily to a MDOF system. The application of damping in a MDOF- system is given in appendix D.4 .

	damping (% of critical)		
	Elastic behaviour		Inelastic behaviour
	Stresses well below yield	Stresses at or near yield	
Structural damping	0.5	1	2
Hydrodynamic damping	0.5	1	1+
soil damping	1	>2	>5
Recommended total	2	4	10

table 3-1 recommended damping ratios for seismic analysis (Barltrop et al., 1991)

3.5 Adopted damping model

The damping is modelled by viscous dampers (linear damping) near the supports. The damping parameter is defined by:

$$c = \alpha k \tag{3-30}$$

where:

$c =$ damping parameter [Ns/m

$\alpha =$ damping coefficient [s]
$k =$ stiffness parameter [N/m]

A schematisation of the damping is given in Figure 3-10.

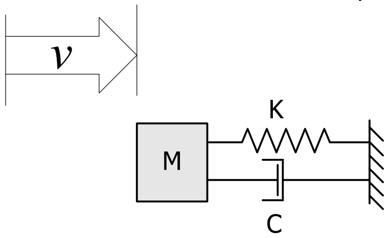

Figure 3-10 Schematisation of stiffness and damping

A damping percentage ξ of 0.05 is taken initially. So,

$$c = \alpha k = \xi c_{cr} = \xi 2\sqrt{km} \tag{3-31}$$

Thus:

$$\alpha \approx \frac{\xi c_{cr}}{k} = \xi 2\sqrt{\frac{m_{total}}{k_{total}}} = 0.0669s \tag{3-32}$$

With the equation (3.24) is assumed that damping is viscous. With equation (3-30) is assumed that the damping coefficient is a percentage of the stiffness coefficient. For a discrete model element, the equation of motion is given by:

$$m\ddot{v} + c\dot{v} + kv = 0 \tag{3-33}$$

substitution of the general solution (3-17) into (3-33) gives the following relation:

$$\omega^2 m - i\omega c + k = 0 \tag{3-34}$$

substitution of (3-30) into (3-34) gives:

$$\omega^2 m - i\omega\alpha k + k = \omega^2 m + (1 - i\omega\alpha)k \tag{3-35}$$

The damping coefficient is assumed to be proportional to the stiffness coefficient and is represented by the complex part in the stiffness parameter ($-i\omega\alpha k$).
The damping is applied discrete at the location of the supports. In this model there is no damping within the beam. In Figure 3-9 is given the resistance force, due to the stiffness and damping, as function of the relative displacement.

3.6 Transfer function

The solution of the model (paragraph 3.3) is given in Appendix B. The first natural frequencies are given by:

1. 2.41 Hz
2. 2.50 Hz
3. 2.93 Hz
4. 4.40 Hz

The mode shapes corresponding these natural frequencies are given in Figure 3-11.

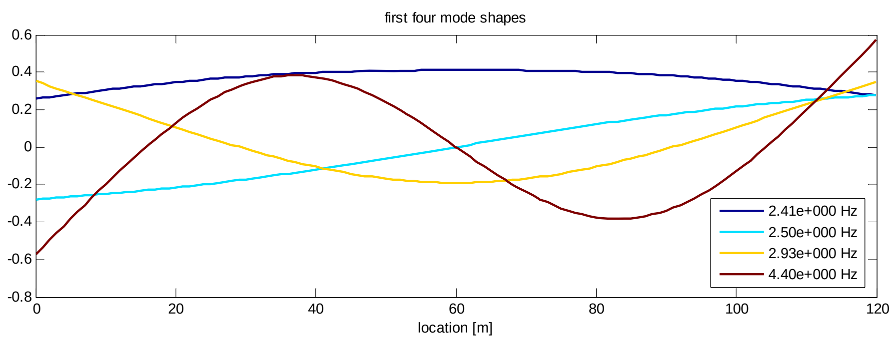

Figure 3-11 Mode shapes corresponding to the first four natural frequencies

Equation (B-8) gives the solution of the displacement. In here the displacement is given as function of x and t. Writing ω as a variable, equation (B-8) can be written as:

$$v(x,\omega,t) = \exp(i\omega t)\cdot V_n(x,\omega) \tag{3-36}$$

The variable t, occurs only in the first factor of the equation, $\exp(i\omega t)$. The second part of the general solution (3-36) doesn't inherit the variable t. The first factor $\exp(i\omega t)$ has an amplitude of "one" and is there fore only responsible for the rotation of the complex number into the complex plane (change of complex angle, see Figure 3-12). The second factor in equation (3-37) represents the solution of the displacement in the frequency domain. This factor is complex and is given by:

$$\begin{aligned}V_n(x,\omega) &= \hat{A}_{n.1}\exp(-i\gamma_{n.1}x) + \hat{A}_{n.2}\exp(-i\gamma_{n.2}x) + \\ &\hat{A}_{n.3}\exp(-i\gamma_{n.3}x) + \hat{A}_{n.4}\exp(-i\gamma_{n.4}x)\end{aligned} \tag{3-37}$$

The maximum value of the solution is given by $\operatorname{Re}\left(v(x,t)\right)\big|_{\max}$

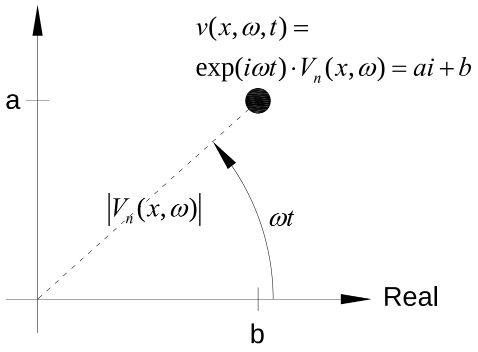

Figure 3-12 general solution in complex plane

In Figure 3-12 is seen that $\operatorname{Re}\left(v(x,t)\right)\big|_{\max}$ is given by $|V(x,\omega)|$. So,

$$\begin{aligned}&\operatorname{Re}\left(v(x,t)\right)\big|_{\max} = v(x,t)\big|_{\max} = |V_n(x,\omega)| = \\ &\left|\hat{A}_{n.1}\exp(-i\gamma_{n.1}x) + \hat{A}_{n.2}\exp(-i\gamma_{n.2}x) + \hat{A}_{n.3}\exp(-i\gamma_{n.3}x) + \hat{A}_{n.4}\exp(-i\gamma_{n.4}x)\right|\end{aligned} \tag{3-38}$$

When the excitation amplitude is assumed to be 1 and the phase shift to be 0 does equation (3-38) represent the transfer function between the base excitation and the structural motion. This response function is given by:

$$H_{v_n y_b}(x,\omega) = \frac{v_n(x,t)}{y_b(t)} = \frac{V_n(x,\omega)}{Y_b} = \frac{V_n(x,\omega)}{1} = V_n(x,\omega) \tag{3-39}$$

The frequency response function for the structural bending moment is calculated in a similar manner. Since the bending moment in the beam is represented by:

$$M(x,t) = -EIv_n''(x,t) \tag{3-40}$$

the bending moment response on the base displacement is given by:

$$H_{My_b}(x,\omega) = \frac{-EIv_n''(x,t)}{y_b(t)} = \frac{-EIV_n''(x,\omega)}{Y_b} = \frac{-EIV_n''(x,\omega)}{1} = -EIV_n''(x,\omega) \tag{3-41}$$

As well the shear force, which is given by:

$$D(x,t) = -EIv_n'''(x,t) \tag{3-42}$$

The corresponding shear force – base displacement transfer function is given by:

$$H_{My_b}(x,\omega) = \frac{-EIv_n'''(x,t)}{y_b(t)} = \frac{-EIV_n'''(x,\omega)}{Y_b} = \frac{-EIV_n'''(x,\omega)}{1} = -EIV_n'''(x,\omega) \tag{3-43}$$

The transfer functions for the case discussed in paragraph 1.2 are given in Figure 3-14 to Figure 3-18. These figures contain the plots of respectively: $|H_{v_n y}(x,\omega)|$, $|H_{M\ddot{y}_b}(x,\omega)|$ and $|H_{D\ddot{y}_b}(x,\omega)|$ at x = 30, 60 and 80m. Their location is arbitrary chosen and given in Figure 3-13.

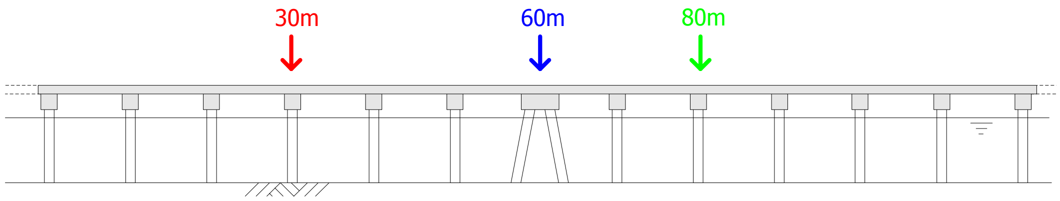

Figure 3-13 Location of the transfer functions

The dominated earthquake/ structural response frequencies are smaller than 5 hz. Therefore the transfer functions are given for the frequencies below 5 hz. Figure 3-14 gives the structural motion base displacement transfer functions.

For the bending moment and shear forces is the base displacement transfer function quadratic proportional to the frequency. The bending moment – base displacement transfer function is given by equation (3-41). The response function seems to be almost quadratic proportional for low frequencies between 0.01 and 2 Hz. Since the base acceleration is given by:

$$\ddot{y}_b(t)=\frac{d^2y_b(t)}{dt^2}=\frac{d^2Y_b\exp(i\omega t)}{dt^2}=\ddot{Y}_b\exp(i\omega t)=-\omega^2Y_b\exp(i\omega t) \qquad (3\text{-}44)$$

holds:

$$\ddot{Y}_b=-\omega^2Y_b \qquad (3\text{-}45)$$

So analogously to (3-41), the transfer function between structural bending moment – base acceleration is given by:

$$H_{M\ddot{y}_b}(x,\omega)=\frac{-EIv_n''(x,t)}{\ddot{y}_b(t)}=\frac{-EIV_n''(x,\omega)}{-\omega^2Y_b}=\frac{EI}{\omega^2}V_n''(x,\omega)=\frac{H_{My_b}(x,\omega)}{-\omega^2} \qquad (3\text{-}46)$$

Where H_{My_b} is nearly quadratic proportional to the frequency, is $H_{M\ddot{y}_b}$ nearly constant for low frequencies (see Figure 3-16). For the low frequencies (smaller than 2 hz), the structural response on the base motion, appears to be constant. The first to fourth natural frequencies 2.41, 2.50, 2.93 and 4.40 Hz are becoming clear in Figure 3-14 and Figure 3-15.

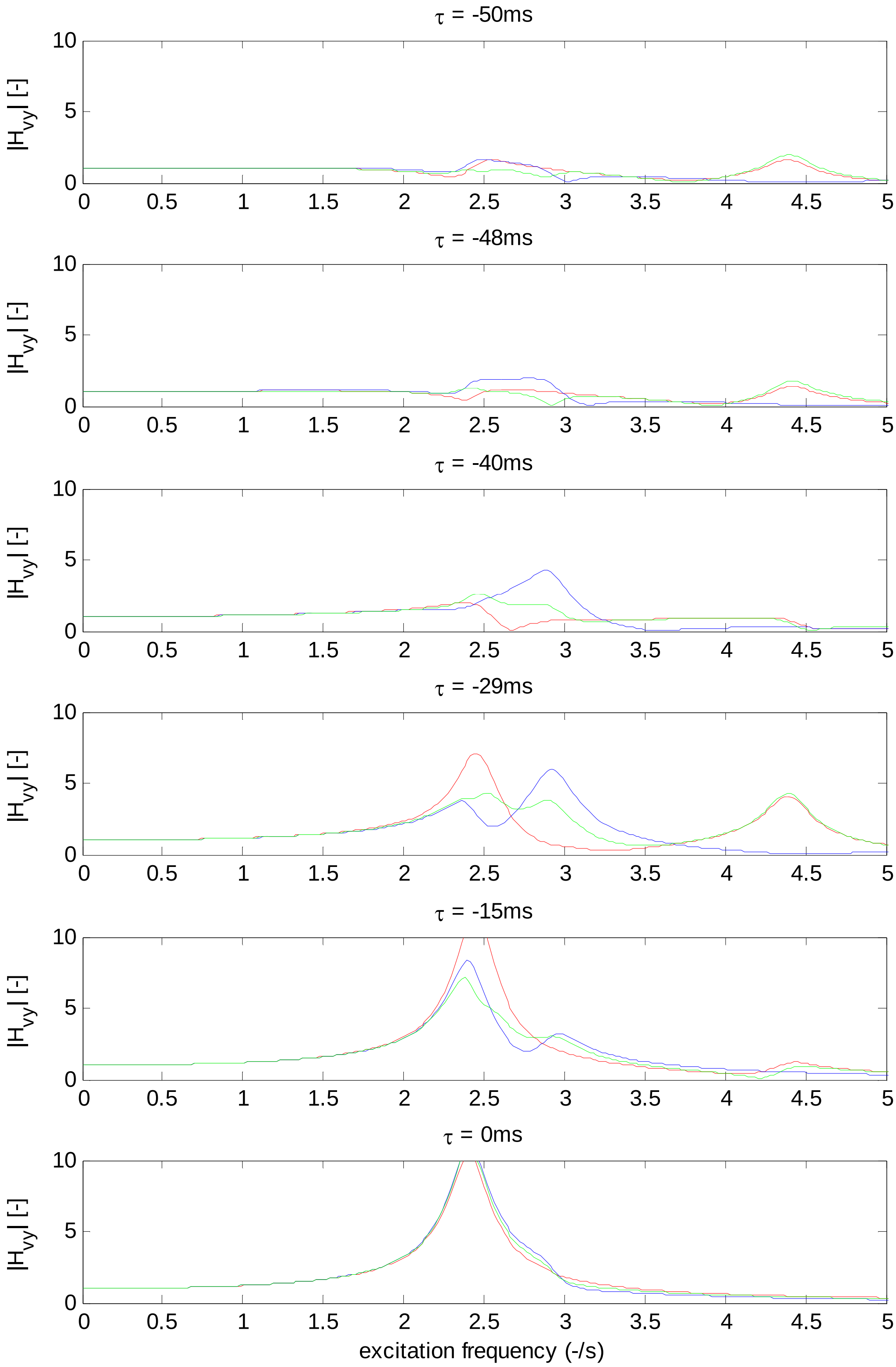

Figure 3-14 structural displacement - base displacement transfer function at 30, 60 and 80m for different values of tau.

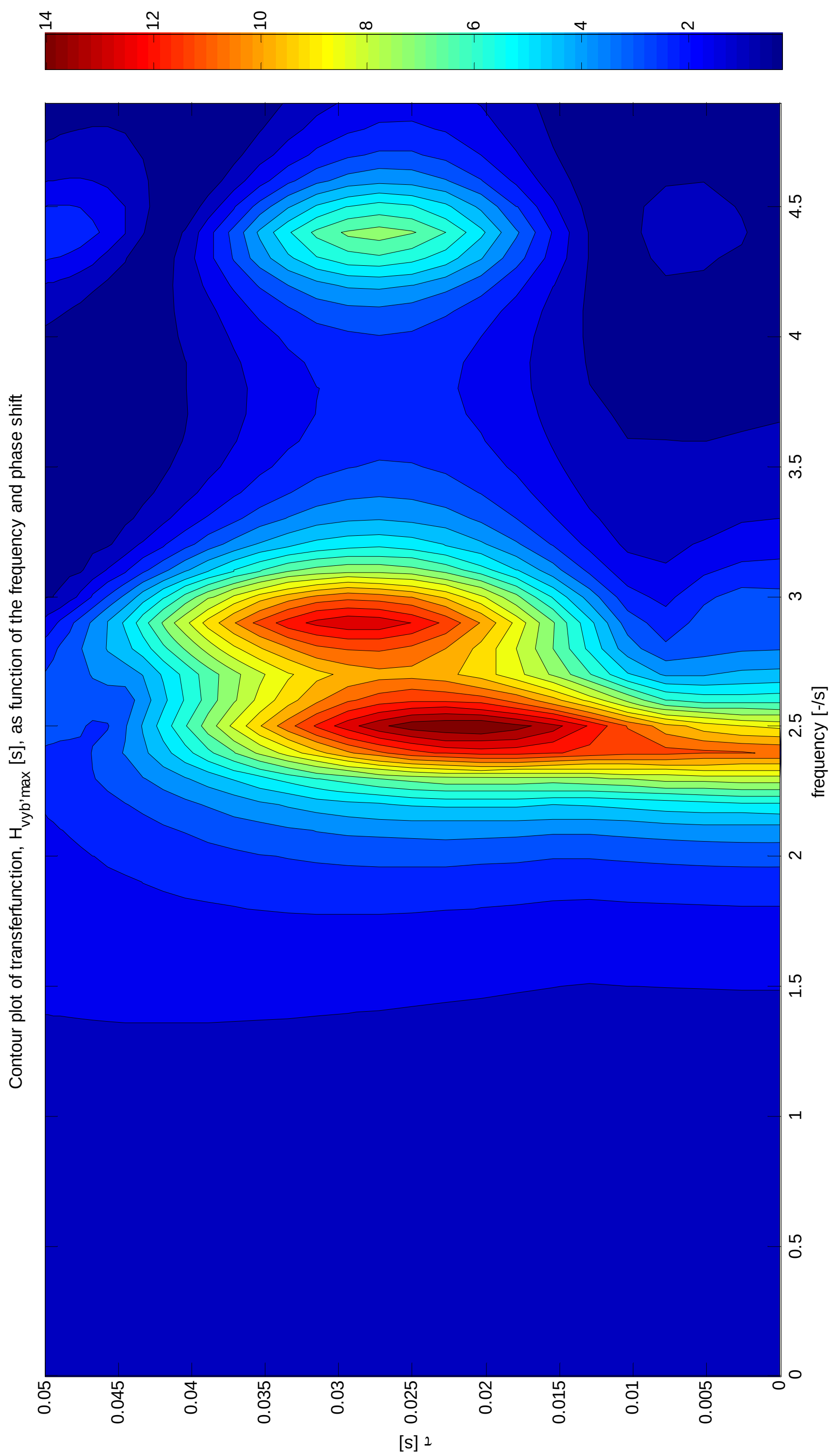

Figure 3-15 Envelope base displacement structural displacement transfer function

The bending moment response increases with an increasing τ for frequencies smaller than 2 hz. The transfer function shows a nearly constant amplitude between 0.01 hz and 2 hz (Figure 3-16). The envelope transfer function is for the total length of the beam is given in Figure 3-17.

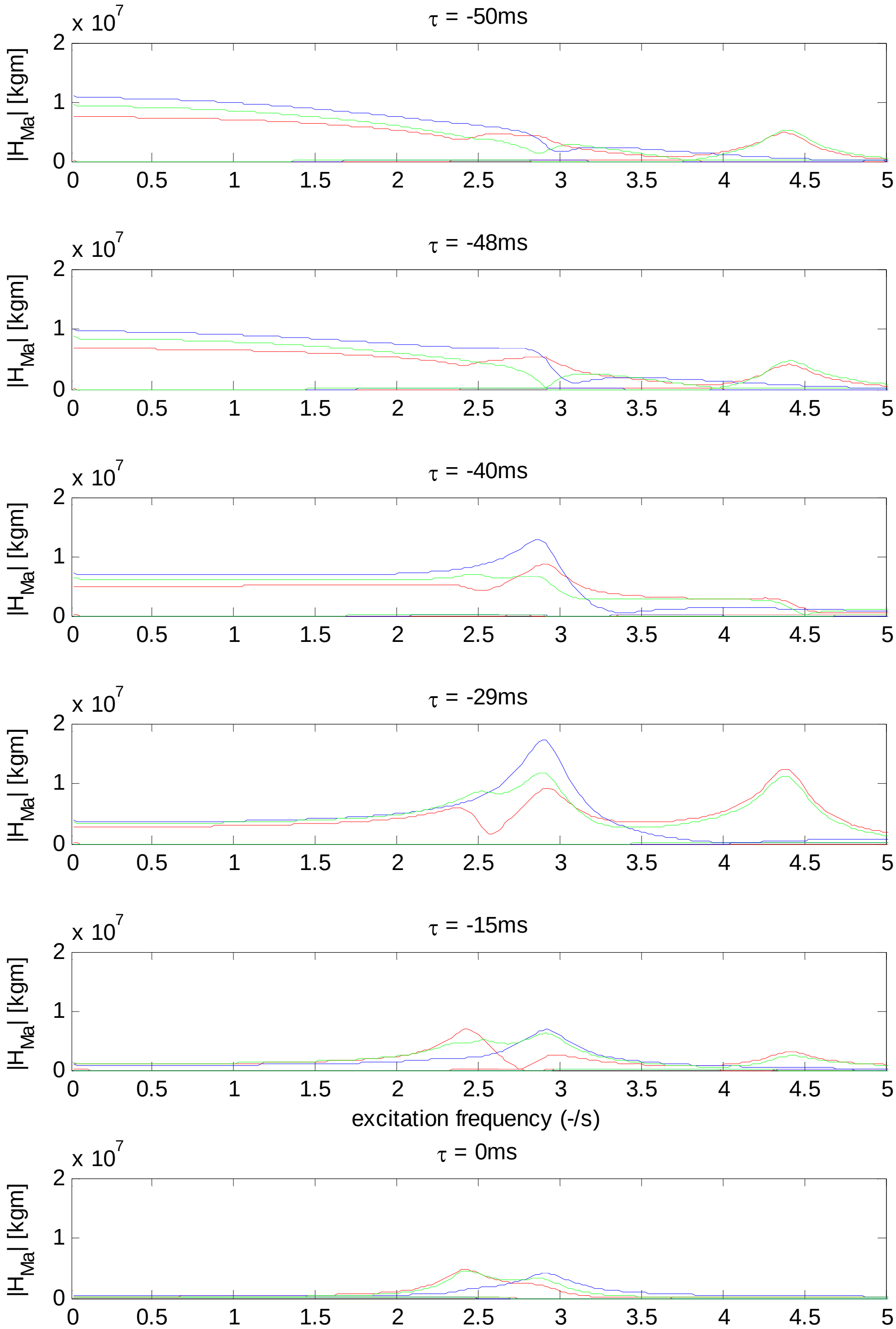

Figure 3-16 Bending moment - structural acceleration transfer function, left column: amplitude, right column: phase shift

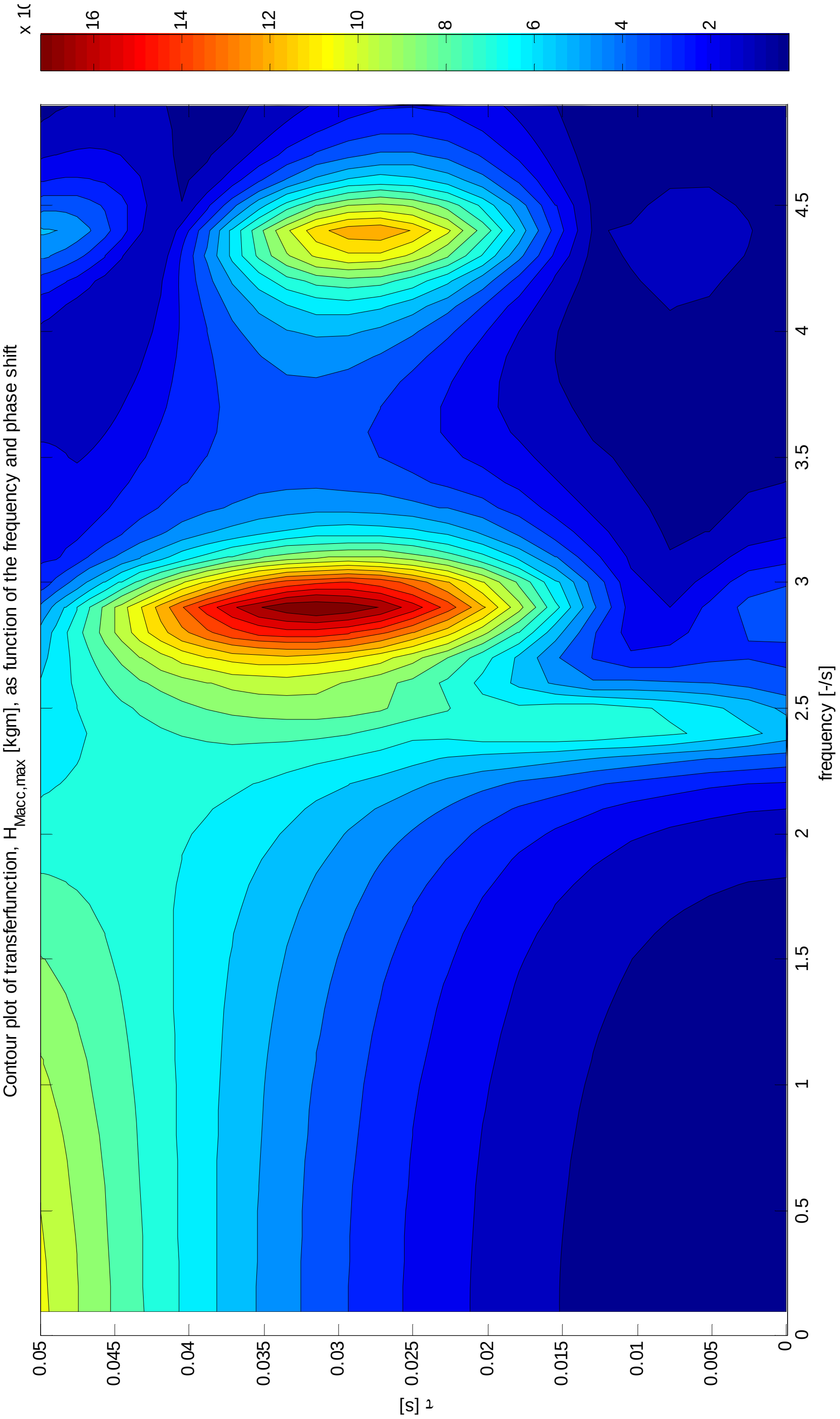

Figure 3-17 Envelope bending moment structural acceleration transfer function

H_{Dy_b} also appears to be nearly quadratic proportional between 0.25 and 2 Hz. $H_{D\ddot{y}_b}$ is given by:

$$H_{D\ddot{y}}(x,\omega) = \frac{-EIv_n'''(x,t)}{a(t)} = \frac{-EIV_n'''(x,\omega)}{-\omega^2 Y} = \frac{EI}{\omega^2} V_n'''(x,\omega) = \frac{H_{Dy}(x,\omega)}{-\omega^2} \tag{3-47}$$

$H_{D\ddot{y}_b}$ is given in Figure 3-18. Figure 3-16 shows the transfer function envelope for the total length of the structure.

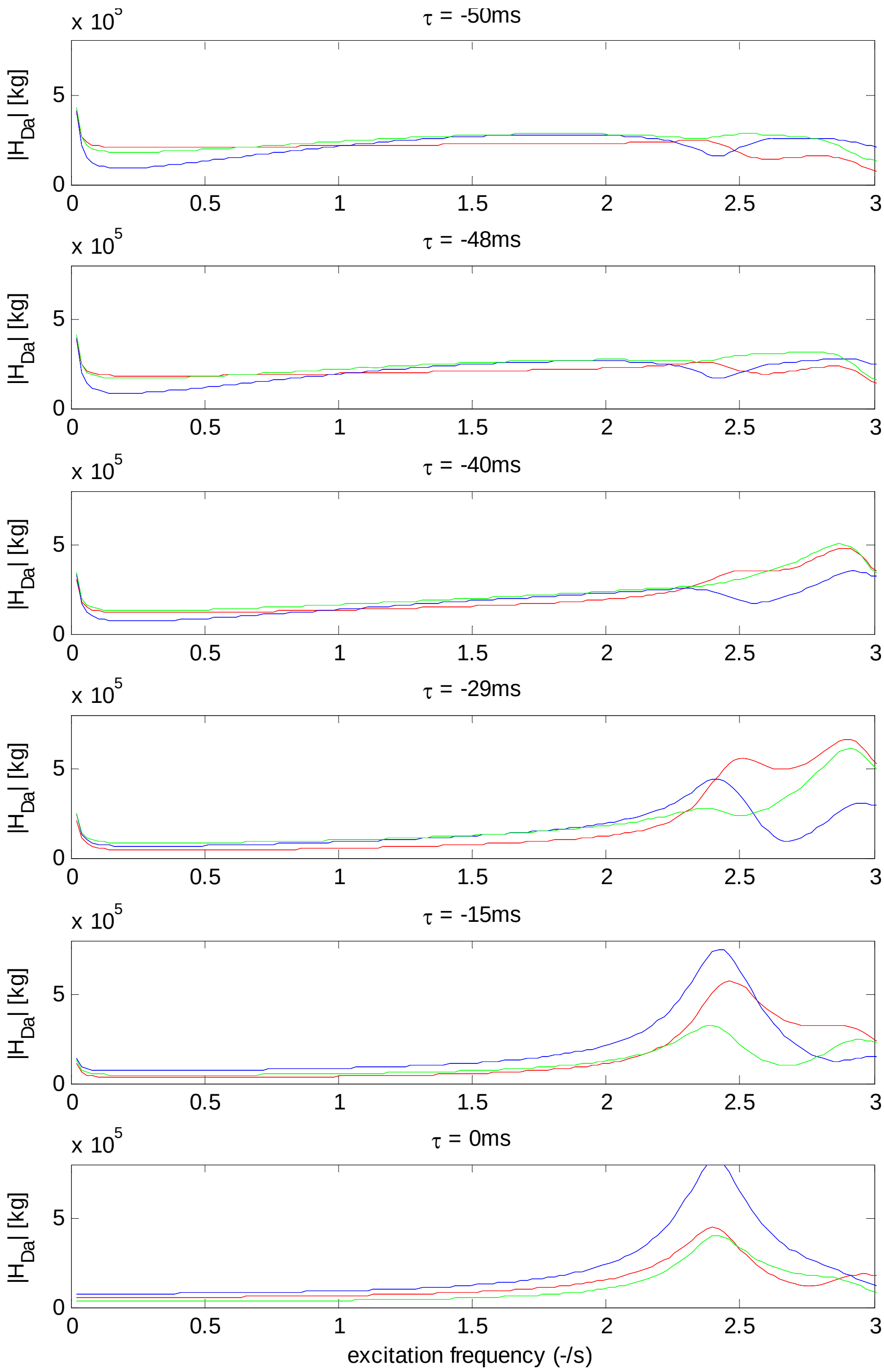

Figure 3-18 shear force - base acceleration transfer function

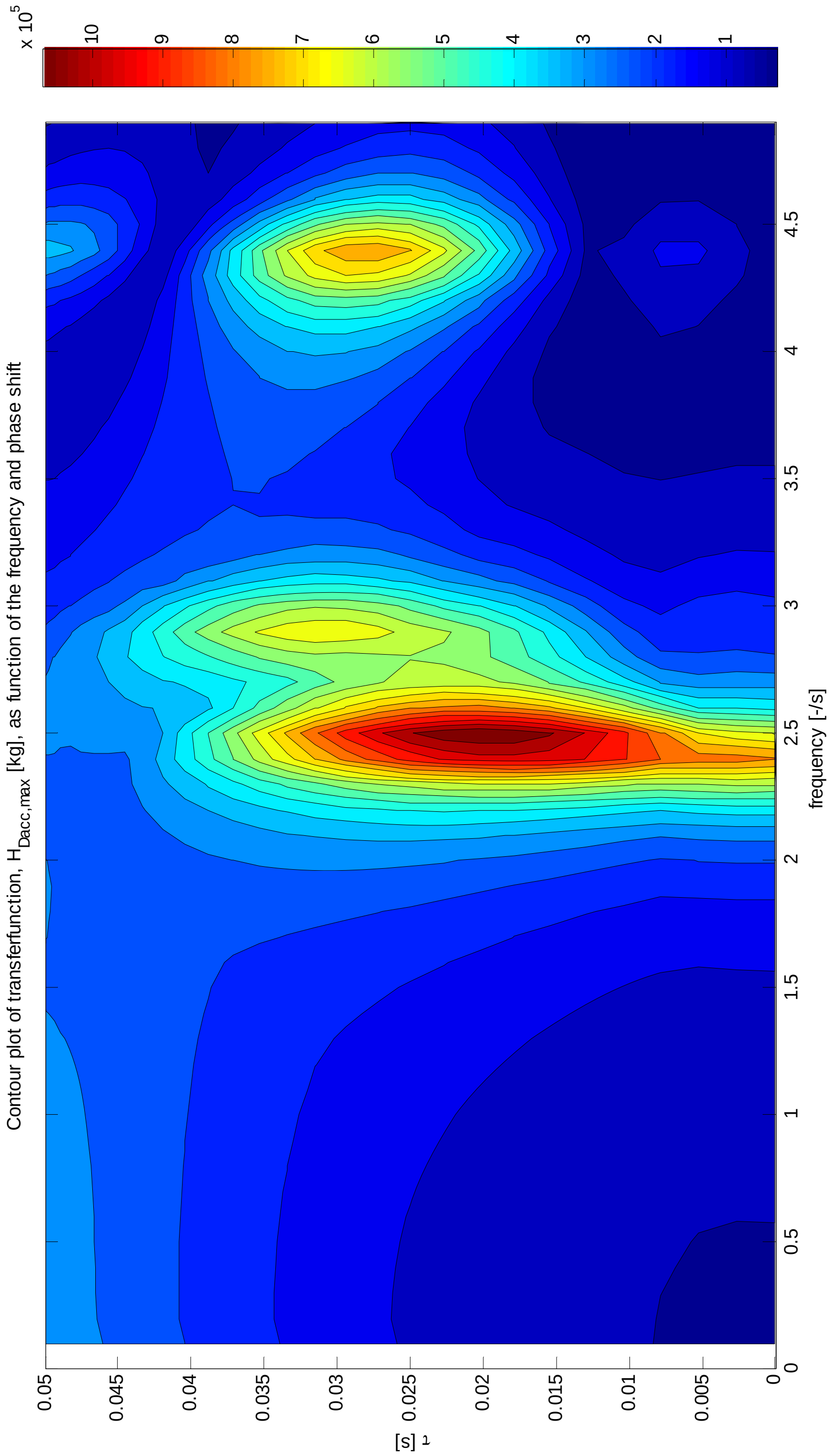

Figure 3-19 Envelope shear force structural acceleration transfer function

From the contour plots in Figure 3-15 Figure 3-17 and Figure 3-19 is becoming clear that for particular values of tau the transfer functions peak. This amplification due to uneven excitation is explained in the following paragraph.

3.7 Uneven excitation amplification

The occurring mode shapes (Figure 3-11 and Figure 3-22) are depending on the frequency of the loading.

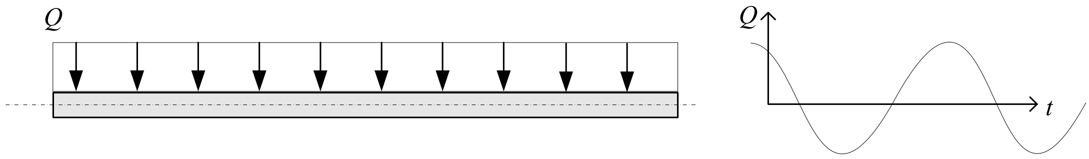

Figure 3-20 Distributed harmonic load

In the previous chapter is discussed the amplification of the structural vibration near the resonance frequencies. Figure 3-22 shows the first four natural modes for the corresponding first four natural frequencies. Extra amplification/ resonance will occur when the harmonic load is distributed in the same way as the corresponding mode shape. E.g. consider the 3rd mode shape. This mode shape will occur when the excitation frequency reaches approximately 2.93 Hz. When the load has the same distribution as the mode shape (Figure 3-21) an extra amplification of the structural motion will occur.

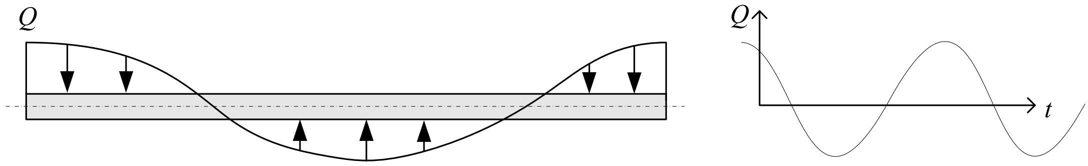

Figure 3-21 Harmonic load (Distributed according to the 3rd mode shape)

In the applied model, the excitation load on the beam is not a distributed load but a discrete force near the supports induced by the relative displacement (approximately) multiplied by the spring stiffness. The uneven excitation amplification occurs when the base displacement corresponds to the mode shape.

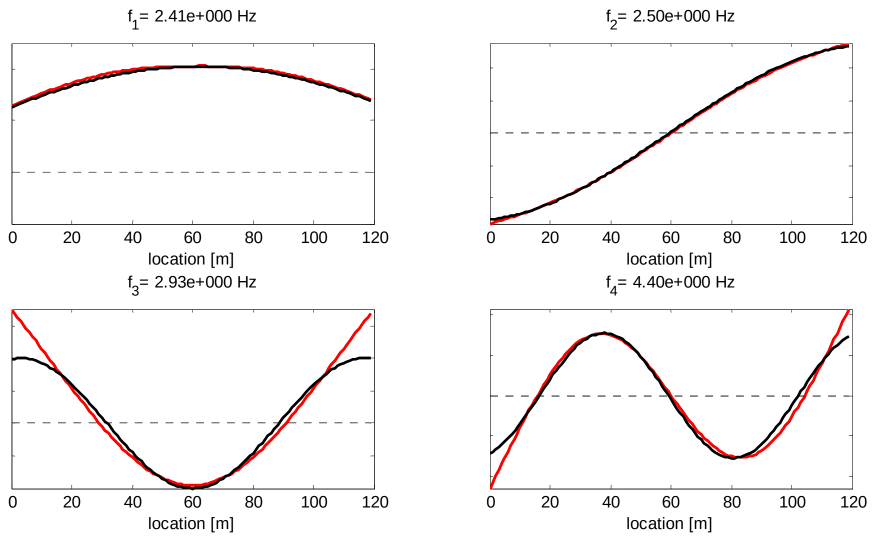

Figure 3-22 First mode shapes (red line) with equivalent "harmonic" shapes (black line)

The base motion investigated is a harmonic motion given by:

$$y_b(t-(N-1)\tau) = Y_b \exp(i\omega(t-(N-1)\tau)) \qquad (3\text{-}48)$$

For each mode shape is determined the time delay τ in such a way that the base displacement corresponds to the natural mode. The wave number (k) of the equivalent harmonic wave are given in table 3-2. The corresponding time delay (τ) in excitation is calculated by:

$$\tau = \frac{k}{f}\cdot d = \frac{k}{f}\cdot 10 \ \text{[s]} \qquad (3\text{-}49)$$

	f [-/s]	k [-/m]	tau [s]
1	2.413	2.33e-3	9.67e-3
2	2.496	3.74e-3	1.50e-2
3	2.925	8.77e-3	3.00e-2
4	4.400	1.17e-2	2.65e-2

table 3-2 frequency, wavenumber and time delay corresponding the first four natural modes.

Figure 3-23 shows the contour plot of the envelope maximum bending moment – base acceleration transfer function amplitude for the total jetty. The phase shift (tau) corresponding the natural frequencies are given by (●) in the contour plot.

The transfer function shows an increase in structural response when the following holds:

- excitation frequency reaches the natural frequency
- load corresponds to the natural mode

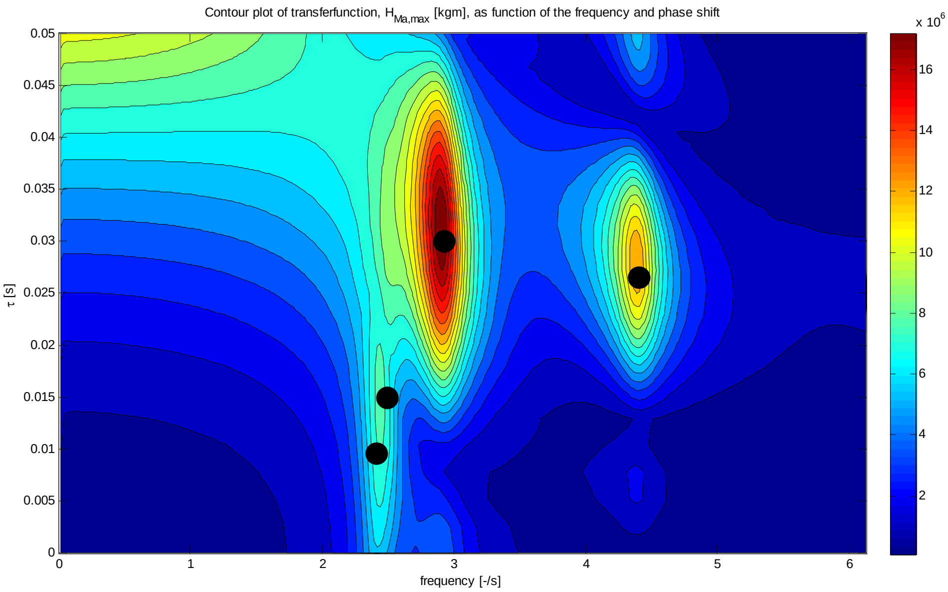

Figure 3-23 Bending moment – base acceleration transfer function maximum for the total jetty length as function of the frequency and phase shift

The maximum bending moments (Figure 4-15) occur at α_{inc} = -36^0. The time delay of excitation between the supports for α_{inc} = -36^0 is given by:

$$\tau = \frac{d}{c}\sin\alpha_{inc} = 0.0294s \text{ [s]} \qquad (3\text{-}50)$$

As seen in Figure 3-23 peaks the bending moment – base acceleration response around 3 Hz at 0.0294s. Figure 3-24 shows the amplification of between the bending moment – base acceleration transfer function at α_{inc} = -36^0 (τ = 0.029s) and α_{inc} = 0^0 (τ = 0s). The figure shows an average amplification of 10 where the amplification at 3 hz contributes most according to Figure 3-23.

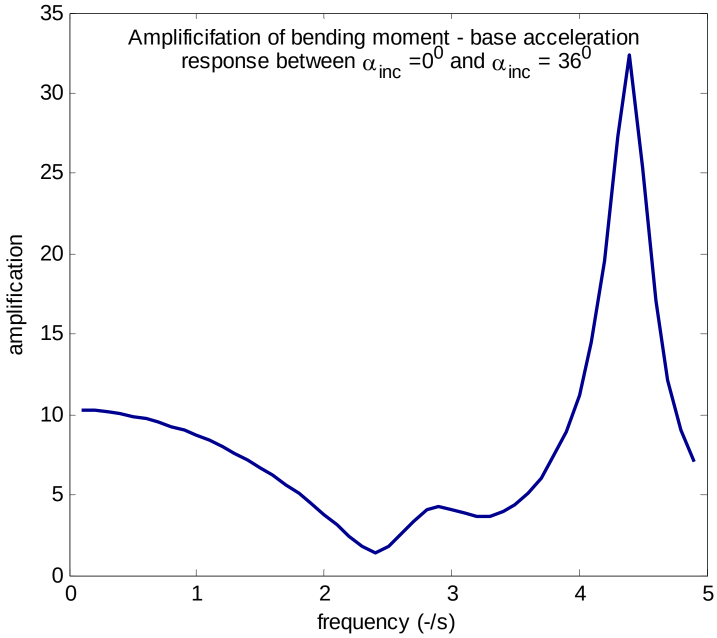

Figure 3-24 amplification of the bending moment response amplitude.

The transfer function is quadratic proportional to the time delay for the excitation frequencies between 0.01 and 2 hz is. Within this range a time delay of excitation causes an amplification of the maximum bending moments. In Appendix J is given the transfer function for variable number of supports N:

- N=3
- N=5
- N=7
- N=9
- N=11
- N=13
- N=15
- N=17

These plots show that for the structures with different lengths uneven excitation has influence on the bending moment in the structure. When the number of supports N is increased:

- The 3rd and 4th natural frequencies become lower. So these natural frequencies are moving towards the area of the earthquake excitation (0 – 5 Hz).
- The bending moment – base acceleration response increases for increasing τ at low frequencies (0 – 1.5 Hz).

Chapter 4 Response

This chapter is about the structural response. First is discussed the modelling models for earthquakes. In paragraph 4.2 is calculated the structural response on the Alkion earthquake for different angles of incidence (α_{inc}). Paragraphs 4.3 to 4.5 are about the results of the structural response.

4.1 Earthquake models

This paragraph is about the modelling of the earthquake. The analysis method for earthquakes is the response spectrum analysis or the time analysis. Appendix E is about the modal response spectrum and this paragraph about the time analysis. The modal response spectrum is only applicable to discrete or lumped mass systems. The time analysis is applicable to continuous and lumped mass systems. The analysing options to evaluate the seismic load are according to section 4 of EN 1998-1:

- Linear static analysis (or named lateral force method of analysis or equivalent static analysis)
- modal response spectrum analysis (linear dynamic analysis)
- non-linear static analysis (pushover analysis)
- (non-) linear dynamic analysis (time- or response- analysis)

Unlike US codes, which consider the linear static analysis as the reference method for the seismic design, Eurocode 8 gives this status to the modal response spectrum method. In the following table is a comparison given for the analysis methods.

Method	Design data	Analysis method	Models ductility
Linear static analysis	Response spectrum	Static	No
Response spectra analysis	Response spectrum	Dynamic	(Yes) No
Ductility Modified response spectra analysis	Response spectrum	Dynamic	Yes
Static pushover analysis	Response spectrum	Static	Yes
Linear dynamic analysis	Time	Dynamic	No
Non- linear dynamic analysis	Time	Dynamic	Yes

Figure 4-1 comparison of seismic analysis methods(Barltrop et al., 1991)

The table is divided in response spectrum and time history modelling. Depending on the phenomenon which is analysed, the design data is chosen. The modal response spectrum gives information about the structural response although not about the phase shift of the structural response. For analysis of the effect of uneven excitation this information is required. Therefore is a time history signal applied onto the model and is the modal response spectrum only treated in the appendix.

4.1.1 Fourier Transform

The transformation between a time domain signal and a frequency domain signal for random earthquake signals is usually done by a Fourier transformation. The general representation of a Fourier transformation for a continuous function is given by:

$$V(x,\omega) = \int_{-\infty}^{\infty} v(x,t) e^{-i\omega t} dt \tag{4.1}$$

The inverse transformation is done by:

$$v(x,t)=\frac{1}{2\pi}\int_{-\infty}^{\infty}V(x,\omega)e^{i\omega t}dt \tag{4.2}$$

Earthquake measurement data consist of a dataset and not of a function. The transformation of a dataset from the time domain into the frequency domain is done by a discrete Fourier transformation. The Discrete Fourier transformation of a signal is given by:

$$X(n)=\frac{1}{N_s}\sum_{k=0}^{N_{s-1}}x(k)e^{\frac{-i\cdot k\cdot n\cdot 2\cdot\pi}{N_s}} \quad \text{for } n=0..N_s-1 \tag{4-3}$$

where:

N_s number of samples

$x(k)=$ random vibration

The frequency is given by:

$$\omega(n)=2\pi\cdot\Delta t\cdot n \tag{4-4}$$

Rewriting the discrete variance spectrum as function of ω gives:

$$S_x(\omega)=X(\omega)=\frac{1}{N_s}\sum_{k=0}^{N_{s-1}}x(k)e^{\frac{-i\cdot k\cdot\frac{\omega}{2\pi\cdot\Delta t}}{N_s}} \tag{4-5}$$

A Fourier transformation of a time domain signal returns a complex number into the frequency domain. Where the transformation from n to omega is given by: ($\omega(n)=2\pi\cdot\Delta t\cdot n$). An inverse Fourier transformation of a frequency domain signal returns a time domain signal.

$$x(k)=\sum_{n=0}^{N_{s-1}}X(n)e^{\frac{-i\cdot k\cdot n\cdot 2\cdot\pi}{N_s}} \quad \text{for } k=0..N_s-1 \tag{4-6}$$

where:

$N_s=$ number of samples

$x(k)=$ random vibration

The transformations do not cause any information loss. The inverse Fourier transformation returns exactly the same initial time domain signal.

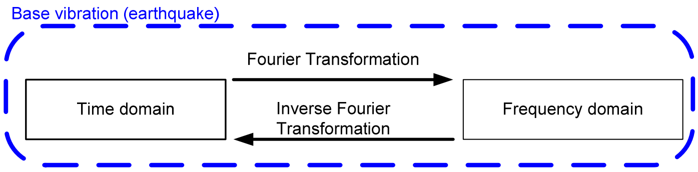

Figure 4-2 transformation between time and frequency domain

4.1.2 Vibration signal

The earthquake motion is given within the blue dashed area. An example of a conversion between time and frequency domain of a base displacement signal is given in Figure 4-3. The blue area is included in the figure for comparison.

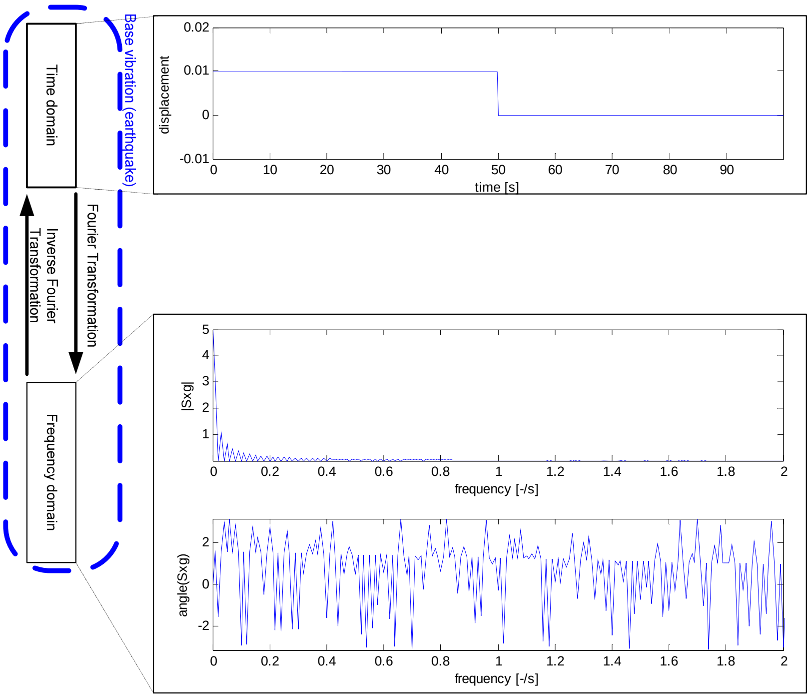

Figure 4-3 pulse displacement signal of 0.01m for 50 seconds followed by a displacement of 0m in the time and frequency domain. (a) base displacement signal (time domain) (b) angle (frequency domain) (c) absolute value (frequency domain)

4.2 Structural response

Multiplication of the earthquake signal (frequency domain) with the transfer function gives the structural motion (frequency domain). The structural motion in the time domain is acquired by an inverse Fourier transformation of the frequency domain signal. A scheme of the transformations is given in Figure 4-4.

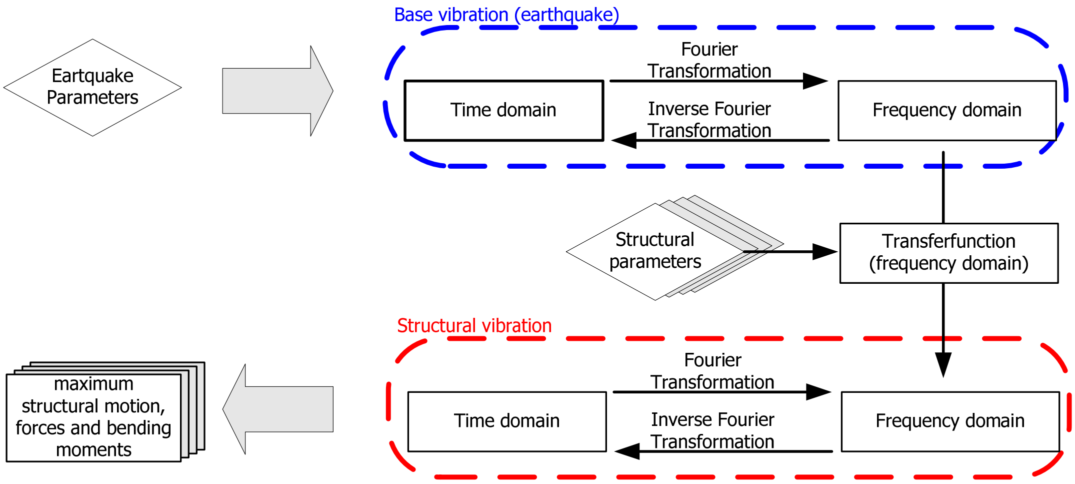

Figure 4-4 Scheme of transformation from base vibration to structural vibration

Explanation of Figure 4-4: The scheme starts with an earthquake dataset. An earthquake is taken/ generated from/ for a specific site. Earthquake data is mainly dependent on site location and soil conditions. The structural parameters determine the transfer function. The earthquake motion (frequency domain) together with the transfer function generates the structural motion (frequency domain).
The transfer function between the base and structural displacement is given by:

$$H_{v_n y}(x,\omega) = \frac{v_n(x,t)}{y(t)} = \frac{V_n(x,\omega)}{Y} \tag{4-7}$$

Rewriting this equation gives the output as function of the input:

$$V_n(x,\omega) = H_{v_n y}(x,\omega) \times Y \tag{4-8}$$

The absolute value in the frequency domain represents the amplitude for a certain frequency contributed to the earthquake signal, $S_x(\omega)$, see equation (4-5). So equation (4-8) becomes:

$$V_n(x,\omega) = H_{v_n y}(x,\omega) \times S_Y(\omega) \tag{4-9}$$

The terms in equation (4-8) and (4-9) are complex numbers. The multiplication of equation (4-9) is graphically given in Figure 4-5 and Figure 4-6. The graphs give the structural response for α_{inc} = 0^0 and α_{inc} = 54^0 at the middle of the jetty (x= 60m). The graphs represent the boxes in Figure 4-4. The bending moments, according to the previous paragraph, turned out to be proportional to the acceleration for low frequencies. Figure 4-7 and Figure 4-8 give the structural bending moments at the middle support for α_{inc} = 0^0 and α_{inc} =36^0. The shear forces are calculated in the same way. The support forces are calculated by:

$$F_s(t) = v_{rel}(t) \times k_t = \big(v(t) - y(t)\big) \times k_t \tag{4-10}$$

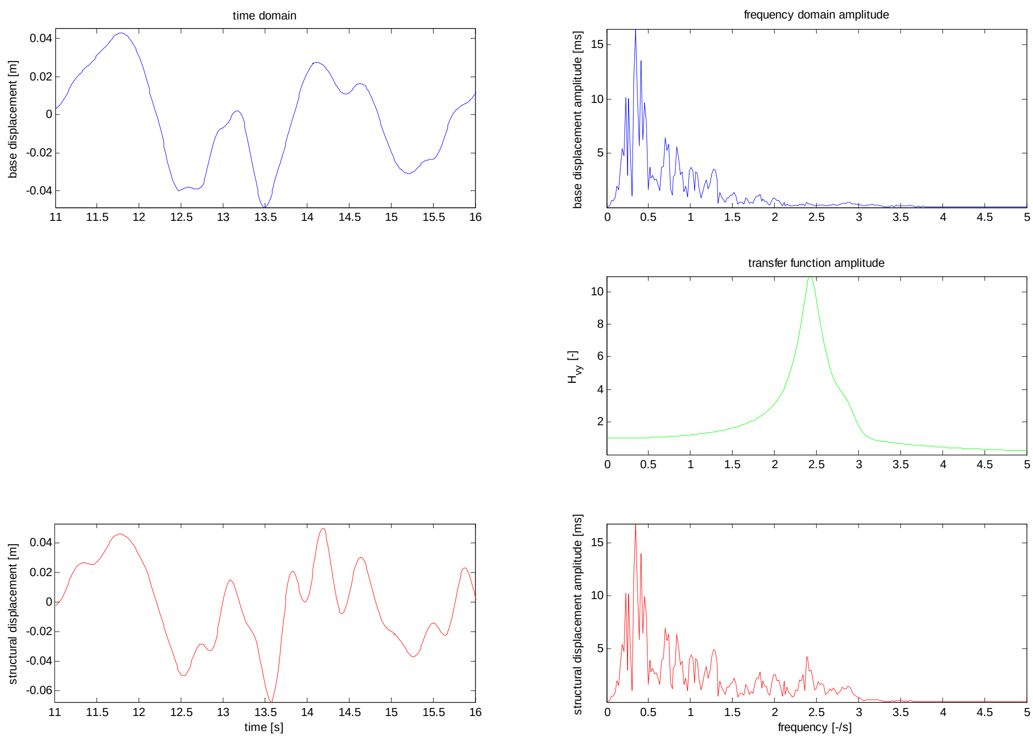

Figure 4-5 structural motion for angle of incidence of 0^0 (time domain between 11s and 16s and frequency domain for total event 0 to 48s), upper row: base motion, middle row: transfer function, bottom row: structural motion, left column time domain, right column frequency domain amplitude.

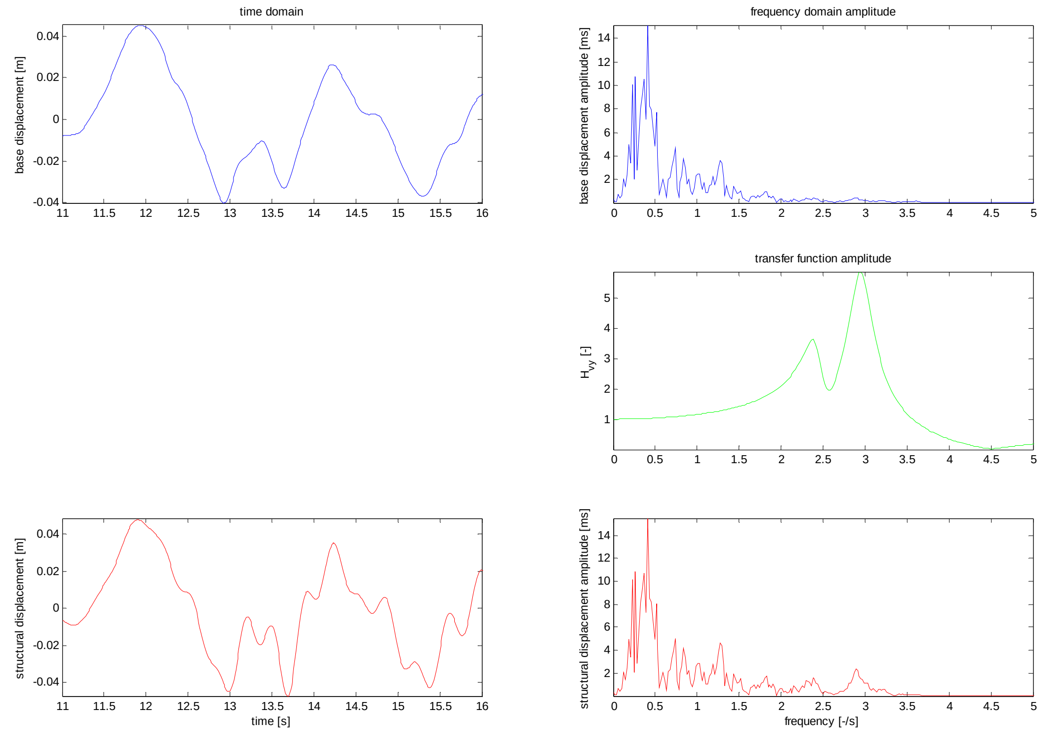

Figure 4-6 structural motion for angle of incidence of 54^0 (time domain between 11s and 16s and frequency domain for total event 0 to 48s), upper row: base motion, middle row: transfer function, bottom row: structural motion, left column time domain, right column frequency domain amplitude.

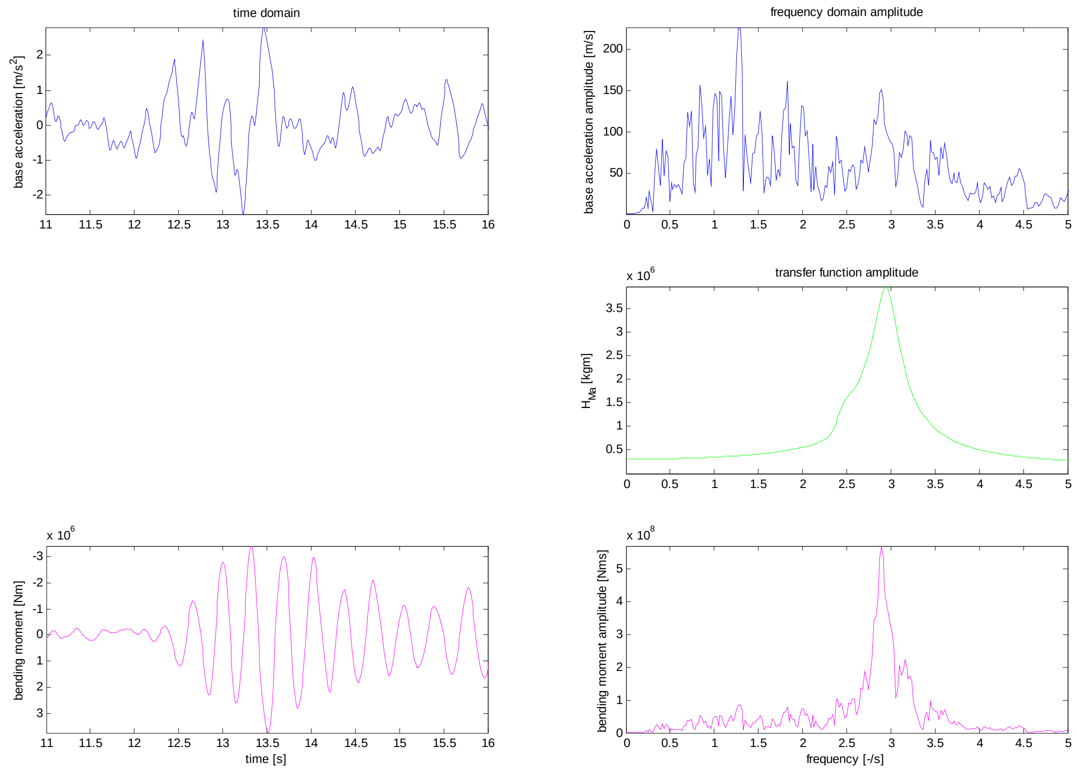

Figure 4-7 structural acceleration for an angle of incidence of 0^0 (time domain between 11s and 16s and frequency domain for total event 0 to 48s), upper row: base acceleration, middle row: transfer function, bottom row: structural bending moment, left column time domain, right column frequency domain amplitude.

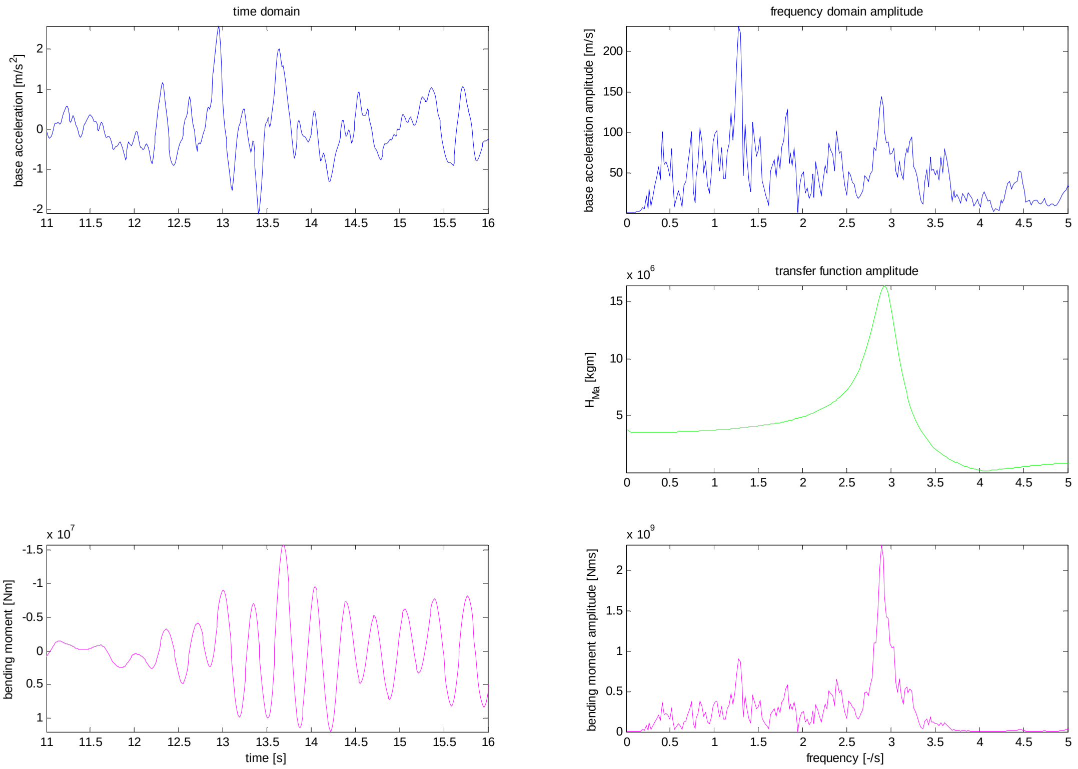

Figure 4-8 structural acceleration for an angle of incidence of 36^0 (time domain between 11s and 16s and frequency domain for total event 0 to 48s), upper row: base acceleration, middle row: transfer function, bottom row: structural bending moment, left column time domain, right column frequency domain amplitude.

4.3 Maxima for α_{inc} =0

In the previous paragraph is discussed how to calculate the structural:

1. displacements
2. bending moments
3. shear forces
4. pile forces

In this paragraph the maximum bending moments will be calculated using a SDOF model. This will be compared to the maximum values calculated with the continuous model with α_{inc} = 0^0.

4.3.1 Static analysis

The jetty structure applied is symmetric. Also is the beam (jetty girder) relatively stiff. So, roughly the maximum acceleration for each location (x) is occurring at the same time and the jetty can be modelled as a SDOF model. Figure 4-9 represents a SDOF model for the "average" support.

In Figure 4-9 is given a SDOF model of the jetty.

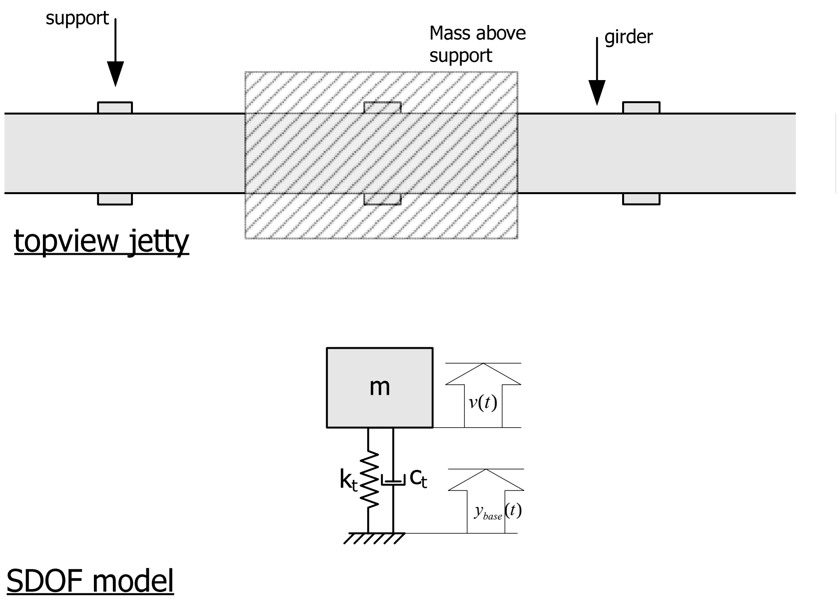

Figure 4-9 SDOF model of the jetty

The average mass/ stiffness on top of the support is given by:

- $m_{average}$ 1.37e5 kg
- $k_{average}$ 3.17e7 N/m

The natural frequency of the SDOF is given by:

$$f_0 = \frac{\sqrt{\frac{k}{m}}}{2\pi} = 2.43Hz \tag{4-11}$$

As expected, this corresponds to the natural frequency calculated with the continuous system equations. The spring forces in the SDOF system are calculated according the linear static analysis by:

$$F_{\max} = m \times \ddot{v}_{\max} \approx k \times v_{rel,\max} \tag{4-12}$$

The maximum absolute acceleration respectively relative displacement is given by the modal response spectrum. The modal response spectrum gives for $T_0 = f_0^{-1} = 0.42s$ the following values (see Figure 2-8 on page 12):

- $\ddot{v}_{\max}$ =5.80 m/s^2
- $v_{rel,\max}$ =0.0249 m

So, the average maximum spring force is given, according the SDOF model, by:

$$\overline{F}_{\max} = m \times \overline{\ddot{v}}_{\max} = 792kN \tag{4-13}$$

This force is normally multiplied with a static safety coefficient C_s of 1.5 (Barltrop et al., 1991). The static coefficient is chosen to be 1. The equivalent distributed load which causes an average support force of 792kN is given by:

$$q_{equivalent} = \frac{\sum F_{\max,s}}{\left(N_s - 1\right)d} = \frac{792kN \times 13}{\left(13-1\right)10m} = 85.8 \text{ [kN/m]} \tag{4-14}$$

Since

$$q(x) \approx \ddot{v}(x) \cdot m(x) \tag{4-15}$$

is the acceleration given by:

$$\ddot{v}(x) \approx \frac{q(x)}{m(x)} \tag{4-16}$$

where:

$\ddot{v}(x)$ = acceleration in transverse direction

$q(x)$ = distributed equivalent load

$m(x)$ = distributed mass

The maximum bending moment, when the continuous jetty model is loaded by the equivalent load, is given by 4.28 MNm (see Figure 4-10, Figure 4-11 and Appendix I)

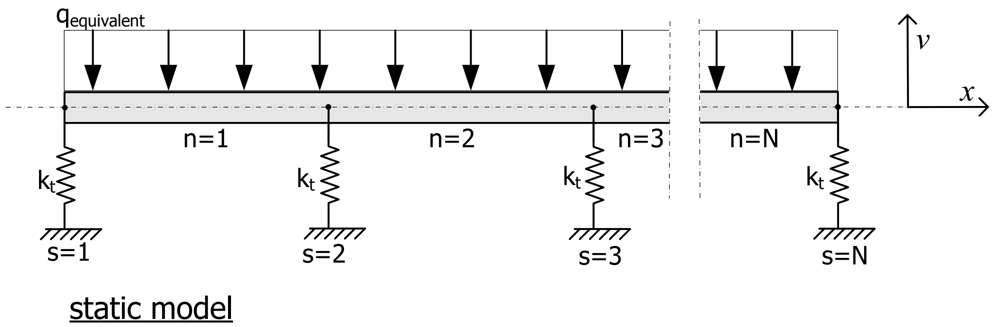

Figure 4-10 equivalent load

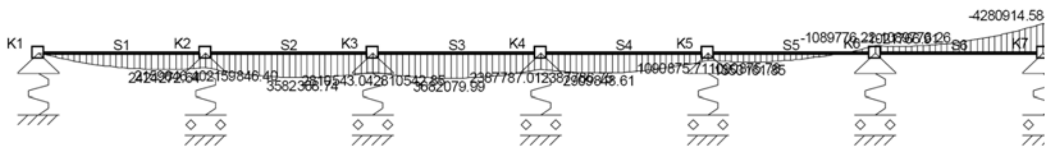

Figure 4-11 Bending moments with equivalent load

4.3.2 Time history analysis

In Figure 4-12 is given the maximum structural response according to the continuous system equations. The green bars/ lines represent the structural response for α_{inc} is 0^0. The base displacement when α_{inc} is 0^0, is given by the longitudinal earthquake displacement, see equation (2.5).

The strong point shows an increase in force because stiffness attracts forces. The average support force is given by 786 kN and the maximum bending moment, at the middle support, is given by 3.80 MNm. The values are compared to the SDOF calculation:

	SDOF model calculation	Continuous model calculation	difference
Average Maximum Forces [kN]	792	786	-1%
Maximum Bending Moment at middle support [MNm]	4.28	3.80	-13%

Table 4-1 Comparison of SDOF model and continuous model calculation

The reduction in comparison to the SDOF calculation is caused by the following:

- In the continuous model, the mass isn't concentrated above the support. At the SDOF – model, the total mass is subjected to the maximum acceleration. At the continuous model, not all the mass has to be subjected to the maximum acceleration at the same time.

The maximum moment, according to the time history analysis, occurs at 55m and 75m. This maximum moment is around 4.25MNm. After all is the bending moment, calculated with the SDOF model, not an over estimation for the maximum bending moment during the earthquake event with α_{inc} =0.

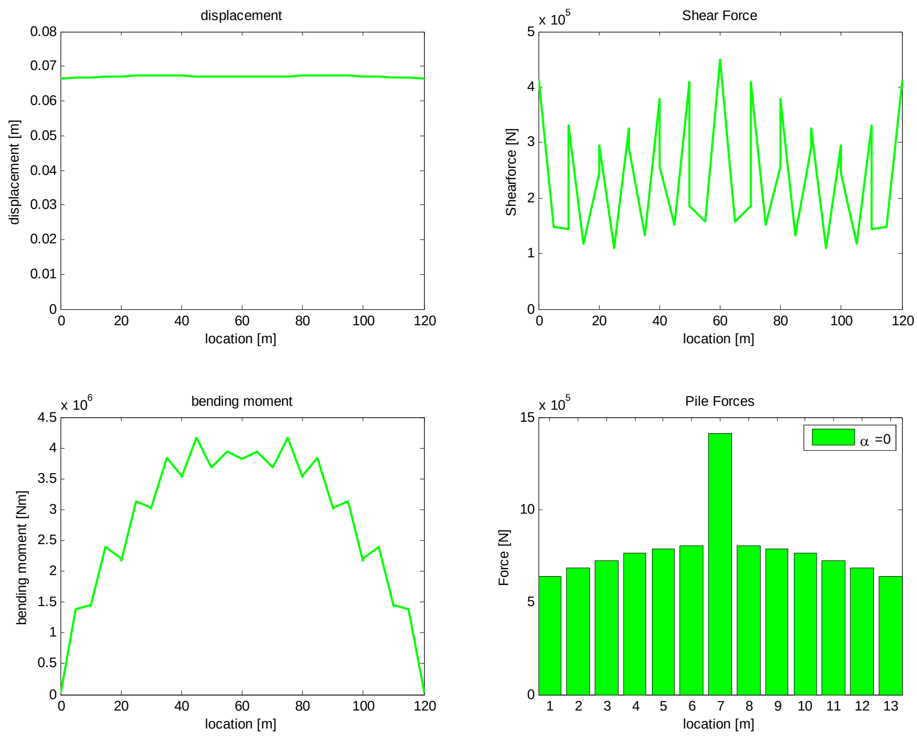

Figure 4-12 Maxima for $\alpha_{inc} = 0^0$

4.4 Maxima for $\alpha_{inc} \neq 0^0$

In this paragraph will be discussed how to calculated the maximum bending moments for a SDOF model when $\alpha_{inc} \neq 0$. This is compared to the maximum values calculated with the time history analysis when $\alpha_{inc} \neq 0$.

4.4.1 Static analysis

An estimation of the structural bending moment is made according to the SDOF – model. A conservative method to calculate the bending moment is to assume that two successive supports have a base displacement dv, corresponding to the maximum pile force, in opposite direction.

$$dv = \frac{dF_{average}}{k_{average}} = \frac{792e3}{3.17e7} = 0.025m \tag{4-17}$$

The bending moment caused by the support displacement is given by (Figure 4-13):

$$M = \frac{6EI}{d^2} 2dv = \frac{6 \times 31e9 \times 13.7}{10^2} \times 2 \times 0.025 = 1.27e3MNm \tag{4-18}$$

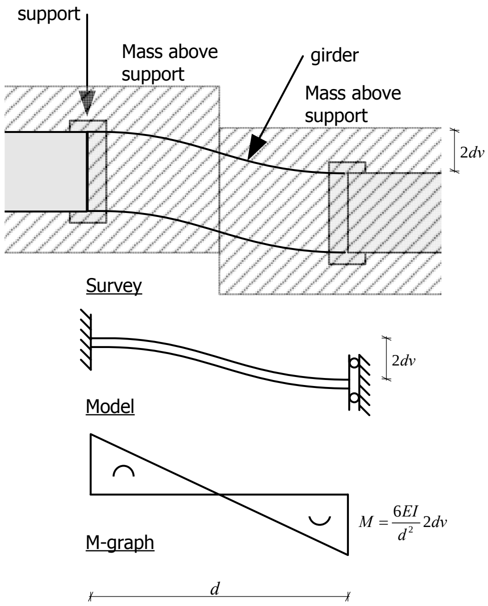

Figure 4-13 Support displacement

4.4.2 Time history analysis

For a changing α_{inc}, changes the transverse base motion and so also the maximum base acceleration/ displacement. These maxima as function of α_{inc} are given in Figure 4-14.

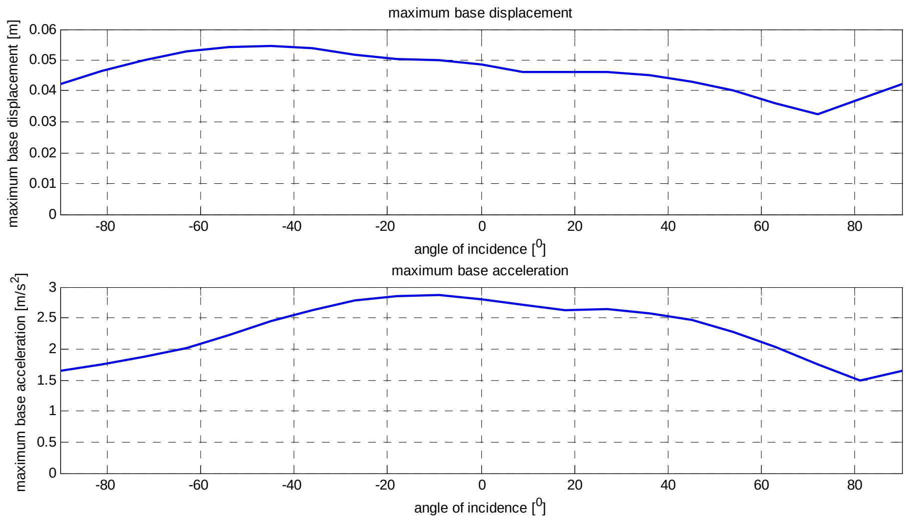

Figure 4-14 maximum displacement/ acceleration as function of α_{inc}

For $\alpha_{inc} \neq 0$ is the time delay $\tau \neq 0$. Since the transfer function is depending on τ is the transfer function indirectly depending on α_{inc} (See Figure 3-14, Figure 3-16 and Figure 3-18). The maximum values during the Alkion earthquake event for different α_{inc} are given in the Figure 4-15:

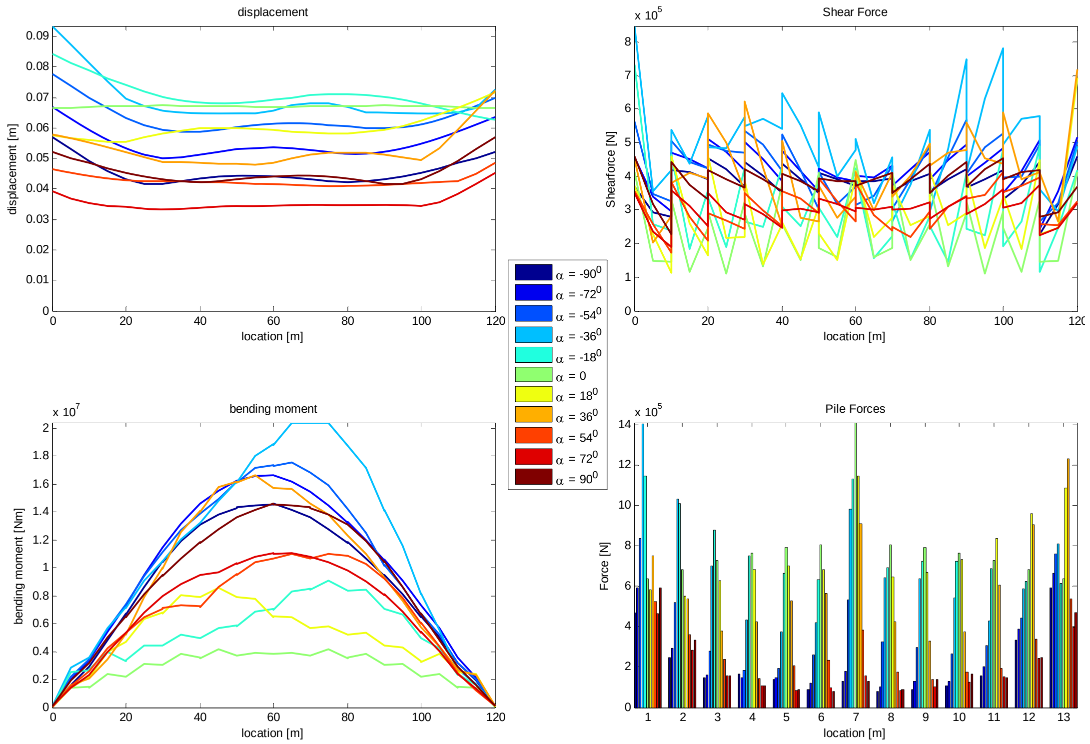

Figure 4-15 Melaka Jetty maxima during earthquake event (Alkion)

The maximum bending moment occurs when α_{inc} = -36^0. For this angle of is incidence is the time delay in excitation between the support around 0.03s. In the previous chapter is determined the existence of an amplification of the transfer functions at τ = 0.03s.

The maximum bending moment is 20.5MNm. The maximum bending moment calculated with the less conservative static model for $\alpha_{inc} \neq 0$ is 19.4MNm, which is a difference of 6%.
In Figure 4-16 is given for comparison the modal response spectra for α_{inc} = -36^0 and α_{inc} = 0. Overall there is a reduction in the modal response spectra for α_{inc} = -36^0. The maximum bending moment calculated with the modal response spectrum when α_{inc} = -36^0 will be less then the calculation of the maximum bending moment when the modal response spectrum for α_{inc} = 0^0 is used.

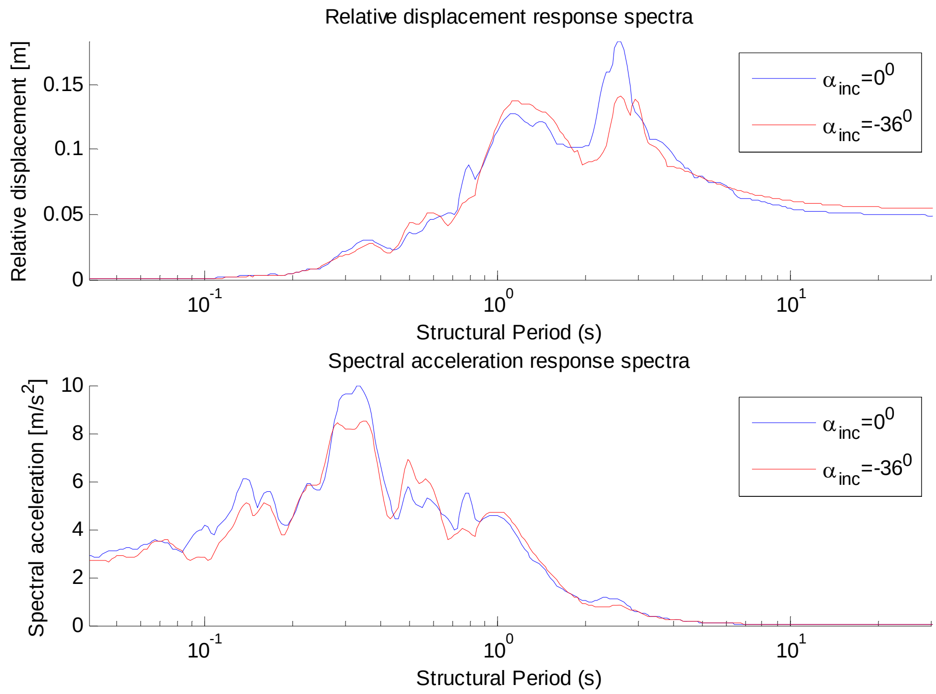

Figure 4-16 modal response spectra for $\alpha_{inc} = -36^0$ and $\alpha_{inc} = 0^0$

An overview of the calculated bending moments are given in table 4-2.

	time history	conservative SDOF
bending moment [MNm]	20.5	1270
difference to time history	0%	+6100%

table 4-2 time history vs. modal response calculation

4.5 Relation

The relation between the angle of incidence and maxima is given in Figure 4-17.

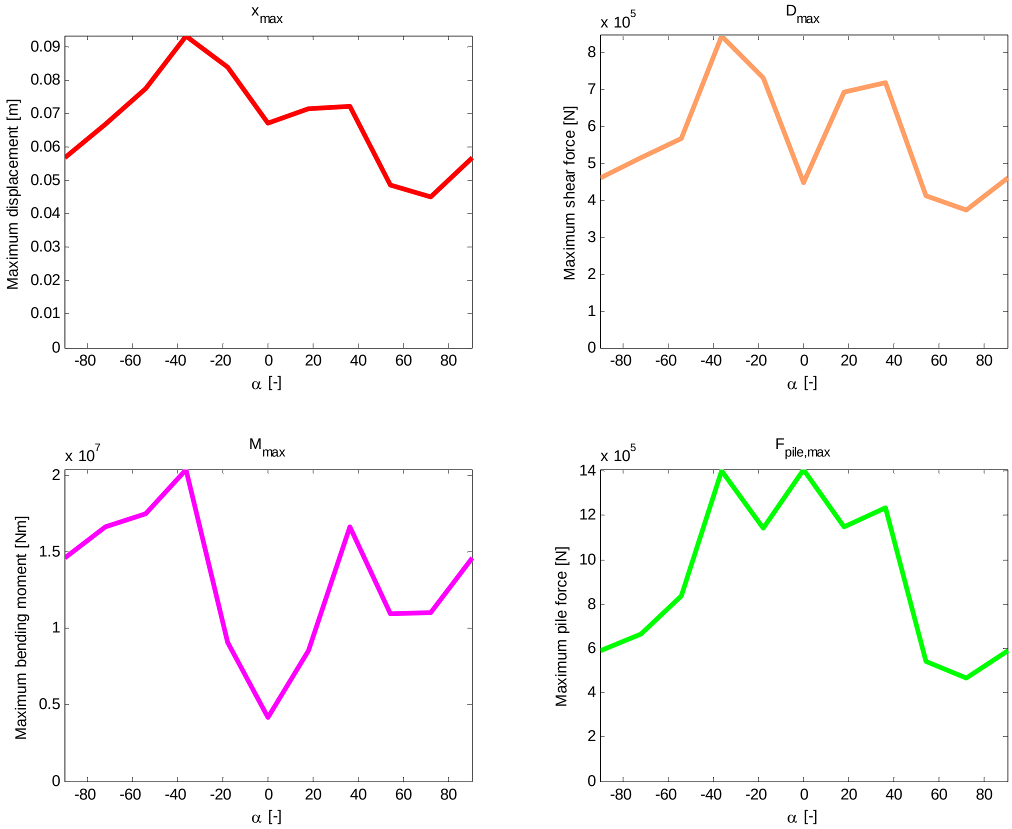

Figure 4-17 Maxima as function of angle of incidence

The maximum base acceleration for α_{inc} = 0 is bigger than when α_{inc} = -36^0. Also the response spectrum will change because base acceleration changes. The static analysis is calculated for a

The maximum values of the four graphs in Figure 4-17 are plotted in Figure 4-18 to Figure 4-21, these employ:

1. displacement
2. bending moment
3. shear force
4. pile force

The following conclusions can be made from Figure 4-17.

1. maximum displacement

The displacement transfer function amplitudes are, for frequencies smaller than 1, equal to 1. The structural displacement is expected to be related to the base motion. The maximum motion occurs for α_{inc} = -36^0 and x=0 (see Figure 4-18). The displacement amplification is more or less 50%

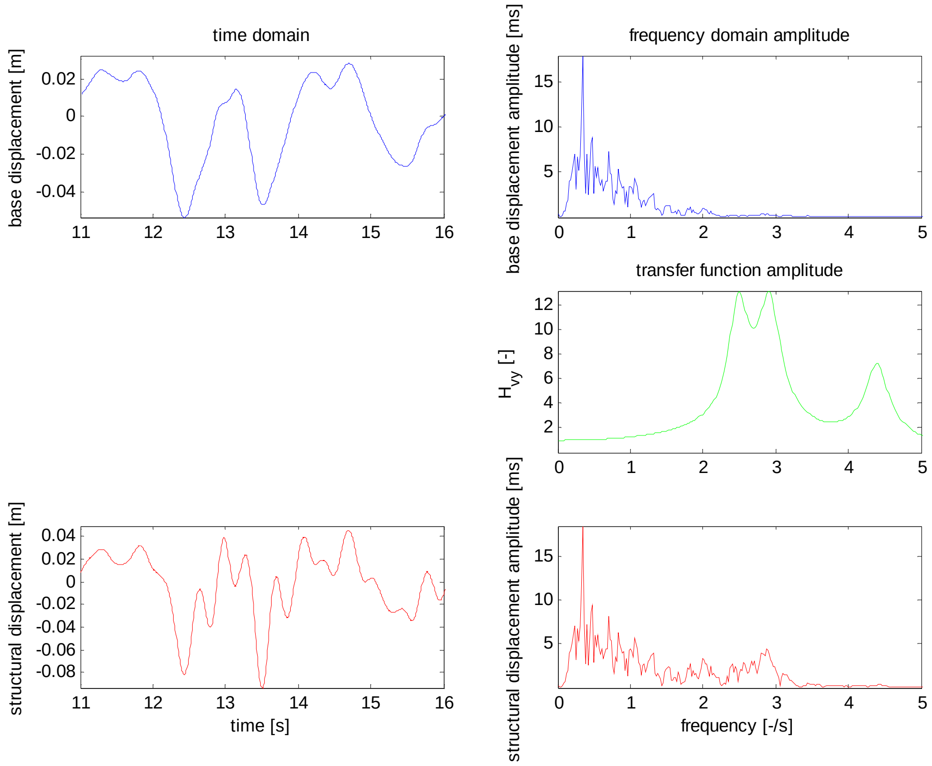

Figure 4-18 Maximum motion at x=0m for α_{inc} = -38^0. time domain between 11s and 16s and frequency domain for total event (0 to 48s), upper row: base acceleration, middle row: transfer function, bottom row: structural bending moment, left column time domain, right column frequency domain amplitude.

2. maximum bending moments

The maximum bending moment occurs between 11 and 16s for α_{inc} = -36^0 (see Figure 3-16). The transfer functions for the bending moment – base acceleration showed an increase in response with an increase in time delay. The bending moment maxima show a similar relation. The bending moments are increased for an increase in the absolute value of the angle of incidence.

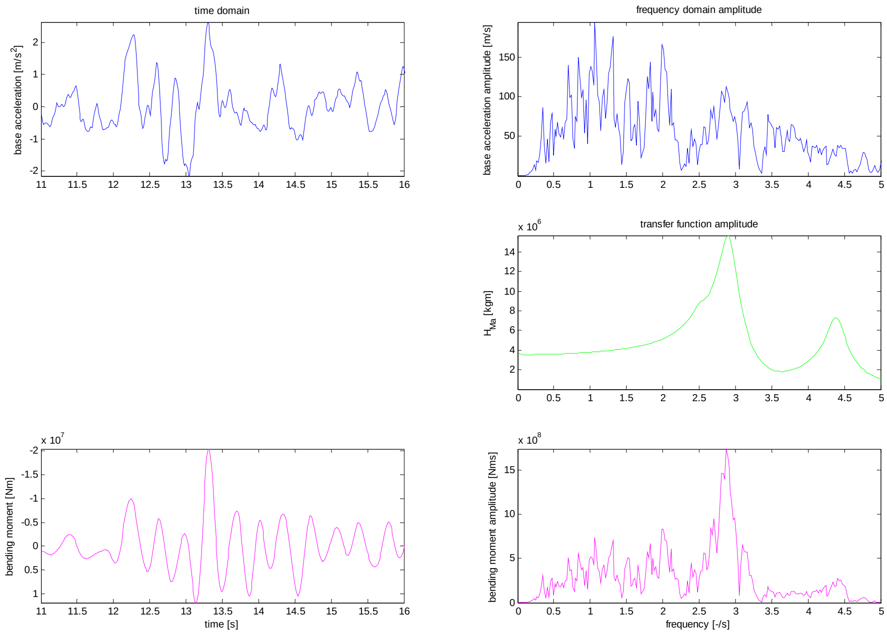

Figure 4-19 Bending moment at x=70m for α_{inc} = -36^0. time domain between 11s and 16s and frequency domain for total event (0 to 48s), upper row: base acceleration, middle row: transfer function, bottom row: structural bending moment, left column time domain, right column frequency domain amplitude.

3. maximum shear forces

For the shear forces is not found a clear relation. The response functions shows a bigger response for an increase in the absolute value of τ. The time history analysis shows a maximum at x=100 for α_{inc} = -36^0.

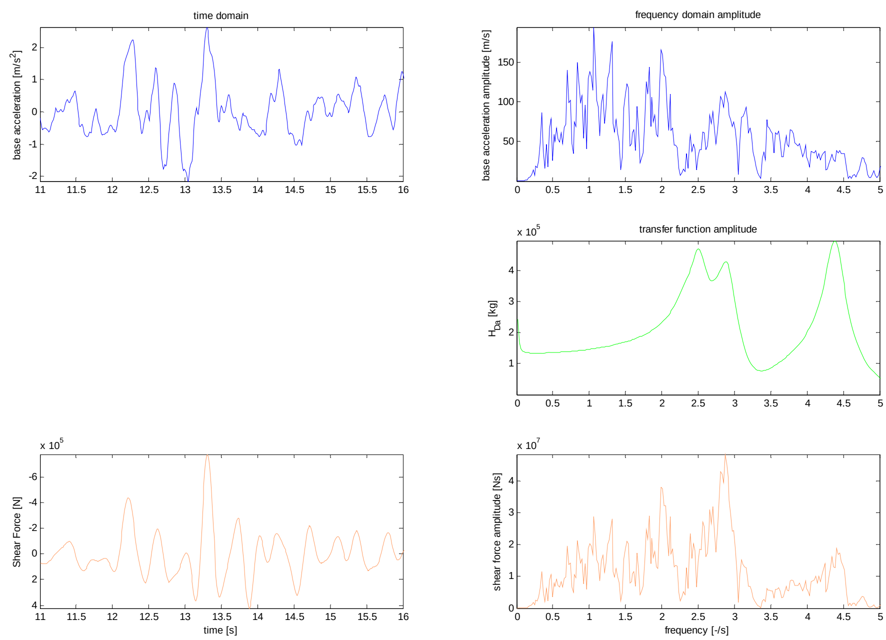

Figure 4-20 shear force for α_{inc} = -36^0 and x=100m. Time domain between 11s and 16s and frequency domain for total event (0 to 48s), upper row: base acceleration, middle row: transfer function, bottom row: structural bending moment, left column time domain, right column frequency domain amplitude.

4. maximum pile forces

The maximum pile forces are decreasing with a increasing of the absolute angle of incidence. When there is a time delay in excitation of the supports, the supports are not excited simultaneously successively the peak load will not reach the support at the same time. This could be an explanation for the reduction in pile forces for $\alpha_{inc} \neq 0$. The maximum pile forces occurs at the middle support (strong point) at 60m with $\alpha_{inc} = 0$

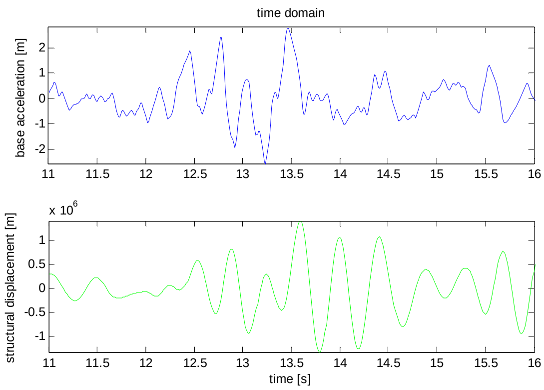

Figure 4-21 pile force for x= 60m and $\alpha_{inc} = 0^0$. Time domain between 11s and 16s and frequency domain for total event (0 to 48s), upper row: base acceleration, middle row: transfer function, bottom row: structural bending moment, left column time domain, right column frequency domain amplitude.

4.6 Variety in parameters

To investigate the influence of the parameters, the following parameters are varied:

- k, stiffness parameter
- ξ, damping parameter
- d, span length
- M_s, support mass
- M_d, distributed mass
- E, youngs modulus

For each variation in variables is made a plot (see Appendix H). The variation is based on the parameters of the Melaka case given in paragraph 1.2. The correlation of the different parameters is given in table 4-3. In here is given for each maximum structural response if it is positively (+), negatively (-) or not (×) correlated to the parameter.

	displacement	bending moment	shear force	pile force
τ	×	+	×	-
k_t	-	×	×	×
ξ	-	-	-	-
d	+	+	+	+
M_s	+	+	+	+
M_d	×	×	+	+
E	×	+	×	×

table 4-3 parameter - structural response correlation, positive (+), negative (-) or no (x) correlation

Overall it can be concluded that the phase shift in excitation in the frequency domain by tau has influences on the structural bending moment and the pile forces, this could already be seen in the transfer functions. The angle of incidence firstly has influence on the transverse base excitation. The maximum values show a significant increase in the maximum bending moment and a significant reduction of the maximum pile force for an increase of α_{inc}. The maximum displacement and the shear forces do not give a clear relation.

Chapter 5 Conclusions and recommendations

The main result of this thesis is that the dynamic response to an earthquake of a long jetty structure depends on the angle of incidence. A significant dynamic amplification of the structural response occurs if the spatial shape of the earthquake loading, at a natural frequency of the structure, closely resembles the structural mode shape that corresponds to this frequency.

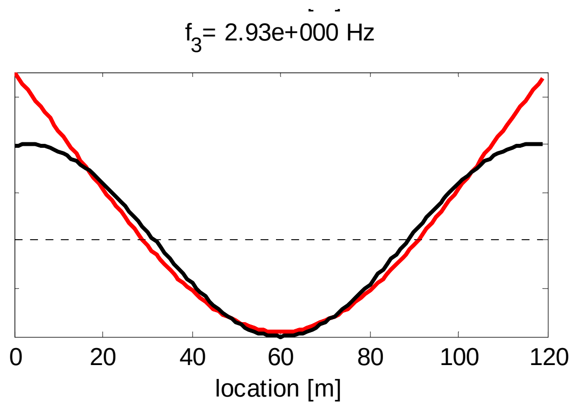

Figure 5-1 Third mode shape (red line), with equivalent base displacement (black line)

An example is given in Figure 5-1 for the Melaka case that was studied in this thesis. The red line represents the 3rd mode shape corresponding to the frequency of 2.93 Hz (period T_3 = 0.34s). The black line represents the earthquake loading shape for a harmonic wave of the same frequency that approaches the structure with a velocity c = 200 m/s and under an incidence angle α_{inc} = 36^0 . The corresponding time delay in loading between the adjacent supports is given by $\tau = d \sin \alpha_{inc} / c \approx 0.029s.$ The wavelength λ of the earthquake loading is given by $\lambda = T\, d/\, \tau \approx 120m.$ Where d is the intermediate support distance.

Thus, long jetty structures can be prone to specific incidence angles of possible earthquakes. We recommend this aspect to be accounted for in the building codes, which is currently not the case.

In order to conclude if the angle of incidence should be accounted for in the design, the following simplistic considerations can be carried out:

1. Estimate the natural frequencies and the corresponding mode shapes.
2. If $\lambda_i > T_i \cdot c$ the incidence angle can be of importance.

If the incidence angle can be of importance, the following approach schematized in Figure 5-2 is recommended for implementation into the codes:

1. Determine the design earthquake event in the frequency domain. (prescribed by the codes)
2. Calculate the transfer functions for different incidence angles.
3. Calculate the structural response to the earthquake in the frequency domain.
4. Transform this response to the time domain using an inverse Fourier transformation.
5. Conclude whether the maximum stresses are reached.

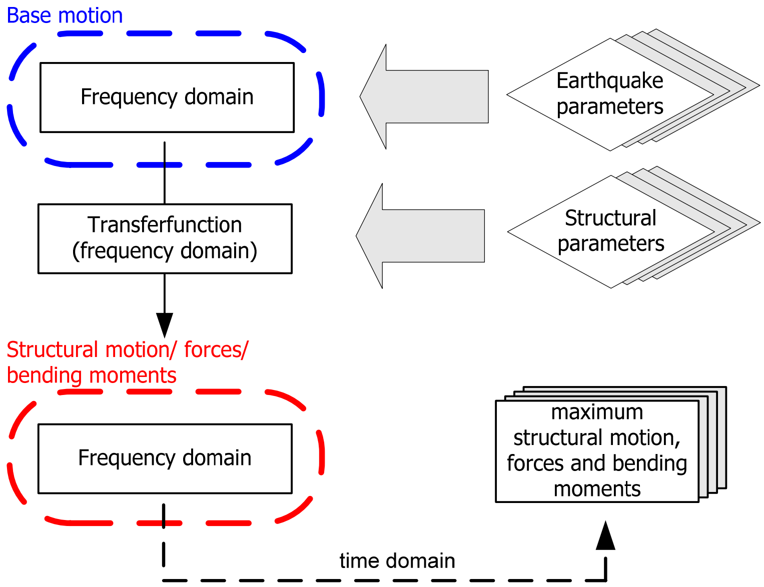

Figure 5-2 Frequency domain calculation

The model employed in this thesis is rather simplistic because it was aimed at exploring qualitatively the effect of the earthquake incidence angle on the structural response. In order to make the proposed model more realistic and explore possibilities of the structural response reduction, it is recommended to include the following factors in the model:

- Possible local failure of Pile – Cap connection
- Possible plastic deformation of the piles/ deck
- Stoppers that would limit the deck motion

Appendix A Drawings

Survey drawings of the Melaka case

Appendix B Solution of continuous equations

B.1 General solution transverse displacement

The equation of motion for a beam is given by the 4th order differential equation (3-14). So, for each span number n is the equation of motion given by:

$$\overbrace{EI\frac{\partial^4 v_n(x,t)}{\partial x^4}}^{\text{stiffness term}}+\overbrace{\rho A\frac{\partial^2 v_n(x,t)}{\partial t^2}}^{\text{inertia term}}=0 \qquad \text{(B-1)}$$

where:

$v =$ the transverse displacement as function of x (place) en t (time) [m]
$EI =$ bending stiffness [Nm^2]
$x =$ location on the beam [m]
$\rho =$ specific weight [kg/m^3]
$A =$ area [m^2]
$n =$ span number

For a derivation of (B-1) is revered to (3-14). The solution of the 4th order differential is given by:

$$v_n(x,t)=\hat{A}_n\exp(i\omega t-i\gamma x) \qquad \text{(B-2)}$$

where:

x = location on the beam [m]
t = time [s]
$\hat{A}_n$ = complex amplitude for span n
ω = frequency [rad/s]
γ_n = wave number [rad/m] for span n

Equation (B-2) inserted into the equation of motion (B-1) and divided by $\exp(i\omega t-\gamma x)$ gives:

$$-\omega^2\rho A+\gamma^4 EI=0 \qquad \text{(B-3)}$$

The four solutions of γ are given by:

$$\gamma_{n.1}=+\sqrt[4]{\frac{\rho A\omega^2}{EI}} \qquad \text{(B-4)}$$

$$\gamma_{n.2}=-\sqrt[4]{\frac{\rho A\omega^2}{EI}} \qquad \text{(B-5)}$$

$$\gamma_{n.3}=+i\sqrt[4]{\frac{\rho A\omega^2}{EI}} \qquad \text{(B-6)}$$

$$\gamma_{n.4}=-i\sqrt[4]{\frac{\rho A\omega^2}{EI}} \qquad \text{(B-7)}$$

Thus the displacement for $v_n(x,t)$ is represented by:

$$v_n(x,t)=\exp(i\omega t)\Big(\hat{A}_{n.1}\exp(-i\gamma_{n.1}x)+\hat{A}_{n.2}\exp(-i\gamma_{n.2}x)+\hat{A}_{n.3}\exp(-i\gamma_{n.3}x)+\hat{A}_{n.4}\exp(-i\gamma_{n.4}x)\Big)=\exp(i\omega t)\cdot V_n(x,\omega) \qquad \text{(B-8)}$$

where:

$V_n(x,\omega)=$ displacement in the frequency domain

The base movements for the first support, y_1 and φ_1 are assumed to be harmonic. Their motion is given by:

$$y_b(t) = Y_b \exp(i\omega t) \tag{B-9}$$

where:

Y_b displacement amplitude

and

$$\varphi_1(t) = \Phi \exp(i\omega t) \tag{B-10}$$

where:

$\Phi =$ rotation amplitude

The time delay between the supports is given by τ so at each support, the excitation of its base is given by:

$$y_s(t) = Y \exp(i\omega(t-(s-1)\tau)) = Y \exp(i\omega t)\exp(-i\omega(s-1)\tau) \tag{B-11}$$

Where:

$s =$ support number

and

$$\varphi_s(t) = \Phi \exp(i\omega(t-(s-1)\tau)) = \Phi \exp(i\omega t)\exp(-i\omega(s-1)\tau) \tag{B-12}$$

B.2 Boundary conditions

At each support holds two boundary condition, (equilibrium of bending moment and equilibrium of forces) and at each intermediate support holds two additional boundary conditions namely the two connection conditions. This paragraph gives the formulation of those boundary conditions.

At x=0 holds: n=1 (span number) and s=1 (support number). The boundaries conditions are defined as follows:

$$EI \cdot v_n''\big|_{x=0} = k_r \left(v_n'\big|_{x=0} - \phi_s(t) \right) \quad \text{(bending moment equilibrium)} \tag{B-13}$$

and

$$EI \cdot v_n'''\big|_{x=0} = -k_t \left(v_n\big|_{x=0} - y_s(t) \right) - m\,\ddot{v}_n\big|_{x=0} \quad \text{(force equilibrium)} \tag{B-14}$$

At x=L holds: n=N-1 and s=N (end support). The boundaries conditions are defined as follows:

$$EI \cdot v_n''\big|_{x=L} = -k_r \left(v_n'\big|_{x=L} - \phi_1(t-(s-1)\tau) \right) \quad \text{(bending moment equilibrium)} \tag{B-15}$$

and

$$EI \cdot v_n''' = k_t \left(v_n - y_1(t-(s-1)\tau) \right) + m\ddot{v}_n \quad \text{(force equilibrium)} \tag{B-16}$$

At x=s d holds: n=s and s=s (support number) and the boundaries conditions are defined as follows:

$$\left(v_n - v_{n+1} \right)\big|_{x=s\cdot d} = 0 \quad \text{(displacement equilibrium)} \tag{B-17}$$

$$\left(v_n' - v_{n+1}' \right)\big|_{x=n\cdot d} \quad \text{(rotation equilibrium)} \tag{B-18}$$

$$EI\left(v_n'' - v_{n+1}'' \right)\big|_{x=n\cdot d} = -k_r \left(v_n'\big|_{x=n\cdot d} - \phi_1\left(t-\left(s-1\right)\tau\right) \right) \quad \text{(bending moment equilibrium)} \tag{B-19}$$

$$EI\left(v_n''' - v_{n+1}''' \right)\big|_{x=n\cdot d} = k_t \left(v_n\big|_{x=n\cdot d} - y_1(t-(s-1)\tau) \right) + m\,\ddot{v}\big|_{x=n\cdot d} \quad \text{(force equilibrium)} \tag{5-20}$$

(B-11) and (B-12) inserted into (B-13) to (5-20) gives respectively equations (B-21)to (B-28) (boxed equations):

$$EI \cdot V_1''' - k_r V_1' = -k_r \Phi \quad \text{(bending moment equilibrium s=1)} \tag{B-21}$$

and

$$EI \cdot V_1''' + k_t V_1 - m\omega^2 V_1 = k_t Y \quad \text{(force equilibrium s=1)} \tag{B-22}$$

At x=L holds: n=N-1 and s=N (end support). The boundaries conditions are defined as follows:

$$EI \cdot V_{N-1}'' + k_r V_{N-1}' = k_r \Phi \exp(-i\omega(s-1)\tau) \quad \text{(bending moment equilibrium s=N)} \tag{B-23}$$

and

$$EI \cdot V_{N-1}''' - k_t V_{N-1} + m\omega^2 V_{N-1} = -k_t Y \exp(-i\omega(s-1)\tau) \quad \text{(force equilibrium s=N)} \tag{B-24}$$

If N>2 (more than two supports) holds:
x=s·d (location of equilibrium determination) and n=s-1 (span number).The boundaries conditions are defined as follows:

$$V_n = V_{n+1} \quad \text{(displacement equilibrium)} \tag{B-25}$$

$$V_n' = V_{n+1}' \quad \text{(rotation equilibrium)} \tag{B-26}$$

$$EI\left(V_n'' - V_{n+1}''\right) + k_r V_{n+1}' = k_r \Phi \exp(-i\omega(s-1)\tau) \quad \text{(bending moment equilibrium)} \tag{B-27}$$

$$EI\left(V_n''' - V_{n+1}'''\right) - k_t V_{n+1} + m\ddot{V}_{n+1} = -k_t Y \exp(-i\omega(s-1)\tau) \quad \text{(force equilibrium)} \tag{B-28}$$

V is given in equation (B-29). The derivatives of V are proportional to V and are given in equation (B-30) to (B-33).

$$\frac{v_n(x,t)}{\exp(i\omega t)} = V_n = \left(\hat{A}_{n.1}\exp(-i\gamma_{n.1}x) + \hat{A}_{n.2}\exp(-i\gamma_{n.2}x) + \hat{A}_{n.3}\exp(-i\gamma_{n.3}x) + \hat{A}_{n.4}\exp(-i\gamma_{n.4}x)\right) \tag{B-29}$$

$$V_n' = \frac{\partial v_n(x,t)}{\partial x} = -i\gamma V_n \tag{B-30}$$

$$V_n'' = \frac{\partial^2 v_n(x,t)}{\partial x^2} = -\gamma^2 V_n \tag{B-31}$$

$$\frac{\partial^3 v_n(x,t)}{\partial x^3} = V_n''' = i\gamma^3 V_n \tag{B-32}$$

$$\frac{\partial^2 v_n(x,t)}{\partial t^2} = \ddot{V}_n = -\omega^2 V_n \tag{B-33}$$

For n spans, the system of equation has 4xn equations, and 4xn unknowns ($A_{n.1}$, $A_{n.2}$, $A_{n.3}$ and $A_{n.4}$). This system of equations is written in matrix form by:

$$\mathbf{B} \times \mathbf{A} = \mathbf{C} \tag{B-34}$$

where:
$\mathbf{B}$ = coefficient matrix with dimension (4n X 4n)
$\mathbf{A}$ = variable vector with dimension (4n x 1)
$\mathbf{C}$ = force vector with dimension (4n x 1)

The solution of the matrix $\mathbf{A}$ is given by:

$$\mathbf{A} = \mathbf{B}^{-1} \times \mathbf{C} \tag{B-35}$$

Substitution of the variables into the general solution (B-8) gives the deflection as function of place (x) and time (t) for each span *n*. With the solution of the displacement, the solutions of the shear forces and bending moments are also known because of the following relations:

$$M(x,t) = -EI\frac{\partial^2 v(x,t)}{\partial x^2} \tag{B-36}$$

and

$$D(x,t) = -EI\frac{\partial^3 v(x,t)}{\partial x^3} \tag{B-37}$$

Without structural damping, equation (B-38) returns the natural frequencies of the structure.

$$\det B(\omega) = 0 \tag{B-38}$$

The mode shapes corresponding to the natural frequencies are calculated according:

$$\begin{bmatrix} b_{1,1} & \cdots & b_{1,n-1} \\ \vdots & & \vdots \\ b_{n-1,1} & \cdots & b_{n-1,n-1} \end{bmatrix} \cdot \begin{bmatrix} a_1 \\ \vdots \\ a_{n-1} \end{bmatrix} = -a_n \begin{bmatrix} b_1 \\ \vdots \\ b_{n-1} \end{bmatrix} \tag{B-39}$$

Where:

$a_{n,n}$ are elements of $\mathbf{A}$

$b_{n,n}$ are elements of $\mathbf{B}$

So

$$\begin{bmatrix} a_1 \\ \vdots \\ a_{n-1} \end{bmatrix} = -a_n \cdot \begin{bmatrix} b_{1,1} & \cdots & b_{1,n-1} \\ \vdots & & \vdots \\ b_{n-1,1} & \cdots & b_{n-1,n-1} \end{bmatrix}^{-1} \cdot \begin{bmatrix} b_1 \\ \vdots \\ b_{n-1} \end{bmatrix} \tag{B-40}$$

B.3 General solution longitudinal motion

The equation of motion for a rod is given by the 2nd order differential equation (B-41). So, for each span number n is the equation of motion given by:

$$\rho A\frac{\partial^2 u_n(x,t)}{\partial t^2} = \frac{\partial}{\partial x}\left(EA\frac{\partial u_n(x,t)}{\partial x}\right) \tag{B-41}$$

where:

$u =$ the longitudinal displacement as function of x (place) en t (time) [m]
$E =$ Young's modulus [N/m^2]
$x =$ location on the beam [m]
$\rho =$ specific weight [kg/m^3]
$A =$ area [m^2]
$n =$ span number

For a derivation of (B-1) is revered to (3-14). The solution of the 4th order differential is given by:

$$u_n(x,t) = \hat{A}_n \exp(i(\omega t - \gamma x)) \tag{B-42}$$

where:

x = location on the beam [m]
t = time [s]
$\hat{A}_n$ = complex amplitude for span n
ω = frequency [rad/s]
γ_n = wave number [rad/m] for span n

Equation (B-2) inserted into the equation of motion (B-1) and divided by $\exp(i\omega t-\gamma x)$ gives:

$$-\omega^2\rho=-\gamma^2 E \tag{B-43}$$

The four solutions of γ are given by:

$$\gamma_{n.1}=\sqrt{\frac{\omega^2\rho}{E}} \tag{B-44}$$

$$\gamma_{n.2}=-\sqrt{\frac{\omega^2\rho}{E}} \tag{B-45}$$

Thus the displacement for $v_n(x,t)$ is represented by:

$$u_n(x,t)=\exp(i\omega t)\left(\hat{A}_{n.1}\exp(-i\gamma_{n.1}x)+\hat{A}_{n.2}\exp(-i\gamma_{n.2}x)\right)=\exp(i\omega t)\cdot U_n(x,\omega) \tag{B-46}$$

where:

$U_n(x,\omega)=$ displacement in the frequency domain

The longitudinal base movements for the first support, x_1 are assumed to be harmonic. Their motion is given by:

$$x_1(t)=X\exp(i\omega t) \tag{B-47}$$

where:

$X=$ longitudinal displacement amplitude

The time delay between the supports is given by τ so at each support, the excitation of its base is given by:

$$x_s(t)=X\exp(i\omega(t-(s-1)\tau))=X\exp(i\omega t)\exp(-i\omega(s-1)\tau)) \tag{B-48}$$

Where:

$s=$ support number

B.4 Boundary conditions

At each support holds one boundary condition, (equilibrium of forces) and at each intermediate support holds one additional boundary conditions namely the connection conditions. This paragraph gives the formulation of those boundary conditions.

At x=0 holds: n=1 (span number) and s=1 (support number). The boundary conditions is defined as follows:

$$EA\cdot u'\big|_{x=0}=k_l\left(u\big|_{x=0}-x_s(t)\right)+m\,\ddot{u}\big|_{x=0}\quad\text{(force equilibrium)} \tag{B-49}$$

At x=L holds: n=N-1 and s=N (end support). The boundaries conditions are defined as follows:

$$EA\cdot u'\big|_{x=0}=-k_l\left(u\big|_{x=0}-x_s(t)\right)-m\,\ddot{u}\big|_{x=0}\quad\text{(force equilibrium)} \tag{B-50}$$

At x=s x d holds: n=s and s=s (support number) and the boundaries conditions are defined as follows:

$$\left(u_n-u_{n+1}\right)\big|_{x=s\cdot d}=0\quad\text{(displacement equilibrium)} \tag{B-51}$$

$$EA\left(u_n'-u_{n+1}'\right)\big|_{x=n\cdot d}=k_l\left(u\big|_{x=n\cdot d}-x_s(t-(s-1)\tau)\right)+m\,\ddot{u}\big|_{x=n\cdot d} \tag{B-52}$$

(force equilibrium)

(B-47) (B-48) inserted into (B-49) to (B-52) gives respectively (B-53) to (B-56)(boxed equations):

$$\boxed{EAU_1'-k_lU_1+m\omega^2U_1=-k_lX\quad\text{(force equilibrium s=1)}} \tag{B-53}$$

At x=L holds: n=N-1 and s=N (end support). The boundaries conditions are defined as follows:

$$EAU'_{N-1} + k_l U_{N-1} - m\omega^2 U_{N-1} = k_l X \exp(-i\omega(s-1)\tau) \quad \text{(force equilibrium s=N)} \tag{B-54}$$

If N>2 (more than two supports) holds:
x=s·d (location of equilibrium determination) and n=s-1 (span number).The boundaries conditions are defined as follows:

$$U_n = U_{n+1} \quad \text{(displacement equilibrium)} \tag{B-55}$$

and

$$EA\left(U'_n - U'_{n+1}\right) + k_l U_{n+1} - m\omega^2 \ddot{U}_{n+1} = k_l X \exp(-i\omega(s-1)\tau) \quad \text{(force equilibrium)} \tag{B-56}$$

V is given in equation (B-29). The derivatives of V are proportional to V and are given in equation (B-30) to (B-33).

$$\frac{u_n(x,t)}{\exp(i\omega t)} = U_n = \left(\hat{A}_{n.1}\exp(-i\gamma_{n.1}x) + \hat{A}_{n.2}\exp(-i\gamma_{n.2}x)\right) \tag{B-57}$$

$$U'_n = \frac{dU}{dx} = -i\gamma U_n \tag{B-58}$$

$$\ddot{U}_n = \frac{d^2U}{dt^2} = -\omega^2 U_n \tag{B-59}$$

For n spans, the system of equation has 4xn equations, and 4xn unknowns ($A_{n.1}$ and $A_{n.2}$). This system of equations is written in matrix form by:

$$\mathbf{B} \times \mathbf{A} = \mathbf{C} \tag{B-60}$$

where:
$\mathbf{B}$ = coefficient matrix with dimension (2n X 2n)
$\mathbf{A}$ = variable vector with dimension (2n x 1)
$\mathbf{C}$ = force vector with dimension (2n x 1)

The solution of the matrix $\mathbf{A}$ is given by:

$$\mathbf{A} = \mathbf{B}^{-1} \times \mathbf{C} \tag{B-61}$$

Substitution of the variables into the general solution (B-8) gives the deflection as function of place (x) and time (t) for each span *n*. With the solution of the longitudinal displacement, the solutions of the stress due to the longitudinal forces are also known because of the following relations:

$$N(x,t) = EA\frac{du(x,t)}{dx} \tag{B-62}$$

The stresses due to the longitudinal forces are given by:

$$\sigma(x,t) = \frac{N(x,t)}{A} = E\frac{du(x,t)}{dx} \tag{B-63}$$

Appendix C Mode shape functions

A mode shape function is a function which represents the mode shape as a function of x.

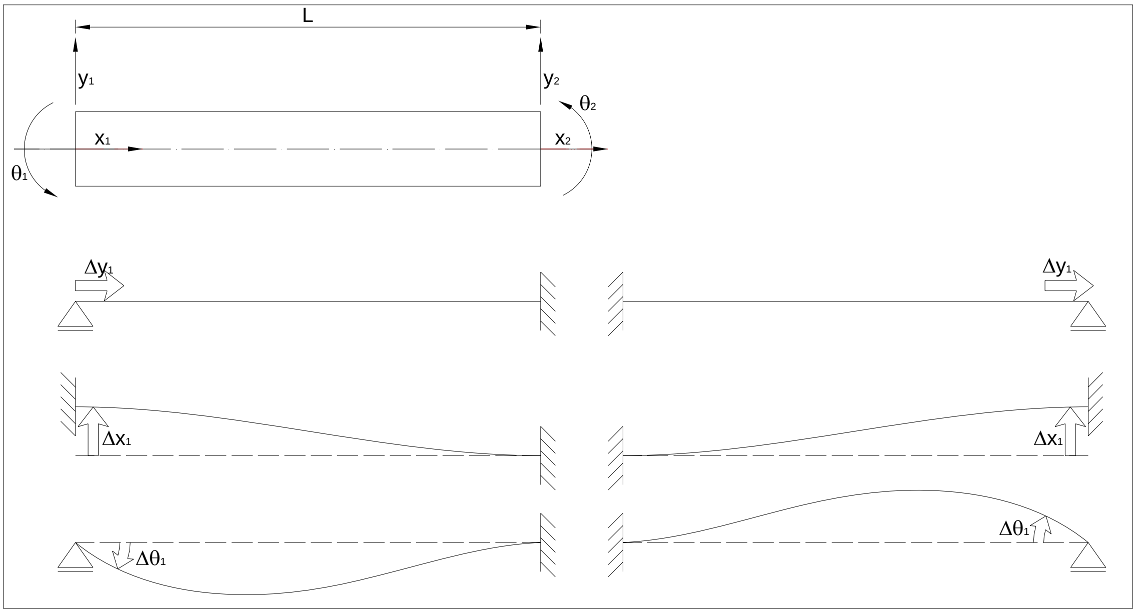

When one of the 6 degrees of freedom is displaced by a unit 1. The displacement of the total element distributed over the length is given by:

$$\Delta x_1(x) = \psi_{x1}(x)\Delta x_1$$

$$\text{where } \psi_{x1}(x) = \left(1 - 3\left(\frac{x}{L}\right)^2 + 2\left(\frac{x}{L}\right)^3\right) \tag{C.64}$$

$$\Delta x_2(x) = \psi_{x2}(x)\Delta x_2$$

$$\text{where } \psi_{x2}(x) = \left(3\left(\frac{x}{L}\right)^2 - 2\left(\frac{x}{L}\right)^3\right) \tag{C.65}$$

$$\Delta \theta_1(x) = \psi_{\theta 1}(x)\Delta \theta_1$$

$$\text{where } \psi_{\theta 1}(x) = x\left(1 - \frac{x}{L}\right)^2 \tag{C.66}$$

$$\Delta \theta_2(x) = \psi_{\theta 2}(x)\Delta \theta_2$$

$$\text{where } \psi_{\theta 2}(x) = \frac{x^2}{L}\left(\frac{x}{L} - 1\right)^3 \tag{C.67}$$

With these function the shape of the element can be expressed in terms of its nodal displacements:

$$d(x) = \psi_{x_1}(x)\Delta x_1 + \psi_{x_2}(x)\Delta x_2 + \psi_{y_1}(x)\Delta y_1 + \psi_{y_2}(x)\Delta y_2 + \psi_{\theta_1}(x)\Delta \theta_1 + \psi_{\theta_2}(x)\Delta \theta_2 \tag{C.68}$$

Appendix D MDOF Modelling

The single degree of freedom method can be extended to perform a much more accurate analysis. In a MDOF- system, the mass M, stiffness K, damping C, loading f and deflections x represent a set of simultaneous equations. These equations can be written in matrix form as:

$$\mathbf{M\ddot{x}} + \mathbf{C\dot{x}} + \mathbf{Kx} = \mathbf{f(t)} \tag{D.1}$$

This chapter will discuss the determination of a mass, damping and stiffness matrix. and the transformation to generalised coordinates.

D.1 Principal or generalised coordinates

Again the equation of motion:

$$\mathbf{M\ddot{x}} + \mathbf{C\dot{x}} + \mathbf{Kx} = \mathbf{f(t)} \tag{D.2}$$

The transformation matrix, to transform the Cartesian axis system to the principal or generalised axis system, is ϕ^t where ϕ is the matrix of eigenvectors (natural shapes or mode shapes) arranged in columns.

$$\mathbf{Z} = \boldsymbol{\varphi}^{\mathbf{T}}\mathbf{X} \text{ or } \mathbf{X} = \boldsymbol{\varphi}\mathbf{Z} \tag{D.3}$$

The transportation from general coordinates back to Cartesian coordinates is done by:

$$\mathbf{x}(t) = \sum_{n=1}^{N} \boldsymbol{\varphi}_n \mathbf{Z}_n(t) = \boldsymbol{\Phi}\mathbf{Z}(t) \tag{D.4}$$

When a matrix is orthogonal with regards to the eigenvector matrix holds:

$$\phi^T ... \phi = \text{diagonal} \tag{D.5}$$

where

ϕ = the matrix of eigenvectors

The equation of motion in principal coordinates becomes then:

$$\mathbf{M_n\ddot{Z}} + \mathbf{C_n\dot{Z}} + \mathbf{K_nZ} = \mathbf{F_n}(t) \tag{D.6}$$

Where:

$\mathbf{M_n}$ = $\boldsymbol{\varphi}^{\mathbf{T}}\mathbf{M}\boldsymbol{\varphi}$

$\mathbf{C_n}$ = $\boldsymbol{\varphi}^{\mathbf{T}}\mathbf{C}\boldsymbol{\varphi} = \mathbf{2\xi_n\omega_nM_n}$ where $\mathbf{\xi_n}$ is the n[th] mode damping ratio

$\mathbf{K_n}$ = $\boldsymbol{\varphi}^{\mathbf{T}}\mathbf{K}\boldsymbol{\varphi}$

$\mathbf{F_n}$ = $\boldsymbol{\varphi}^{\mathbf{T}}\mathbf{f}$

$\mathbf{M_n}$, $\mathbf{C_n}$ and $\mathbf{K_n}$ are diagonal matrices and represent the mass, damping and stiffness participation in mode n. $\mathbf{F_n}$ is the force participating in mode n. The matrices M, C and K have to be orthogonal to be transformed into diagonal matrices. The advantage of diagonal matrices is that the set of equations are fully decoupled (only diagonal terms).

D.2 Stiffness matrix

The spring force in a mass spring system is represent by:

$$f_s = k \cdot x \tag{D.7}$$

The factor k represent the stiffness of the system. For a MDOF system is the stiffness represent by set of equations depending on the degrees of freedom. The equation ordered give the stiffness matrix K. The elements of the stiffness matrix for plane beam column are given by:

$$k_{ij} = \int_0^L EI(x)\psi_i^{"}(x)\psi_j^{"}(x)dx \tag{D.8}$$

Where:

$\psi(x)$ = shape function

The stiffness matrix for a plane frame column (6 degrees of freedom) is given in equation (D.9). The stiffness matrix for a plane beam column is given by the same matrix without the 1st and 4th rows/ columns.

$$\mathbf{K} = \begin{bmatrix} \frac{EA}{L} & 0 & 0 & \frac{-EA}{L} & 0 & 0 \\ 0 & \frac{12EI}{L^3} & \frac{6EI}{L^2} & 0 & -\frac{12EI}{L^3} & \frac{6EI}{L^2} \\ 0 & \frac{6EI}{L^2} & \frac{4EI}{L} & 0 & \frac{-6EI}{L^2} & \frac{2EI}{L} \\ \frac{-EA}{L} & 0 & 0 & \frac{EA}{L} & 0 & 0 \\ 0 & -\frac{12EI}{L^3} & \frac{-6EI}{L^2} & 0 & \frac{12EI}{L^3} & \frac{-6EI}{L^2} \\ 0 & \frac{6EI}{L^2} & \frac{2EI}{L} & 0 & \frac{-6EI}{L^2} & \frac{4EI}{L} \end{bmatrix} \tag{D.9}$$
$$= \begin{bmatrix} \mathbf{K_{11}} & \mathbf{K_{12}} \\ \mathbf{K_{21}} & \mathbf{K_{22}} \end{bmatrix}$$

D.3 Mass matrix

The mass matrix can be construct as a (Clough and Penzien, 1993):

- Lumped- mass matrix
- Consistent- mass matrix

The lumped mass matrix is the simples way to construct the mass matrix. Here is assumed that the entire mass is concentrated at the point at which the translational displacements are defined (the nodes). The point mass will be associated with each degree of freedom. The mass associated with any rotational degree of freedom will be zero. Because the mass is assumed to be lumped the inertia mass is assumed to be zero. Thus the lumped- mass matrix is a diagonal matrix which will include zero diagonal elements for the rotational degrees of freedom.

$$\mathbf{M} = \begin{bmatrix} m_1 & & & & & \\ & m_1 & & & & \\ & & I_1 & & & \\ & & & m_2 & & \\ & & & & m_2 & \\ & & & & & I_2 \end{bmatrix} = \begin{bmatrix} \mathbf{M_{11}} & \\ & \mathbf{M_{22}} \end{bmatrix} \tag{D.10}$$

$m_i =$ the mass of element i

$I_i =$ the inertia mass of element I [kgm^2] = 0

The consistent matrix posses for each mass, like the stiffness matrix, the influence on the nodes. Like the stiffness matrix is the consistent matrix also not a diagonal matrix like the lumped mass matrix. The consistent plane- beam column is given by:

$$m_{ij} = \int_0^L m(x)\psi_i(x)\psi_j(x)dx \tag{D.11}$$

Where:

$\psi(x)$ = shape function

The mass matrix for a plane- frame element is modelled in the way. The mass matrix for a plane- frame element is given in (D.13). The mass matrix of a plane- beam column is given by the same matrix without the 1st and 4th rows/ columns.

$$\mathbf{M} = \frac{\rho AL}{420}\begin{bmatrix} 140 & 0 & 0 & 70 & 0 & 0 \\ 0 & 156 & 22L & 0 & 54 & -13L \\ 0 & 22L & 4L^2 & 0 & 13L & -3L^2 \\ 70 & 0 & 0 & 140 & 0 & 0 \\ 0 & 54 & 13L & 0 & 156 & -22L \\ 0 & -13L & -3L^2 & 0 & -22L & 4L^2 \end{bmatrix} = \begin{bmatrix} \mathbf{M_{11}} & \mathbf{M}_{12} \\ \mathbf{M}_{21} & \mathbf{M_{22}} \end{bmatrix} \tag{D.12}$$

ρ = the specific weight (kg/m^3)

A = area (m^2)

L = length of the beam element (m)

The determination of the shape functions is given in 0.

D.4 Damping Matrix

The damping matrix can be determined in the same way as the consistent mass and the stiffness matrix (Clough and Penzien, 1993):

$$c_{ij} = \int_0^L c(x)\psi_i(x)\psi_j(x)dx \tag{D.13}$$

Where:

$\psi(x)$ = shape function

$m(x)$ = distributed mass as function of x

In practice, the evaluation of the damping property c(x) is impracticable.
The most easy way to formulate a damping matrix, which is orthogonal to natural mode matrix, is to construct it proportional to the mass and stiffness matrix. This is called mass or stiffness proportional damping.

$$C = a_0 M \text{ or } C = a_1 K \tag{D.14}$$

Where:

a_0 and a_1 are proportional constant [s^{-1}] and [s]

or

$$C_n = a_0\phi^T M\phi \text{ or } C_n = a_1\phi^T K\phi \tag{D.15}$$

or in terms of damping ratio (see equation (D.6))

$$2\omega_n M_n \xi_n = a_0 M_n \text{ or } C_n = 2\omega_n M_n \xi_n = a_1 K_n \tag{D.16}$$

From which

$$\xi_n = \frac{a_0}{2\omega_n} \text{ or } \xi_n = \frac{a_1\omega_n}{2} \tag{D.17}$$

From equation (D.16) it can be seen that for mass proportional damping the damping ratio is inversely proportional to the frequency and on the other hand the stiffness proportional damping is directly in proportion with the frequency. The dynamic response include contributions form all modes. When the MDOF system has significant natural frequencies which span a wide range, the amplitude of the different modes will be distorted by inappropriate damping ratios.
An improvement can be made when the damping matrix is expressed as a sum of the stiffness and mass proportional damping matrix. Thus:

$$c = a_0 m + a_1 k \text{ (Rayleigh damping)} \tag{D.18}$$

So combining the formulas in (D.17) gives:

$$\xi_n = \frac{a_0}{2\omega_n} + \frac{a_1 \omega_n}{2} \tag{D.19}$$

The damping ratio as function of the natural frequency is given in the following figure:

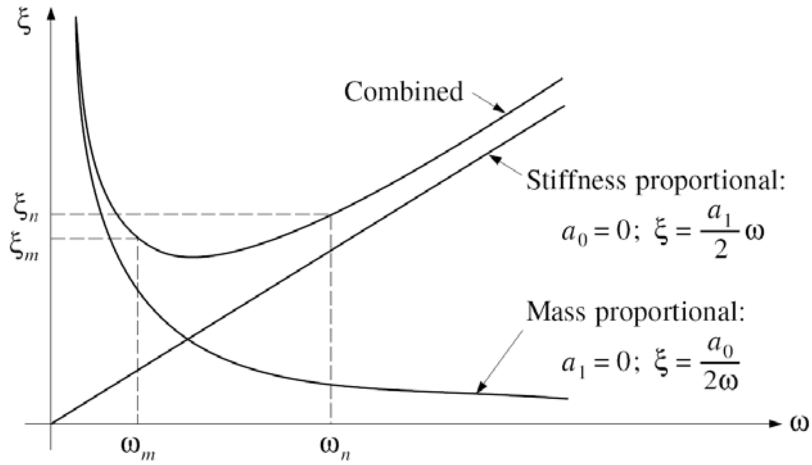

Figure 5-3 relationship between damping ratio and frequency, for Rayleigh damping (Clough and Penzien, 1993).

The solution of the a coefficients is gained by writing the damping as a set of equations:

$$\begin{bmatrix} \xi_m \\ \xi_n \end{bmatrix} = \tfrac{1}{2} \begin{bmatrix} 1/\omega_m & \omega_m \\ 1/\omega_n & \omega_n \end{bmatrix} \begin{bmatrix} a_0 \\ a_1 \end{bmatrix} \tag{D.20}$$

And the factors resulting from the simultaneous solution are:

$$\begin{bmatrix} a_0 \\ a_1 \end{bmatrix} = 2 \frac{\omega_m \omega_n}{\omega_n^{\,2} - \omega_m^{\,2}} \begin{bmatrix} \omega_n & -\omega_m \\ 1/\omega_n & -1/\omega_m \end{bmatrix} \begin{bmatrix} \xi_m \\ \xi_n \end{bmatrix} \tag{D.21}$$

The mass and stiffness matrices used to formulate Rayleigh damping are not the only matrices which are orthogonal to the natural vector matrices. In fact an infinite number of matrices has this property $(\phi^T ... \phi = \text{diagonal})$. A proportional damping matrix can be made up of any combination of these matrices:

$$\mathbf{C} = \mathbf{M} \sum_b a_b \left[\mathbf{M}^{-1} \mathbf{K} \right]^b \equiv \sum_b \mathbf{C}_b \tag{D.22}$$

In here, the different a-coefficients are arbitrary. For b=0 and b=1 the formula stated in (D.18) is gained. In Figure 5-4 is seen the damping ratio versus the frequency of a three term solution and a four term solution.

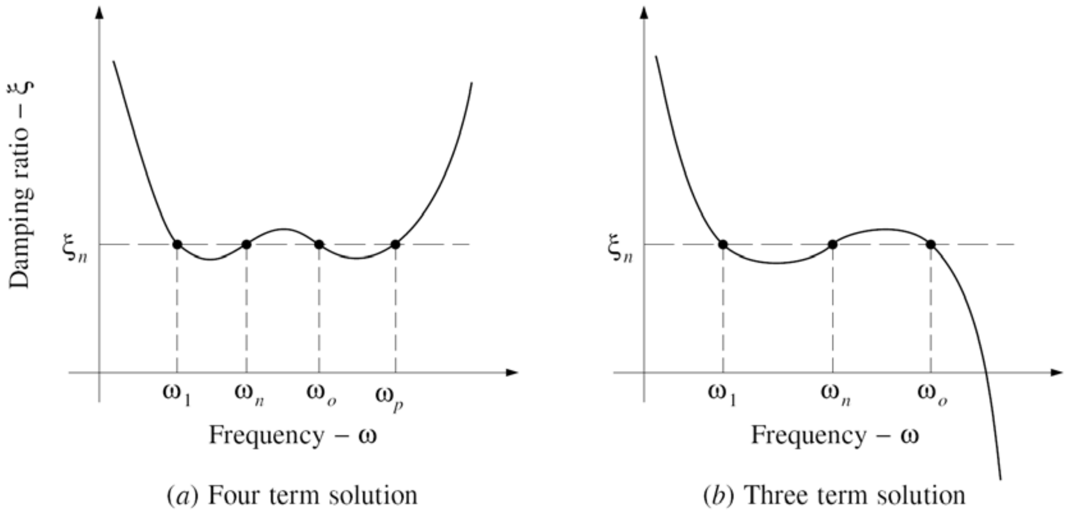

Figure 5-4 extended Rayleigh damping, damping ratio versus frequency (Clough and Penzien, 1993).

Alternative formulation of the damping matrix is a damping matrix associated with a given set of modal damping ratios. The set of modal damping ratios reflects the damping in each mode shape.

$$\mathbf{C}_n = \mathbf{\Phi}^{\mathbf{T}}\mathbf{C}\mathbf{\Phi} = 2\begin{bmatrix} \xi_1\omega_1 M_1 & 0 & 0 & \cdots \\ 0 & \xi_2\omega_2 M_2 & 0 & \cdots \\ 0 & 0 & \xi_3\omega_3 M_3 & \cdots \\ \vdots & \vdots & \vdots & \ddots \end{bmatrix} \quad \text{(D.23)}$$

The matrix of the damping matrix in (D.23) is given in Cartesian coordinates by:

$$\mathbf{C} = \mathbf{M}\left[\sum_{n=1}^{N} \frac{2\xi_n\omega_n}{M_n}\boldsymbol{\varphi}_n\boldsymbol{\varphi}_n^T\right]\mathbf{M} \quad \text{(D.24)}$$

In this matrix, the contribution of the damping for each undamped mode will contribute nothing to the damping matrix. Only the modes included in the formation of the damping matrix will have damping and all the other modes will be undamped. To avoid undesirable amplification of an undamped modal response, damping should be increased with stiffness proportional damping matrix as in equation (D.14). The matrix should be calculated to provide the damping ratio ξ_c of the highest mode ω_c for which damping is specified. Thus:

$$a_1 = \frac{2\xi_c}{\omega_c} \quad \text{(D.25)}$$

Combining (D.25) with the stiffness part of equation (D.17) gives the damping ratio $\hat{\xi}_n$ of the stiffness proportional damping matrix as function of the frequency ω_n:

$$\hat{\xi}_n = \frac{a_1\omega_n}{2} = \xi_c\left(\frac{\omega_n}{\omega_c}\right) \quad \text{(D.26)}$$

The total damping ratio desired in any mode *n* is ξ_n. To satisfy with this condition, the symbol ξ_n has to be degreased with the stiffness proportional damping part. Thus the total damping at each mode is given by ξ_n. The new modal equivalent damping ratio $\left(\overline{\xi}_n\right)$ is given by:

$$\bar{\xi}_n = \xi_n - \xi_c \left(\frac{\omega_n}{\omega_c} \right) \tag{D.27}$$

The final result of this development is a proportional damping matrix c given by

$$\mathbf{C} = a_1\mathbf{K} + \mathbf{M}\left[\sum_{n=1}^{c-1} \frac{2\bar{\xi}_n \omega_n}{M_n} \boldsymbol{\varphi}_n \boldsymbol{\varphi}_n^T \right]\mathbf{M} \tag{D.28}$$

Which provides the desired modal damping ratios for frequencies less than or equal to ω_c and which has linearly increasing damping for higher frequencies.

D.5 Axis transformation

When the local axis system of a beam is at an angle (α) to the global axis system, it is convenient to transform beam to the global access system. The stiffness relation in the direction of α is $f_\alpha = K_\alpha x_\alpha$:

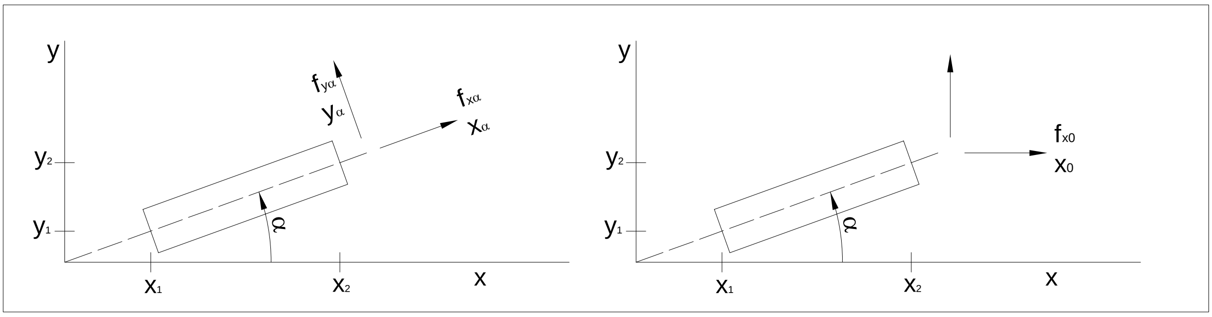

Figure 5-5 transformation of local to global axes

The rotation of the vectors f_α and x_α with respect to the global x – y axis is given by(Ghali and Neville, 1989):

$$\mathbf{f_\alpha} = \mathbf{Tf_0} \text{ and } \mathbf{x_\alpha} = \mathbf{Tx_0} \tag{D.29}$$

Where:

$$\mathbf{T} = \begin{bmatrix} \cos\alpha & \sin\alpha & 0 \\ -\sin\alpha & \cos\alpha & 0 \\ 0 & 0 & 1 \end{bmatrix} \text{ or } \begin{bmatrix} \lambda_{x^*x} & \lambda_{x^*y} & 0 \\ \lambda_{y^*x} & \lambda_{y^*y} & 0 \\ 0 & 0 & 1 \end{bmatrix}$$

Where:

$$\lambda_{x^*x} = \frac{x_2 - x_1}{l_{12}}$$

$$\lambda_{x^*y} = \frac{y_2 - y_1}{l_{12}}$$

$$\lambda_{y^*x} = -\lambda_{x^*y}$$

$$\lambda_{y^*y} = \lambda_{x^*x}$$

Because $T^{-1} = T^T$, holds the following: $f_0 = T^T f_\alpha$ and $x_0 = T^T x_\alpha$. With these equations the transformed stiffness matrix can be determined:

$$\mathbf{f}_\alpha = \mathbf{K}_x \mathbf{x}_\alpha$$
$$\mathbf{T}\mathbf{f}_0 = \mathbf{K}_\alpha \mathbf{T}\mathbf{x}_0$$
$$\mathbf{f}_0 = \left[\mathbf{T}^\mathrm{T}\mathbf{K}_\alpha\mathbf{T}\right]\mathbf{x}_0$$
$$\mathbf{f}_0 = \mathbf{K}_0\mathbf{x}_0$$
$$\mathbf{K}_0 = \mathbf{T}^\mathrm{T}\mathbf{K}_\alpha\mathbf{T} \tag{D.30}$$

D.6 Multiple beams

Structures can be modelled as multiple beams. For n elements the size of the M and K matrices will be (n x n). The elements in the M matrix will be zero at the off-diagonals. The stiffness of each beam element has to be transformed to a global stiffness matrix.
The transformation to an integral global stiffness matrix is given in Figure 5-6. The beam stiffness for the separate beams (A,B and C) have to be summed for each element.

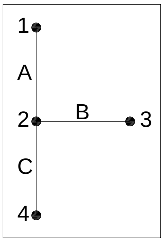

$$\mathbf{K}_\mathrm{g} = \begin{bmatrix} \mathbf{A}_{11} & \mathbf{A}_{12} & \mathbf{0} & \mathbf{0} \\ \mathbf{A}_{21} & \mathbf{A}_{22}+\mathbf{B}_{11}+\mathbf{C}_{11} & \mathbf{B}_{12} & \mathbf{C}_{12} \\ \mathbf{0} & \mathbf{B}_{21} & \mathbf{B}_{22} & \mathbf{0} \\ \mathbf{0} & \mathbf{C}_{21} & \mathbf{0} & \mathbf{C}_{22} \end{bmatrix}$$

Figure 5-6 example structure, transformation partial beam stiffness to integral stiffness matrix

Appendix E Modal response spectrum

E.1 Modal response spectrum analysis

A modal response spectrum analysis is a plot of the maximum response versus the corresponding frequency of period results in a response spectrum for a particular ground motion. In this paragraph will be first explained how to generate a response spectrum for a single degree of freedom model (SDOF) and thereafter for a multi degree of freedom model (MDOF). A important note: the modal response spectrum has to be applied to the modal coordinate system. This holds also for a MDOF model. For a continuous system model this is not applicable. The application of a modal response spectrum is given in Appendix E.

E.2 SDOF

For a SDOF mass spring system holds:

$$x_t = x_g + x_r \tag{E.1}$$

where:

x_t = the total displacement

x_g = the ground displacement

x_r = the displacement of the structure relative to the ground

The equation of motion becomes then:

$$M\ddot{x}_t = C\left(\dot{x}_g - \dot{x}_t\right) + K\left(x_g - x_t\right) \tag{E.2}$$

This can be rewritten as:

$$M\ddot{x}_r + C\dot{x}_r + Kx_r = -M\ddot{x}_g \tag{E.3}$$

Or in terms of ω and ξ:

$$\ddot{x}_r + 2\xi\omega_n\dot{x}_r + \omega_n{}^2 x_r = -\ddot{x}_g(t) \tag{E.4}$$

where:

ω_n = $\sqrt{K/M}$

ξ = $\dfrac{C}{2\sqrt{KM}}$

In equation (E.4), the response ($\ddot{x}_r$, $\dot{x}_r$ and x_r) can be calculated for a given ground acceleration as a function of the time($\ddot{x}_g(t)$). The response is determined only by T_n (natural period for SDOF system) and ξ (critical damping percentage). Measured time histories of earthquake ground movement are applied to the SDOF- systems and a time history of the motion x_r relative to the ground is calculated. An overview of this numerical calculation is given in 0. This calculation is repeated for a range of T_n ($2\pi/\omega_n$) and ξ. The peak relative response to the ground motion time history is noted for each T_n and ξ. This value is called the spectral displacement S_d.

$$S_d = x_{r(\max)} \tag{E.5}$$

It is also convenient to define approximate velocity an acceleration spectra (pseudo velocity, or pseudo acceleration).

$$S_v = \omega_n S_d \tag{E.6}$$

$$S_a = \omega_n^2 S_d \tag{E.7}$$

For the El Centro earthquake from 1940 is the response spectrum given in Figure 5-7.

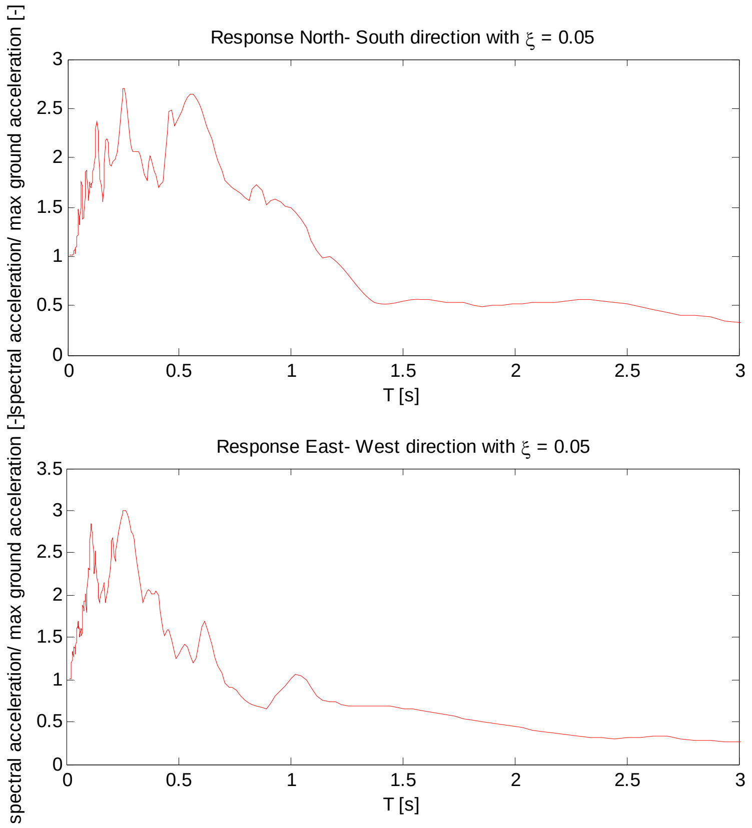

Figure 5-7 Response spectrum for El Centro earthquake

S_v and S_a are approximations, their definition assumes that the response is at the frequency ω_n which is not necessarily true. Because of the relationship between the S_d, S_v and S_a it is convenient to plot these in one figure (Figure 5-8).

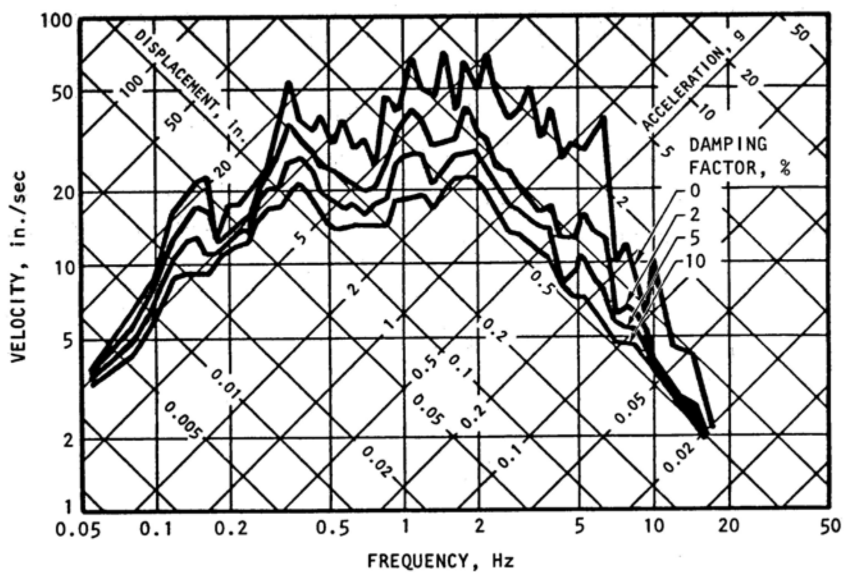

Figure 5-8 response spectra, El Centro earthquake may18 1940 direction North- South (Newmark and Hall, 1982)

The response spectrum is given in codes as the basis of design for real structures. Although the response spectrum contains simplifications and consumptions it is widely used because it's analytical convenient and the result are thought to be conservative.

Even when two 2D analyses in two orthogonal horizontal directions, X and Y, satisfy it is preferable to do the modal analysis for a full 3D structural model.
The fist step in a modal response spectrum analysis is the determination of the 3D modal shapes and natural frequencies of vibration (eigenmodes and eigenvalues).
The response of the lowest-frequency mode is usually the most significant. For a application to a MDOF- model is referred to 0. For ductility modified response spectra is referred to E.4 .

E.3 Influence of the soil

With the help of a response spectrum is becoming clear which frequencies or periods are dominant. The response spectrum is besides the earthquake also depended on the soil classification. The local soil conditions have influence on how the structure is excited and there fore also on the response spectrum. Numerous investigations in response spectra as function of the soil conditions are being done (Seed and Idriss, 1982). Their results are given in Figure 5-9 and Figure 5-10. There is a difference in response whether the construction is founded at a hard underground or soft clay. The response on weak soil is in general higher than the response on soft soil. The peak responds for stiff soil is around 0.2 – 0.5 hz.

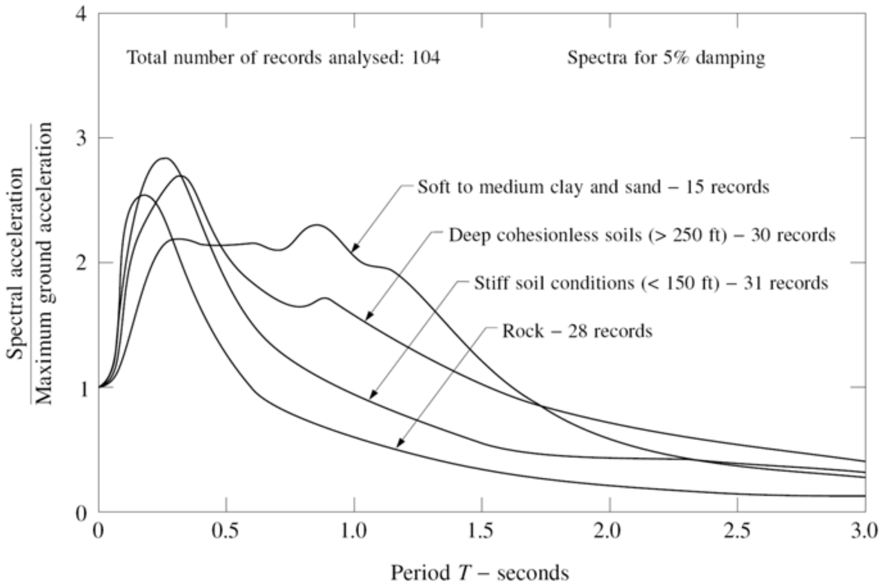

Figure 5-9 Average acceleration spectra for different site conditions (Seed and Idriss, 1982)

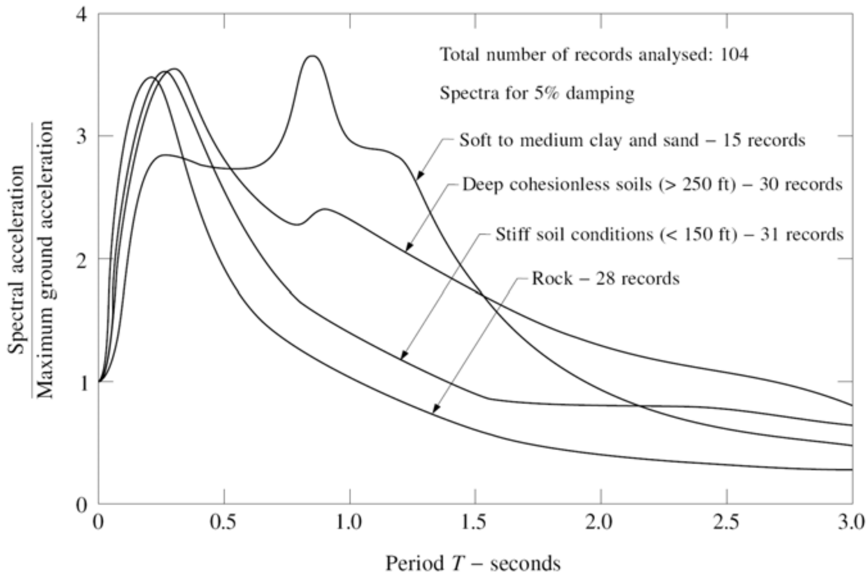

Figure 5-10 84 percentile acceleration spectra for different site conditions (Seed and Idriss, 1982)

Figure 5-11 and Figure 5-12 give the response spectra according the API and the Eurocode 8. Both response spectra build up in the same matter. In here is schematically given the influence of the soil type on the response spectrum. On the y-axis is given the response acceleration divided by the maximum excitation acceleration. The response spectra according the eurocode is classified in 5 soil types where the response spectra according the API is classified in 3 soil types. For most areas in world the design earthquake acceleration is known. Therefore these graphs are integrally applicable.

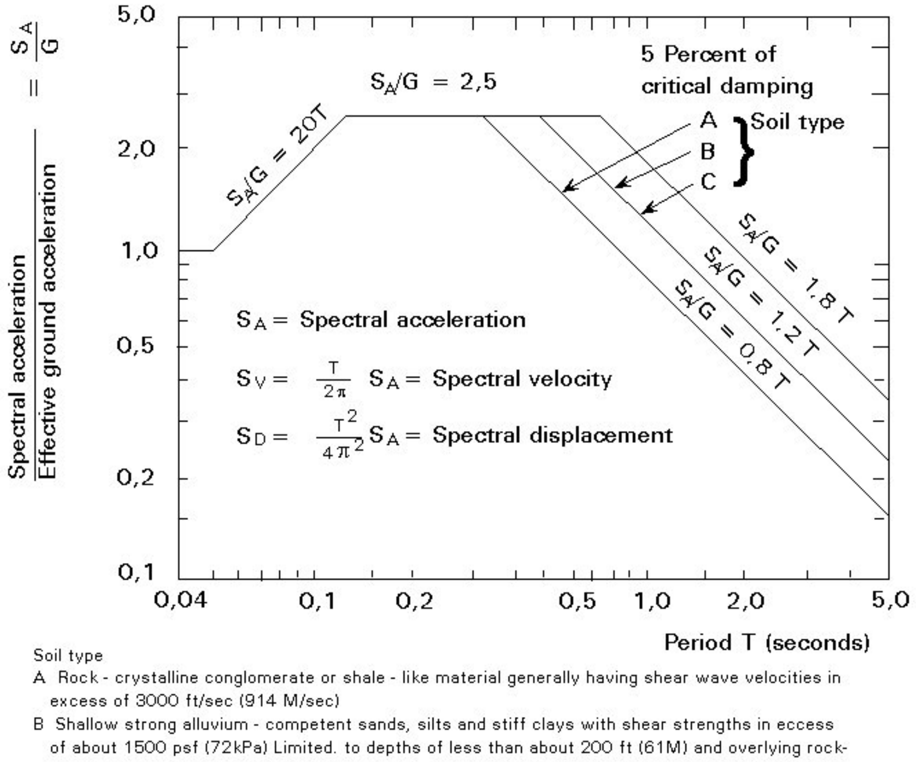

Soil type

A Rock - crystalline conglomerate or shale - like material generally having shear wave velocities in excess of 3000 ft/sec (914 M/sec)

B Shallow strong alluvium - competent sands, silts and stiff clays with shear strengths in eccess of about 1500 psf (72kPa) Limited. to depths of less than about 200 ft (61M) and overlying rock-like materials

C Deep strong alluvium-competent sands, silts and stiff clays with thicknesses in excess of about 200 feet (61M) and overlying rock-like materials

Figure 5-11 design response spectra [API p. 150.]

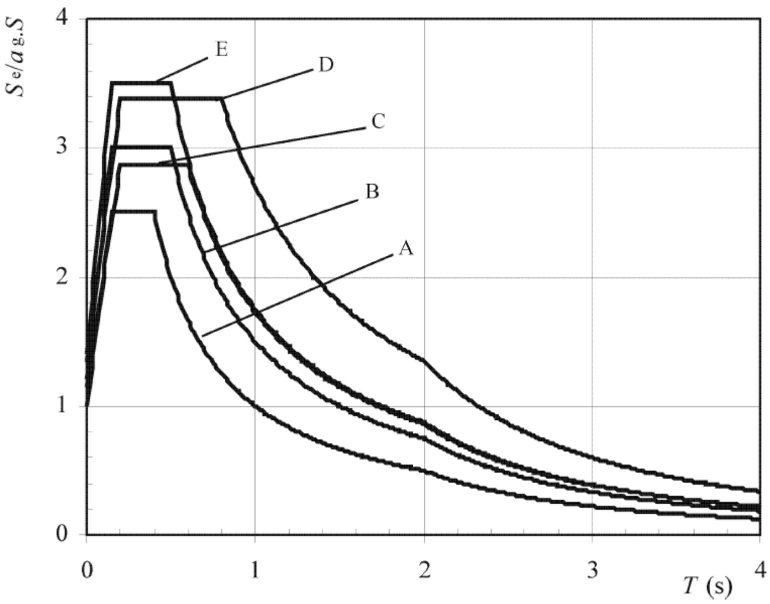

A	Rock or toher rock- like geological formation, including at most 5 m of weaker material at the surface
B	Deposits of very dense san, gravel or ervy stiff clay, at least several tens of m in thickness, characterised by a gradual increase of mechanical properties with depth
C	Deep deposits of dense or medium-dense sand, gravel or stiff clay with thickness from several tens to many hundreds of meter
D	Deposits of loose-to-medium cohesion less soil (with or without some soft cohesive layers), or of predominantly soft-to-firm cohesive soil
E	A soil profile consisting of a surface alluvium layer with v_s values of type C or Dand thickness varying between about 5 m and 20 m, underlain by stiffer material with v_s> 800 m/s

Figure 5-12 Elastic response spectra type 1 according the eurocode, with 5% damping

Many structures rely on plastic behaviour to resist major earthquakes. The loading calculated from the linear assumptions in the static pushover analysis is an approximation of the actual behaviour. During severe shaking several types of non-linear behaviour may occur:

- plastic hinge formation
- brace buckling
- P- Δ effects
- Member strength decay under cyclic load
- Soil pore water pressure generation under cyclic load
- Soil strength degradation under cyclic loading.

With the help of a numerical calculation, non-linear behaviour can be introduced into the calculation. The result will be an accurate representation of the appearing forces. A time domain history analysis is done with the following formula:

$$\mathbf{M\ddot{x}} + \mathbf{C\dot{x}} + \mathbf{Kx} = \mathbf{f(t)} \quad \text{(E.8)}$$

The force vector is the earthquake excitation force (relative base movement times support stiffness). With the mass, damping, stiffness matrices and two initial conditions known the structural behaviour for this event can be calculated numerically with e.g. the Runke Kutta method (see 0).

For non-linear models, the damping and stiffness resistance are depending on the structural displacement. In a numerical calculation this condition is relative easy to program.

Non- linear calculations are difficult to understand. The change of initial conditions for instance can result in a totally different outcome. Insight into the problem is therefore difficult to acquire and the result are equivocal.

E.4 Ductility factor

So far the response spectrum, besides damping, didn't include ductility. Ductility is energy dissipation due to inelastic behaviour of the construction material. In this paragraph the influence of ductility on the response spectra will be analysed. The response spectra will be analysed for an elastic-plastic model relatively to the elastic model. The equation of motion for a non linear model is given by:

$$\ddot{x}_r + 2\xi\omega\dot{x}_r + \frac{f_s(x_r)}{m} = -\ddot{x}_g(t) \qquad \text{(E.9)}$$

where:

$$\omega = \sqrt{k/m}$$

$$\xi = c/2m\omega$$

The maximum value of the displacement is expressed in terms of the ductility factor μ.

$$\mu = \frac{|x(t)|_{\max}}{x_y} \qquad \text{(E.10)}$$

where:

$x_y =$ the displacement at which yielding starts

For μ < 1 the entire response, like in the previous response calculations the system is assumed to be elastic. When μ > 1, the system respond inelastic in certain time intervals. The maximum displacement $|x(t)|_{\max}$ and the maximum spring force $|f_s(t)|_{\max}$ are compared for the two cases. For both cases, the values ξ, ω and m kept constant during a certain earthquake event $\ddot{x}_g(t)$. The results are given in Figure 5-13.

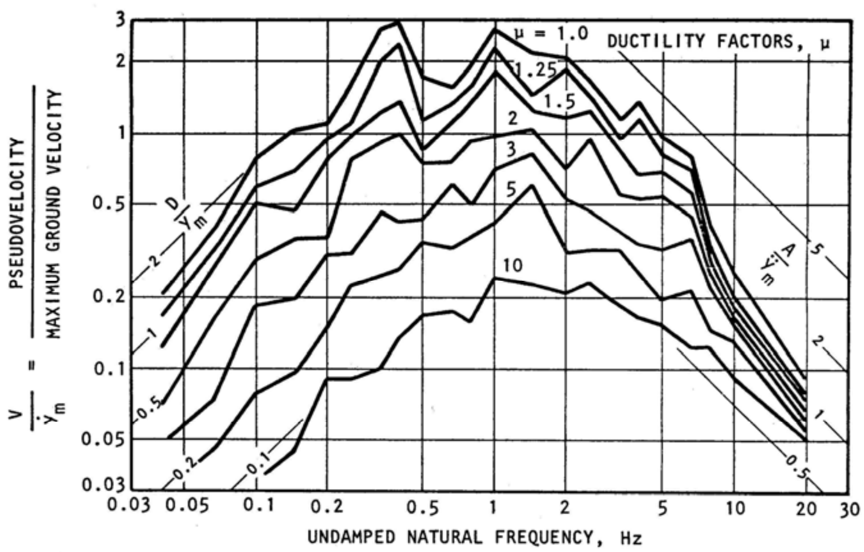

Figure 5-13 Deformation spectra, elastoplastic systems, 2 % critical damping, El Centro Earthquake (Newmark and Hall, 1982).

In the following analysis the maximum values for the elastic case are supplemented with the subscript "el" and in the elastic- plastic case with "elpl". The values are obtained numerically. The first system considered is a flexible system having a value of natural frequency $0 < f < 33Hz$. In this system the structural resistance is insignificant. Consequently both x_{el} and x_{elpl} will approach the maximum ground displacement $|\ddot{x}_g(t)|_{\max}$.

$$\left.\begin{aligned} x_{el} &= x_{elpl} = \left| x_g(t) \right|_{\max} \\ f_{s,y} &= k \left| x_g(t) \right|_{\max} \Big/ \mu \end{aligned}\right\} 0 < f < 0.3Hz \tag{E.11}$$

For systems with a natural period between 0.3 and 2 Hz, x_{el} and x_{elpl} won't reach the maximum ground displacement. Numerous earthquake excitations show that the relative displacement still holds. An example is given in Figure 5-13.

$$\left.\begin{aligned} x_{el} &= x_{elpl} \\ f_{s,y} &= f_{s,el} \big/ \mu \end{aligned}\right\} 0.3 < f < 2Hz \tag{E.12}$$

In the frequency range $2 < f < 8Hz$, the results indicate (see Figure 5-14) that the deformation energy is well preserved. The areas under the elastic and the elastic-plastic curves in Figure 5-14 are nearly equal. The elastic- plastic displacement/ force (x_{elpl} and $f_{s,y}$) expressed in terms of elastic displacement/ force (x_{el} and $f_{s,el}$) and the ductility factor μ gives:

$$\left.\begin{aligned} x_{elpl} &= \frac{\mu}{\sqrt{2\mu - 1}} x_{el} \\ f_{s,y} &= \frac{1}{\sqrt{2\mu - 1}} f_{s,el} \end{aligned}\right\} 2 < f < 8Hz \tag{E.13}$$

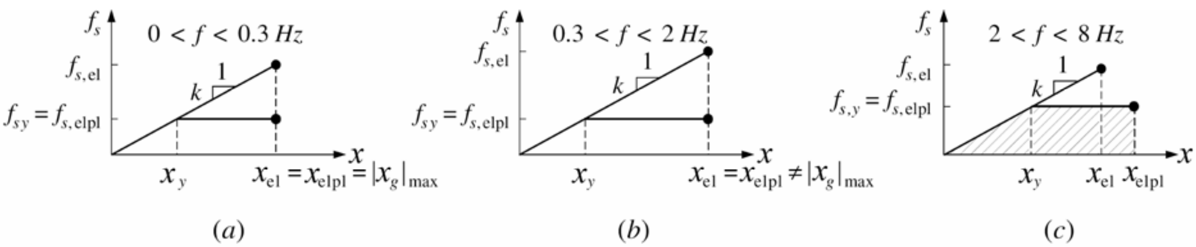

Figure 5-14 Elastic and elastic- plastic force- displacement relations (Clough and Penzien, 1993)

When the natural frequency goes to infinity ($k \to \infty$) yielding of the rigid will occur with the slightest reduction of $f_{s,y}$. In this case $x_y \to 0$. For finite values of the ductility factor the force must be limited. This is true of frequencies $f > 33Hz$. Thus

$$\left.\begin{aligned} x_{elpl} &= \mu x_{el} \\ f_{s,y} &= f_{s,el} = m \left| \ddot{x}_g(t) \right|_{\max} \end{aligned}\right\} f > 33Hz \tag{E.14}$$

The natural frequencies in the range $8 < f < 33Hz$ respond transitional between the systems discussed before in equation (E.13) and (E.14). Fortunately, the fundamental frequencies of most structures are below $8Hz$. Thus in most cases, the equations below $8Hz$ will suffice in estimating the maximum force.

Appendix F Numerical Calculation

The equation of motion is given by:

$$M\ddot{x} + C\dot{x} + Kx = f(t) \tag{F.1}$$

This second order differential equation can be written as two dependent single order differential equations (Vuik, 2005). E.g. when:

$$\begin{aligned} v &= x \\ w &= \dot{v}(= \dot{x}) \\ \dot{w}&(= \ddot{x}) \end{aligned} \tag{F.2}$$

Then equation (F.1) can be written as:

$$\begin{aligned} \dot{v} &= w \\ \dot{w} &= \frac{-Cw - Kv - M\left\{r\ddot{x}_g\right\}}{M} = -\frac{K}{M}v - 2\xi\sqrt{\frac{K}{M}}w - r\ddot{x}_g \end{aligned} \tag{F.3}$$

Or in matrix notation:

$$\begin{bmatrix} \dot{v} \\ \dot{w} \end{bmatrix} = \begin{bmatrix} 0 & 1 \\ -\boldsymbol{\omega}^2 & -2\xi\boldsymbol{\omega} \end{bmatrix} \begin{bmatrix} v \\ w \end{bmatrix} - \begin{bmatrix} 0 \\ r\ddot{x}_g(t) \end{bmatrix}$$

which is:

$$\dot{\mathbf{x}} = \mathbf{A}\mathbf{x} - \mathbf{f}(t) \tag{F.4}$$

Where matrix $\mathbf{A}$ is given by:

$$\begin{bmatrix} 0 & 1 \\ -\boldsymbol{\omega}^2 & -2\xi\boldsymbol{\omega} \end{bmatrix}$$

The Runge- Kutta method is given by:

$$\omega_{n+1} = \omega_n + \tfrac{1}{6}\left[k_1 + 2k_2 + 2k_3 + k_4\right]$$

Where:

$$\begin{aligned} k_1 &= hf(t_n, d_n) \\ k_2 &= hf(t_n + \tfrac{1}{2}h, d_n + \tfrac{1}{2}k_1) \\ k_3 &= hf(t_n + \tfrac{1}{2}h, d_n + \tfrac{1}{2}k_2) \\ k_4 &= hf(t_n + h, d_n + k_3) \end{aligned} \tag{F.5}$$

The local truncation error of the runge kutta method is given by:

$$\mathbf{G}_{RK}(h\mathbf{A}) = I + h\mathbf{A} + \frac{h^2}{2}\mathbf{A} + \frac{h^3}{6}\mathbf{A} + \frac{h^4}{24}\mathbf{A} \tag{F.6}$$

The matrix **A** diagonalised for every power according to:

$$\mathbf{S}^{-1}\mathbf{A}^k\mathbf{S} = \mathbf{\Lambda}^k \tag{F.7}$$

Because $\mathbf{\Lambda}^k$ is diagonal for every value of k, $\mathbf{G}_{RK}(h\mathbf{\Lambda})$ will also be diagonal.

$$\mathbf{G}_{RK}(h\mathbf{\Lambda}) = \mathrm{Diag}[Q(h\lambda_1), Q(h\lambda_1), \ldots\ldots, Q(h\lambda_k)] \tag{F.8}$$

The matrix $\mathbf{G}_{RK}(h\mathbf{\Lambda})$ is a diagonal matrix with amplification factors on its diagonals.

The numerical calculation is stable when all the amplification factors are smaller than 1, because the local truncation error is then limited. When the relative damping factor ξ is constant, the amplification matrix **A** is only dependent on the natural frequency $\boldsymbol{\omega}$ (see equation (F.3)). Therefore the diagonal amplification matrix $\mathbf{G}_{RK}(h\mathbf{\Lambda})$ with a constant damping percentage is only dependent on $\boldsymbol{\omega}$ and h (step size). In practice does this mean that the natural frequency at a certain stepsize are limited (see Figure 5-15). The maximum applicable natural frequency are given in table F-1.

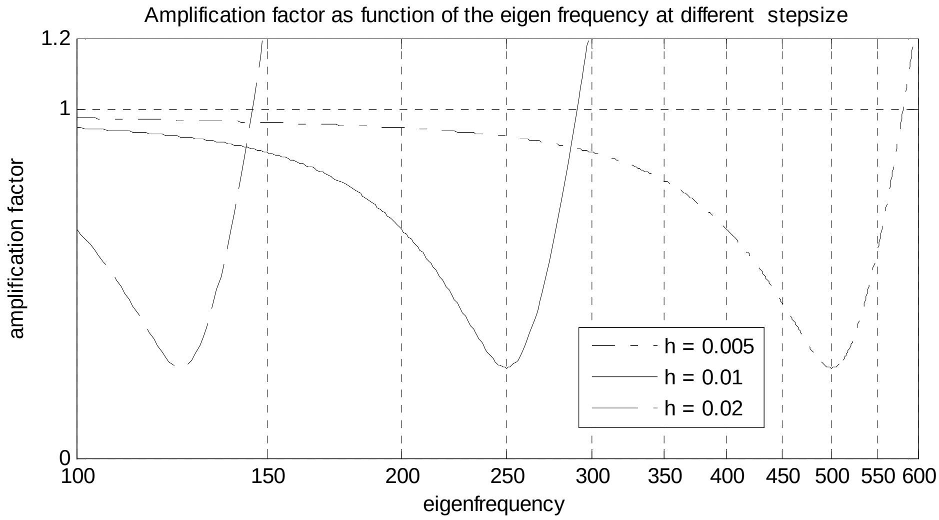

Figure 5-15 amplification factor as function of the natural frequency at different step size (h= 0.005/0.01/0.02)

Stepsize	0.02	0.01	0.05
Maximum natural frequency [rad/s]	145	290	580

table F-1 maximum natural frequency at stepsize

Appendix G Modal Response Spectrum Application

This appendix discusses the application of a modal response spectrum to a:

- Linear static analysis
- MDOF modal response spectrum analysis

G.1 Linear static analysis

The linear static analysis is usually conservative. No dynamic analysis is made of the structure. Assumed is the structural peak acceleration. The structural mass is multiplied by this acceleration to acquire the earthquake forces. The forces are applied statically and distributed in proportion to the structural mass. The forces are magnified by a static coefficient, which accounts for the differences between the static and dynamic responses of a structure. For a SDOF system holds:

$$F = C_s \left(S_a\right)_{peak} m \tag{G.1}$$

where:

$F =$ equivalent static load

$C_a =$ static coefficient

$S_{a\,peak} =$ peak of acceleration response spectrum

$m =$ mass of system

G.2 MDOF

In analogy with the SDOF

$$x_t = x_g + x_r \tag{G.2}$$

where:

x_t = the total displacement

x_g = the ground displacement

x_r = the displacement of the structure relative to the ground

The equation of motion becomes then:

$$M\ddot{x}_r + C\dot{x}_r + Kx_r = -M\{r\ddot{x}_g\} \tag{G.3}$$

This equation can be solved using a numerical calculation described in 0. Although, the equations can be transformed to a normal mode coordinate system. The response of each mode can than be treated as a single degree of freedom system whereon the response spectrum can be applied.

$$x = \Phi Z \tag{G.4}$$

where:

Φ = the matrix of eigenvectors (φ, mode shapes) arranged in columns

Substitution of (G.4) into equation (G.5) and multiplied by −Φ gives:

$$\Phi^T M\Phi\ddot{Z} + \Phi^T C\phi\dot{Z} + \Phi^T K\phi Z = -\Phi^T M\{r\ddot{x}_g\} \tag{G.5}$$

The terms $\Phi^T ... \Phi$ have only non-zero values on their leading diagonals. Therefore equation (G.5) can be written as N independent scalar equations (one for each mode) of the form:

$$M_n\ddot{Z}_n + C_n\dot{Z}_n + K_nZ_n = -L_n\ddot{x}_g \quad (G.6)$$

where:

M_n	= generalised mass for mode n	$= \phi_n{}^T M\phi_n$
C_n	= generalised damping for mode n	$= \phi_n{}^T C\phi_n = 2\xi_n\omega_n M_n$
K_n	= generalised stiffness for mode n	$= \phi_n{}^T K\phi_n = \omega_n{}^2 M_n$
Z_n	= displacement for mode n, $Z_n(t)$	$= \phi_n{}^T x_n(t)$
L_n	= modal participation factor	$= \phi_n{}^T M_r$

L_n, the modal participation factor, has dimensions of mass and is a measure of the responsiveness of each mode to ground vibration in the direction r. The value of L_n s dependent on the

$$M_n\ddot{Z}_n + C_n\dot{Z}_n + K_nZ_n = -L_n\ddot{x}_g \quad (G.7)$$

where:

= the matrix of eigenvectors (φ, mode shapes) arranged in columns

The equation (G.7) is in normal mode equivalent to equation (G.3). The maximum displacement(in normal mode coordinates) in mode n is:

$$Z_{n\max} = \frac{L_n}{M_n} S_{dn} \quad (G.8)$$

The displacement due to mode n, in Cartesian coordinates, is equal to:

$$x_{n\max} = \phi_n Z_n = \phi_n \frac{L_n}{M_n} S_{dn} \quad (G.9)$$

$x_{n\max}$ consist of a vector. Member forces for the mode n displacement are calculated from the element stiffness relation.

$$\mathbf{f}_{n\max} = \mathbf{K}\mathbf{x}_{n\max} = \mathbf{K}S_{nd} \quad (G.10)$$

Another way for defining the stiffness force, because $M = K/\omega^2$ and $S_a = \omega^2 S_d$. Subsequently:

$$\mathbf{f}_{n\max} = MS_{na} \quad (G.11)$$

An method of calculating the maximum element forces is by the square root of sum of squares (SRSS) method. Where the maximum force is calculated by:

$$\mathbf{f}_{\max} \approx \sqrt{\sum_{n=1}^{n} \mathbf{f}_{n\max}^2} = \sqrt{\mathbf{f}_{1\max}^2 + \mathbf{f}_{2\max}^2 + \dots\dots + \mathbf{f}_{n\max}^2} \quad (G.12)$$

When the natural frequencies of two modes are closely spaced the SRSS method can be non- conservative. In this case the method can be refined by the "ten percent rule". In this method the natural periods which are less then 10% apart are summed absolutely and the SRSS of these and all the other modes. So when mode 1 and 2 are closely spaced equation 7.18 becomes:

$$\mathbf{f}_{\max} \approx \sqrt{\sum_{n=1}^{n} \mathbf{f}_{n\max}^2} = \sqrt{\left(\mathbf{f}_{1\max} + \mathbf{f}_{2\max}\right)^2 + \dots\dots + \mathbf{f}_{n\max}^2} \quad (G.13)$$

Appendix H Variation in parameters

- stiffness parameter

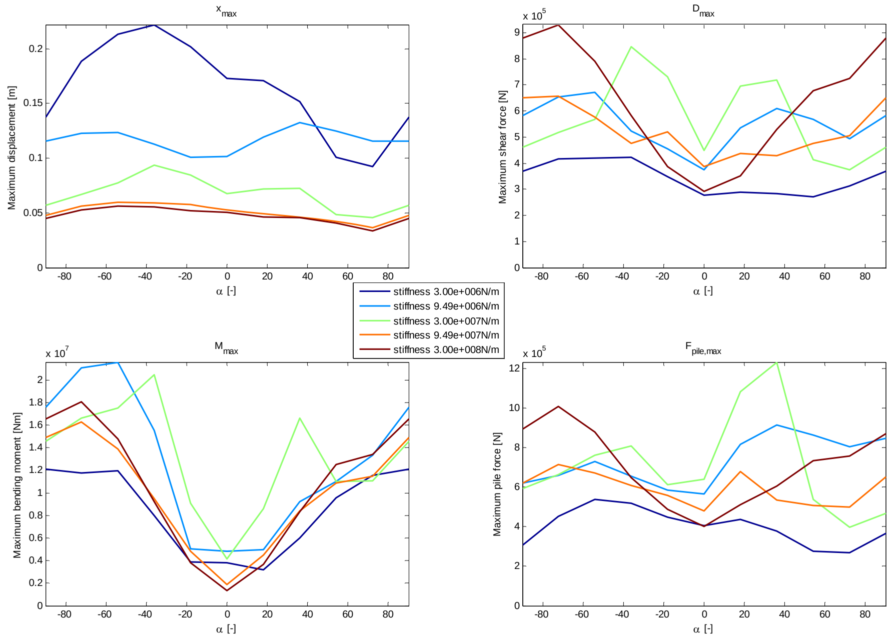

- damping percentage parameter

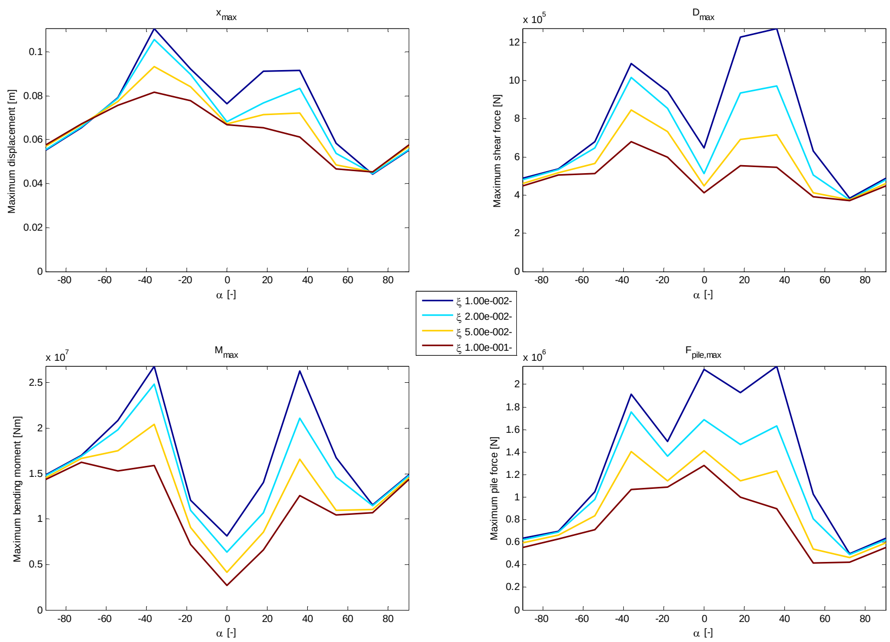

- span length parameter

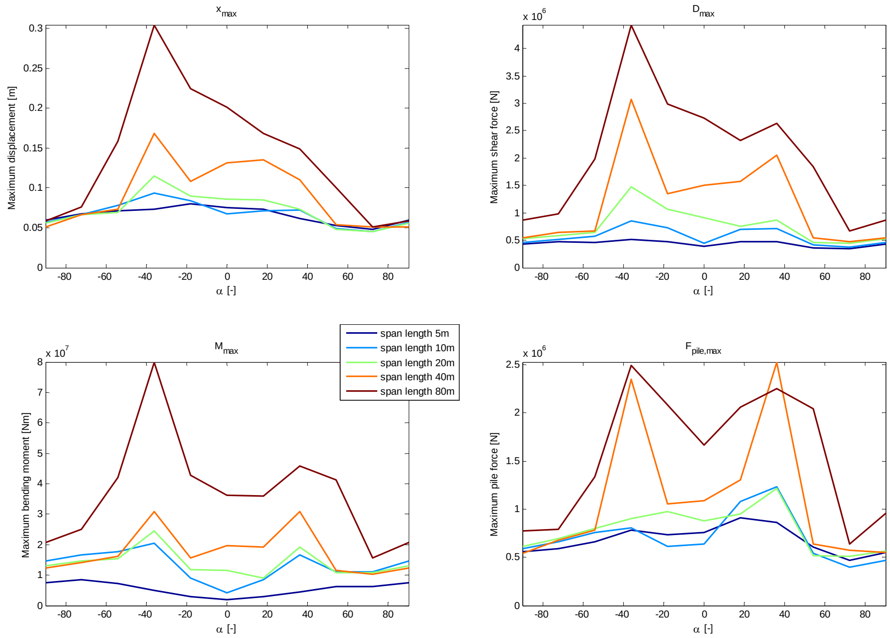

- support mass parameter

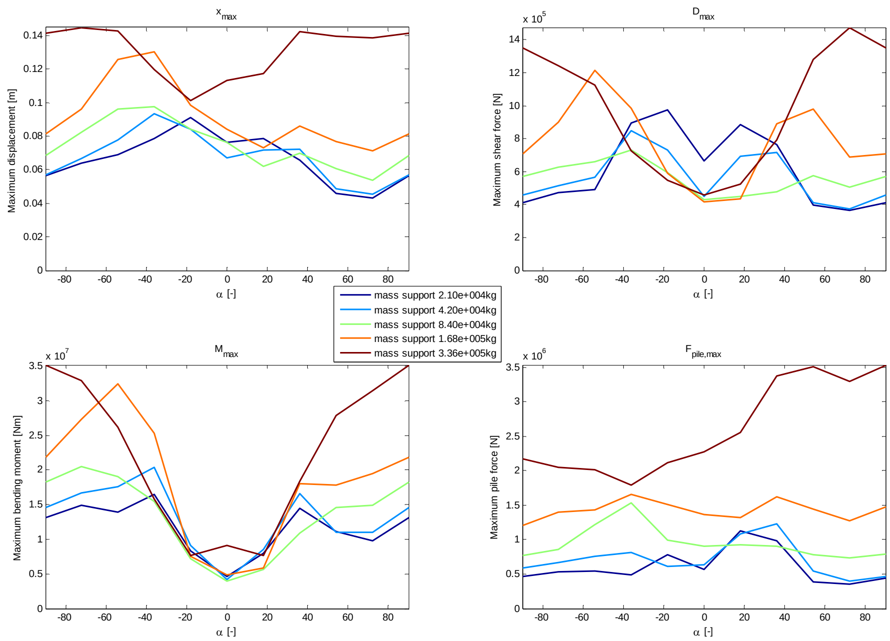

- distributed mass parameter

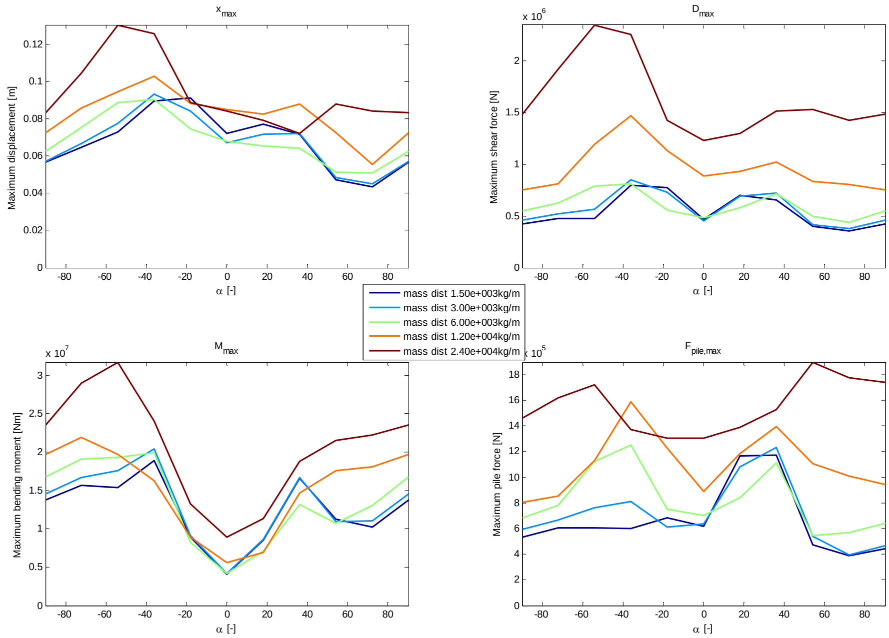

- Young's modulus parameter

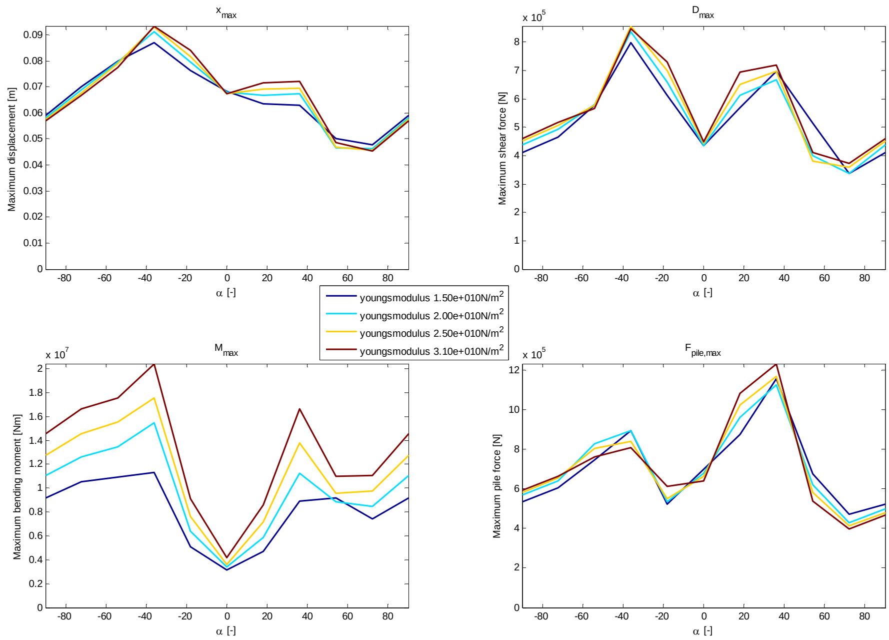

Appendix I Matrix frame calculations

- “normal” support resistant
- strong point support resistant

Appendix J Transfer functions

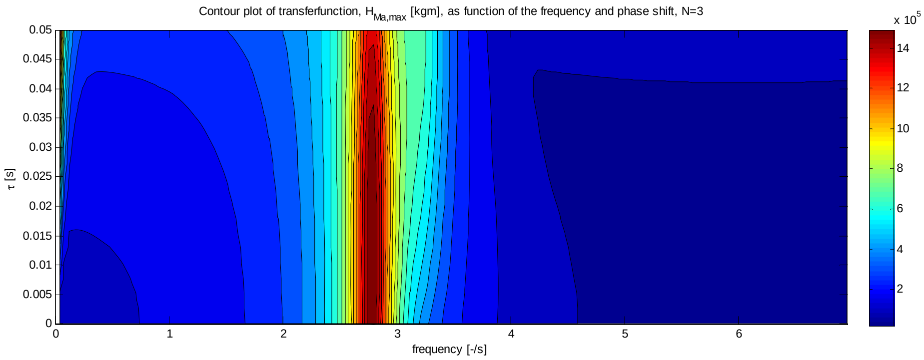

Figure 5-16 Transfer function for N=3

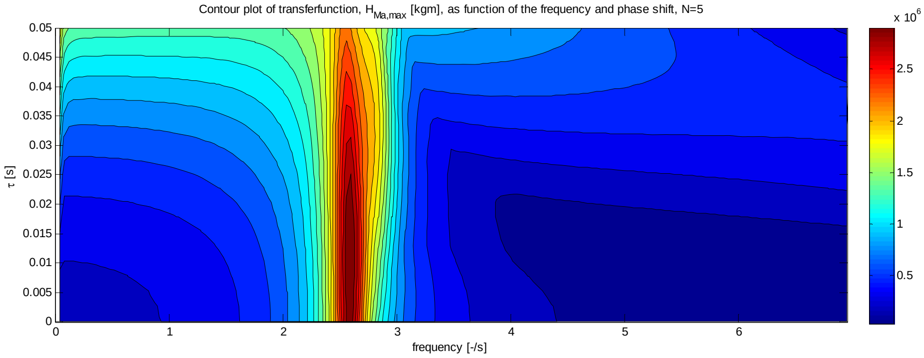

Figure 5-17 Transfer function for N=5

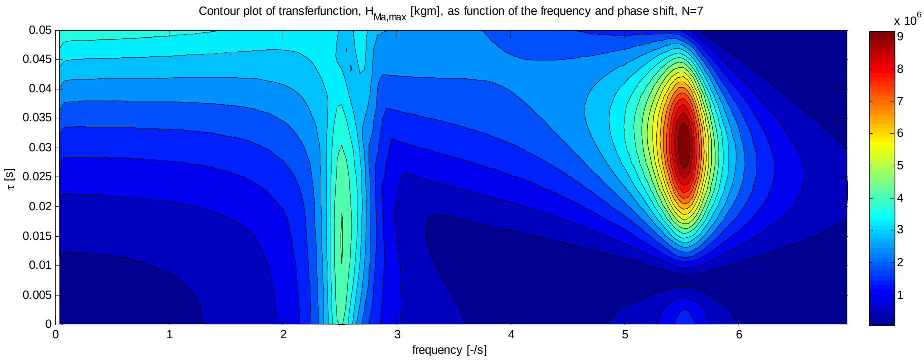

Figure 5-18 Transfer function for N=7

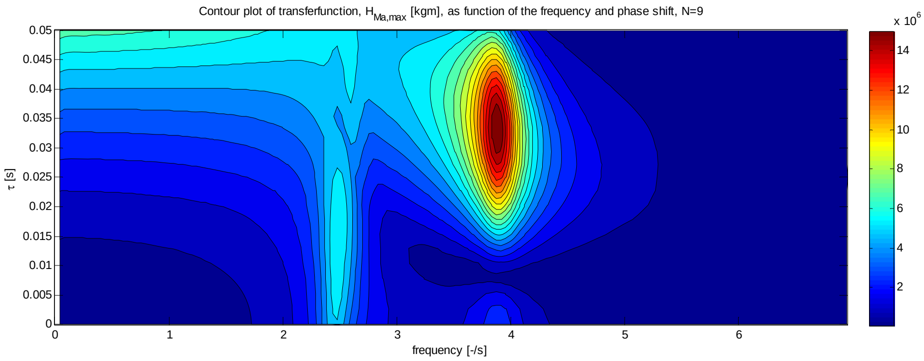

Figure 5-19 Transfer function for N=9

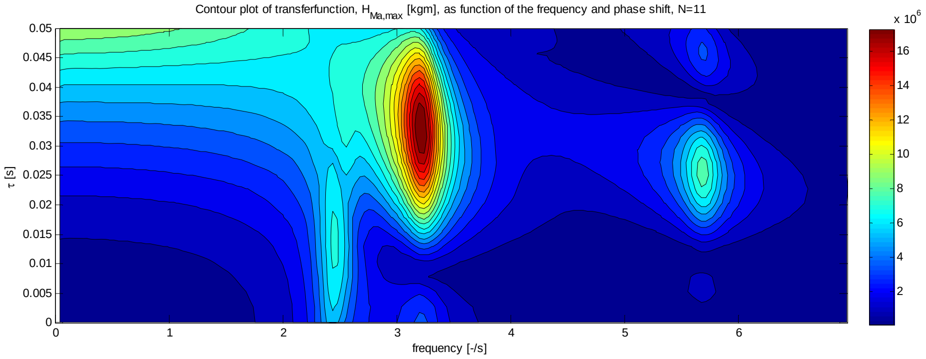

Figure 5-20 Transfer function for N=11

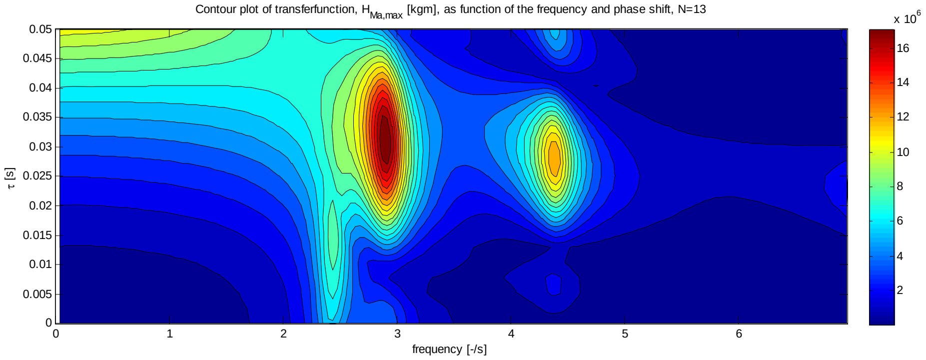

Figure 5-21 Transfer function for N=13

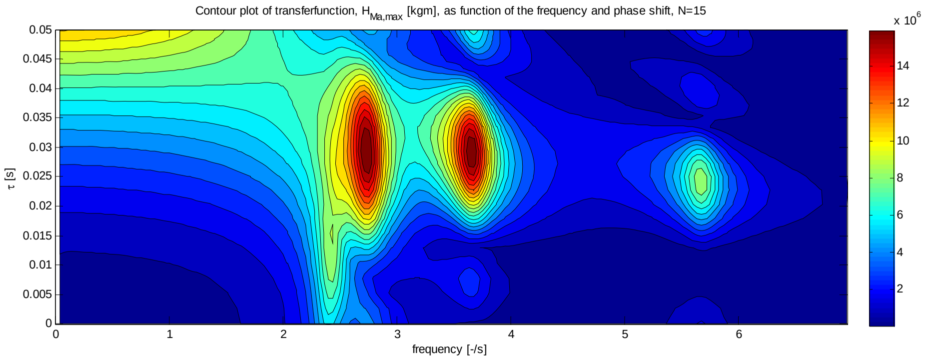

Figure 5-22 Transfer function for N=17

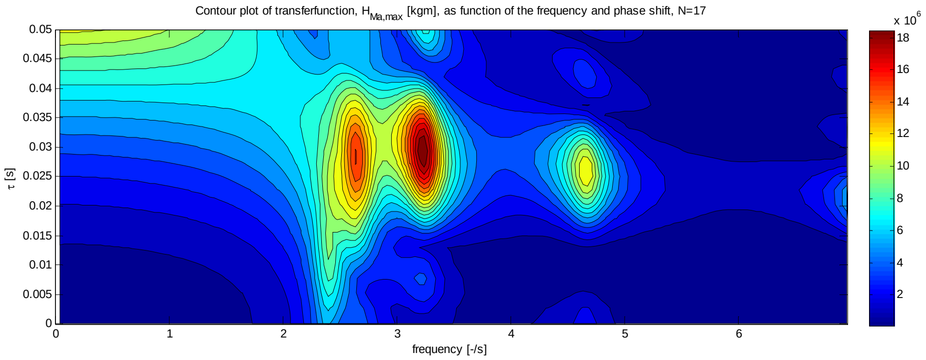

Figure 5-23 Transfer function for N=19

Appendix K Bibliography

Ambraseys N., P.S., R. Berardi, D. Rinaldis, F. Cotton and C. Berge- Thierry, 2000. Dissemination of European strong- motion Data. CD-ROM collection. European Council, Environment and Climate Research Programme.

Barltrop, N.D.P., Marine Technology Directorate Ltd and Adams, A.J., 1991. Dynamics of fixed marine structures. Marine Technology Directorate Ltd publication 91/102. Butterworth-Heinemann, Oxford, 764 pp.

Clough, R.W. and Penzien, J., 1993. Dynamics of Structures. McGraw-Hill, New York, 738 pp.

Fardis, M., 2005. Designers' guide to EN 1998-1 and EN 1998-5 Eurocode 8: Design of structures for earthquake resistance general rules, seismetic actions, design rules for buildings, foundations and retaining structures. Designers' guides to the Eurocodes. Telford, London, 279 pp.

Ghali, A. and Neville, A.M., 1989. Structural analysis: a unified classical and matrix approach. Chapman and Hll, London, 870 blz. pp.

Maritime Navigation Commission Working Group 34, 2001. Seismic design guidelines for port structures report of Working Group no. 34 of the Maritime Navigation Commission. PIANC, Brussels, 44 pp.

Nederlands Normalisatie-Instituut, 1995. Eurocode 8; ontwerpbepalingen voor de bestandheid van constructies tegen aardbevingen. Dl. 1-3. Algemene regels. Bijzondere bepalingen voor verschillende materialen en elementen (voornorm). NNI, Delft, 126 pp.

Newmark, N.M. and Hall, W.J., 1982. Earthquake spectra and design. Engineering monographs on earthquake criteria, structural design, and strong motion records ; v. 3. Earthquake Engineering Research Institute, Berkeley, Calif., 103 pp.

Sarpkaya, T. and Isaacson, M., 1981. Mechanics of Wave Forces on Offshore Structures. Van Nostrand Reinhold, New York, 651 pp.

Seed, H.B. and Idriss, I.M., 1982. Ground motions and soil liquefaction during earthquakes. Earthquake Engineering Research Institute, Berkeley, Calif., 134 pp.

Spijkers, J.M.J., Metrikine, A. and Delft University of Technology Faculty of Civil Engineering and Geosciences., 2005. Structural dynamics: college ct4140. TU Delft, Delft.

Tsinker, G.P., 1997. Handbook of port and harbor engineering; geotechnical and structural aspects. Chapman and Hall, New York, 1054 pp.

Vrijling, J.K., Vrouwenvelder, A.C.W.M. and Delft University of Technology Faculty of Civil Engineering and Geosciences., 2005. Probabilistic design: college ct4130. TU Delft, Delft.

Vuik, C., 2005. Numerieke methoden voor differentiaalvergelijkingen: college wi3097tu. Tu Delft, Faculteit Civiele Techniek en Geowetenschappen, Delft.